

UNIVERSITY OF OKLAHOMA

GRADUATE COLLEGE

MECHANICAL PROPERTIES OF HUMAN MIDDLE EAR TISSUES

A DISSERTATION

SUBMITTED TO THE GRADUATE FACULTY

in partial fulfillment of the requirements for the

degree of

Doctor of Philosophy

By

TAO CHENG
Norman, Oklahoma
2007

UMI Number: 3256649



UMI Microform 3256649

Copyright 2007 by ProQuest Information and Learning Company.
All rights reserved. This microform edition is protected against
unauthorized copying under Title 17, United States Code.

ProQuest Information and Learning Company
300 North Zeeb Road
P.O. Box 1346
Ann Arbor, MI 48106-1346

MECHANICAL PROPERTIES OF HUMAN MIDDLE EAR TISSUES

A DISSERTATION APPROVED FOR THE
SCHOOL OF CHEMICAL, BIOLOGICAL AND MATERIAL ENGINEERING

BY

Dr. Rong Z. Gan (Chair)

Dr. Feng-Chyuan Lai

Dr. Robert L. Rennaker II

Dr. Harold L. Stalford

Dr. Vassilios I. Sikavitsas

ACKNOWLEDGMENTS

I would like to sincerely thank my advisor, Professor Rong Z. Gan, for her guidance, teaching, discussion and support during my study at the University of Oklahoma (OU) over the past five years. Her endless enthusiasm for the research and new ideas coming out from discussions are greatly impressed on my memory, which will, for sure, encourage me to go through difficulties I might meet in my future career development. Dr. Gan not only gave me this opportunity to work in her research team, but also trained me for many skills through different research projects, such as soft tissue biomechanics, finite element modeling and analysis, electromagnetic analysis and implantable medical devices. The skills and knowledge I have gained through the training are priceless and will definitely benefit me over the whole lifetime.

I would also like to gratefully acknowledge all the members of my dissertation committee: Professor Feng-Chyuan Lai, Professor Robert L. Rennaker, Professor Harold L. Stalford and Professor Vassilios I. Sikavitsas, who have spent their time to read my dissertation and offered valuable advices. Without their works, I would never have come to this step.

I also wish to express my heartfelt thanks to Professor Edgar A. O'Rear who is the director of OU bioengineering program (OUBC), and Professor Matthias U. Nollert who is the graduate liaison of OUBC. They provided suggestions and conveniences for me to complete my study as the first graduate with Ph.D. in bioengineering at OU.

Many thanks also go to my team members in the Biomedical Engineering lab at OU. Chenkai Dai helped me harvest middle ear tissues and assisted me in the experiments.

Don Nakmali helped me prepare specimens and provided technical support to all my experiments. Benny Feng and Dr. Qunli Sun are former lab members who shared their experiences on research projects during my early years in the lab. Dr. Xuelin Wang joined our group one and half years ago and we had a lot of discussions on theoretical analysis of soft tissue properties.

Thanks Professor Hongbing Lu and Dr. Gang Huang from Oklahoma State University for their discussions on my research and providing the digital image correlation software. Without their help, this project would not be finished.

Thanks school of Aerospace and Mechanical Engineering (AME) for providing teaching assistantship and staffs at AME and OUBC, they are Billy Mays, Greg Williams, Margaret Phillips, Suzi Skinner, Lawana Cavins, Vicki Pollock, Debbie Mattax, and Donna King, for their help and assistances during my study at OU.

Outside the academic community, I shared my tears and laughs over this dissertation with my family members. There is no word to express my appreciation to my parents and parents-in-law for their understanding and endless love. I would like to thank my sisters and brothers-in-law for their encouragement and support. I am greatly indebted to my wife, Jessica G. Guo, for her unconditional support and love. I would also like to dedicate this dissertation to my sons, Justin G. Cheng and Derick T. Cheng for the happiness they brought to us since they were born.

This research is supported by NIH/NIDCD R01DC006632 and NSF/CMS 0510563 Grants. The sincere thanks go to the NIH and NSF.

TABLE OF CONTENTS

	Page
ACKNOWLEDGMENTS	iv
TABLE OF CONTENTS	vi
LIST OF TABLES	ix
LIST OF FIGURES	x
ABSTRACT	xvi
CHAPTER 1 INTRODUCTION	1
1.1 Structures and Functions of Human Ear	1
1.2 Middle Ear Tissues	4
1.2.1 The Tympanic Membrane	4
1.2.2 The Ossicular Chain with Suspensory Ligaments and Tendons ...	5
1.3 Motivations and Objectives	7
1.4 Approaches	9
CHAPTER 2 BACKGROUND	11
2.1 Published Mechanical Properties of Human Tympanic Membrane	11
2.2 Published Mechanical Properties of Middle Ear Ligaments and Tendons ..	19
2.3 Fundamentals of Biomechanics	20
2.3.1 Mechanical Experiments	20
2.3.2 Computational Modeling	22
2.3.2.1 Constitutive Modeling	23
2.3.2.2 Finite Element Method	26
CHAPTER 3 METHODS	31
3.1 Mechanical Experiments	31
3.1.1 Machine Calibration	31
3.1.1.1 Load Cell Calibration	31

3.1.1.2 Correction Coefficient (k) Determination	33
3.1.2 Specimen Preparation	38
3.1.2.1 Tympanic Membrane (TM) Preparation	38
3.1.2.2 Stapedial Tendon Preparation	40
3.1.2.3 Tensor Tympani Tendon Preparation	41
3.1.2.4 Anterior Malleolar Ligament Preparation	43
3.1.3 Experimental Protocols	45
3.1.3.1 Uniaxial Tensile Test	49
3.1.3.2 Stress Relaxation Test	49
3.1.3.3 Failure Test	50
3.2 Digital Image Correlation (DIC) Method	50
3.2.1 DIC Algorithm	51
3.2.1.1 Displacement Mapping	51
3.2.1.2 Bicubic Spline Interpolation	52
3.2.1.3 Least Squares Correlation	52
3.2.2 DIC Implementation for Ear Tissues	53
3.3 Modeling Analysis	56
3.3.1 Analysis on Tympanic Membrane	56
3.3.2 Analysis on Stapedial Tendon	58
3.3.3 Analysis on Tensor Tympani Tendon	59
3.3.4 Analysis on Anterior Malleolar Ligament	62
 CHAPTER 4 RESULTS OF THE TYMPANIC MEMBRANE	 65
4.1 Mechanical Properties of the Tympanic Membrane	65
4.2 Discussion on the Results	76
 CHAPTER 5 RESULTS OF TENDONS AND LIGAMENT	 81
5.1 Stapedial Tendon	81
5.1.1 Mechanical Properties of the Stapedial Tendon	81
5.1.2 Discussion on Stapedial Tendon Results	89
5.2 Tensor Tympani Tendon	90

5.2.1 Mechanical Properties of the Tensor Tympani Tendon	90
5.2.2 Finite Element Modeling Results	96
5.2.3 Discussion on Tensor Tympani Tendon Results	97
5.3 Anterior Malleolar Ligament	99
5.3.1 Mechanical Properties of the Anterior Malleolar Ligament	99
5.3.2 Material Modeling Results	104
5.3.3 Discussion on Anterior Malleolar Ligament Results	106
 CHAPTER 6 SUMMARY AND COMPARISON OF RESULTS	110
6.1 Constitutive Behaviors of Middle Ear Tissues	110
6.2 Young's Modulus-Stress Relationships of Middle Ear Tissues	112
6.3 Stress Relaxation Functions of Middle Ear Tissues	114
6.4 Ultimate Stress and Stretch Ratio of Middle Ear Tissues	115
6.5 Comparison based on Structures and Functions	116
 CHAPTER 7 APPLICATION	118
7.1 Finite Element Model of Human Ear	118
7.2 Finite Element Analysis	120
7.3 Results	121
7.4 Discussion	127
 CHAPTER 8 CONCLUSIONS AND FUTURE WORK	128
8.1 Conclusions	128
8.2 Future Work	130
8.2.1 Age-Related Study	130
8.2.2 Micro-Structural Modeling	130
8.2.3 Dynamic Experiment	131
 REFERENCES	132

LIST OF TABLES

Tables	Page
2.1 Published elastic modulus of the tympanic membrane from experiments ...	17
2.2 Published elastic modulus of the tympanic membrane used for finite element model of human middle ear	18
2.3 Published elastic modulus of three middle ear ligament and tendons used for finite element model of human middle ear	20
3.1 Experimental reading from the load cell on testing weight	34
3.2 Dimensions of stapedial tendon (ST) specimens (N=12)	41
3.3 Dimensions of tensor tympani tendon (TTT) specimens (N=10)	43
3.4 Dimensions of anterior malleolar ligament specimens (N=9).....	44
4.1 Ultimate stress and stretch ratio of TM specimens (N=11)	75
5.1 Ultimate stress and stretch of stapedial tendon (ST) specimens	89
5.2 Ultimate stress and stretch of tensor tympani tendon (TTT) specimens	96
5.3 Material constants of tensor tympani tendon obtained from FE models	96
5.4 Ultimate stress and stretch of anterior malleolar ligament (AML) specimens	104
5.5 Material parameters of the hyperelastic model for the AML	104
6.1 The mean initial stress and fully relaxed stress of middle ear tissues	114
6.2 The ultimate stress and stretch ratio of tested middle ear tissues	115
7.1 Young's modulus of middle ear tissues in Gan's model and this study	119

LIST OF FIGURES

Figures	Page
1.1 A schematic diagram of a human ear [Flanagan 1965]	1
1.2 The tympanic membrane of a left human ear (lateral view)	4
1.3 The ossicular chain	5
1.4 A human middle ear model (left ear)	7
2.1 Arrangement for measurement of the elastic coefficient of human eardrum. A calibration hair was used to produce a known bending force on a tongue like piece cut from the eardrum [von Békésy 1949]	12
2.2 Measuring apparatus of Young's modulus of human eardrum [Kirikae 1960]	13
2.3 Stress-length relation of human eardrum [Decraemer 1980]	15
2.4 Line of points where vibration measurements were taken (left). Real and imaginary part of the vibration in the posterior section of the eardrum (right) [Fay et al. 2005]	17
2.5 Preconditioning and stress relaxation of soft tissues [Fung 1993]	21
3.1 Main menu of the material testing system	32
3.2 Calibration menu of the material testing system	33
3.3 (A~G) Experimental load reading by the load cell at different weights	37
3.4 The correction coefficient (k) of the load cell	37
3.5 (A) The left ear TM harvested from a temporal bone with malleus and tympanic annulus attached. The TM strip was cut from the posterior site of the TM near the outer edge. (B) The TM specimen fixed at the mounting fixture along the longitudinal direction. A ruler was attached to the metal holder at the load cell side for dimension measurement	39
3.6 (A) The stapedial tendon harvested from a human temporal bone with the stapes and pyramidal eminence connected. (B) The stapedial tendon specimen fixed at the mounting fixture along the longitudinal direction in a	

material testing system (MTS). A ruler was attached to the metal holder at the load cell side as a reference for dimension measurement	41
3.7 (A) The tensor tympani tendon in middle ear cavity connecting to the malleus head and cochleariform was viewed in a human cadaver temporal bone. (B) The tensor tympani tendon specimen was fixed at the mounting fixture along the longitudinal direction in material testing system (MTS). A ruler was attached to the metal holder at the load cell side as a dimensional reference	42
3.8 The anterior malleolar ligament of the Human Middle Ear with two bony ends (the malleus and roof of epitympanum). A ruler was attached to the metal holder at the load cell side as a dimensional reference	44
3.9 The experimental setup	46
3.10 Preconditioning of the TM specimen	47
3.11 Preconditioning of the stapedial tendon specimen	48
3.12 Preconditioning of the tensor tympani tendon specimen	48
3.13 Preconditioning of the anterior malleolar ligament specimen	49
3.14 Illustration of the digital image correlation (DIC) method for calculating the strain distribution of the TM specimen under the uniaxial loading process	54
3.15 Illustration of the digital image correlation (DIC) method for calculating the strain distribution of the stapedial tendon specimen under the loading process	55
3.16 Illustration of the digital image correlation (DIC) method for calculating the strain distribution of the tensor tympani tendon specimen under the loading process	55
3.17 Illustration of the digital image correlation (DIC) method for calculating the strain distribution of the anterior malleolar ligament specimen under the loading process	56
3.18 (A) SEM picture of the tensor tympani tendon at 3000x magnification. (B~F) Five FE model of the tensor tympani tendon with different collagen fiber-ground substance ratio (k) or fiber density	60

3.19	Microstructure of the anterior malleolar ligament under SEM (5000x)	62
4.1	Stress-stretch ratio curves of three TM specimens obtained from uniaxial tensile tests after preconditioning. The wave-like lines were original stress-stretch ratio curves recorded in MTS. The smooth lines were obtained after the Ogden model fitting process. The hysteresis was seen on each specimen with the unloading curve lower than the loading curve (pointed by arrows) ..	67
4.2	(A, C) Comparison of stress-stretch ratio curves of two TM specimens obtained from the MTS measurement (solid lines) and DIC analysis (broken lines). (B, D) Transverse strain distribution across the TM specimen calculated from DIC analysis at four time steps	69
4.3	(A) Stress-stretch ratio curves of eleven TM specimens under uniaxial loading tests. The stretch ratio λ was around 1.15 and the strain rate was 0.1 mm/sec. (B) The mean value of stress-stretch ratio relationship of eleven TM specimens with standard deviation (S.D.) bars	71
4.4	(A) Young's modulus-stress curves of eleven TM specimens under uniaxial loading tests obtained from three stress ranges: 0~0.1, 0.1~0.3 and 0.3~1 MPa. (B) The mean value of Young's modulus-stress curves of eleven TM specimens with standard deviation (S.D.) bars over three stress ranges as in (A)	73
4.5	Normalized stress relaxation function $G(t)$ of nine TM specimens from stress relaxation tests. The solid line shows the mean value of $G(t)$ with standard deviation (S.D.) bars	75
4.6	Effect of TM thickness on stress-stretch ratio curves and Young's modulus-stress curves. The thickness (h) was changed from 0.03 to 0.05, 0.08 and 0.1 mm	79
5.1	(A) Transverse strain distribution across the tendon specimen calculated from DIC analysis at four time steps. The time interval for each step is 5 sec. (B) Comparison of stress-stretch loading curves of a stapedial tendon specimen obtained from MTS experiment (solid line) and DIC analysis (broken line)	83
5.2	Stress-stretch curves of a stapedial tendon specimen obtained from the	

	uniaxial tensile test. The wave-like lines were the original stress-stretch curve recorded in MTS. The smooth lines were obtained after the Ogden model fitting process. A hysteresis loop was observed for the stapedial tendon	84
5.3	(A) Stress-stretch curves of twelve stapedial tendon (ST) specimens under uniaxial loading processes. The maximum stretch ratio λ was around 1.4 and the displacement rate was 0.01 mm/sec. (B) The mean curve of stress-stretch relationships obtained from twelve stapedial tendon specimens with standard deviation (S.D.) bars	85
5.4	(A) Young's modulus-stress curves of twelve stapedial tendon specimens under uniaxial loading tests. (B) The mean value of Young's modulus-stress curves of twelve stapedial tendon specimens with standard deviation (S.D.) bars	87
5.5	(A) Normalized stress relaxation function $G(t)$ obtained from nine stapedial tendon specimens in stress relaxation tests. (B) The mean curve of $G(t)$ of nine tendon specimens with standard deviation (S.D.) bars	88
5.6	(A) Transverse strain distribution across the tensor tympani tendon specimen calculated from DIC analysis at four time steps. (B) Comparison of the stress-stretch curve of a tensor tympani tendon specimen obtained from DIC analysis (broken line) and MTS measurement (solid line)	91
5.7	(A) Stress-stretch curves of ten tensor tympani tendon specimens under uniaxial loading processes. The maximum stretch ratio λ was around 1.4 and the elongation rate was 0.01 mm/sec. (B) The mean value of stress-stretch relationships of ten tensor tympani tendon specimens with standard deviation (S.D.) bars	92
5.8	(A) Young's modulus-stress curves of ten tensor tympani tendon specimens under uniaxial loading processes. (B) The mean value of Young's modulus-stress curves of ten tensor tympani tendon specimens with standard deviation (S.D.) bars	94
5.9	(A) Normalized stress relaxation functions $G(t)$ of ten tensor tympani tendon specimens from stress relaxation tests. (B) The mean value of $G(t)$ of	

ten tensor tympani tendon specimens with standard deviation (S.D.) bars	95
5.10 Comparison between stress-stretch curves of the tensor tympani tendon obtained from FE models and the mean curve measured from ten tendon specimens in uniaxial tensile tests. The broken lines with symbols representing modeling results from five FE tendon models. The solid line without symbols represents the experimental mean curve	97
5.11 (A) Normal strain distribution across the transverse surface of the AML specimen calculated from DIC analysis at four time steps. The No. of nodes represents 8 locations (from left to right) across the specimen in the middle part of the grid. (B) Comparison of the strain obtained from MTS experiment (broken line) and DIC analysis (solid line)	100
5.12 (A) Stress-stretch curves of nine AML specimens under uniaxial loading processes. The maximum stretch ratio λ was around 1.5 and the displacement rate was 0.01 mm/sec. (B) The mean curve of stress-stretch relationships obtained from nine AML specimens with standard deviation (S.D.) bars	102
5.13 (A) Normalized stress relaxation function $G(t)$ obtained from nine AML specimens in stress relaxation tests. (B) The mean curve of $G(t)$ of nine AML specimens with standard deviation (S.D.) bars	103
5.14 The stress-stretch curve of the AML obtained from modeling analysis and the mean stress-strain curve measured from nine AML specimens in uniaxial tensile tests	105
5.15 The Young's modulus-stress relationship of the AML obtained from the material model. The Young's modulus is linearly increasing with respect to the stress. The values varied from 0.12 to 6.5 MPa when the stress increases from 0 to 0.5 MPa	106
6.1 Stress-stretch relationships of tested middle ear tissues	111
6.2 Young's modulus-stress relationships of tested middle ear tissues	112
6.3 Normalized stress relaxation functions of tested middle ear tissues	114
6.4 (A) Microstructure of the TM under SEM (5000x), (B) Microstructure of the stapedial tendon under SEM (5000x)	117

7.1	A 3-dimensional finite element model of human left ear with outer and middle ear parts	119
7.2	Mean peak-to-peak displacement curves measured at the umbo of the TM under the control and ligament cut sequence: C5→C3→C7→C1. (A) Magnitude; (B) phase angle	122
7.3	Mean peak-to-peak displacement curves measured at the stapes footplate under the control and ligament cut sequence: C5→C3→C7→C1. (A) Magnitude; (B) phase angle	123
7.4	FE model-derived umbo displacement curves under the normal and ligament removal sequence: C5→C3→C7→C1. (A) Magnitude; (B) phase angle	125
7.5	FE model-derived stapes footplate displacement curves under the normal and ligament removal sequence: C5→C3→C7→C1. (A) Magnitude; (B) phase angle	126

ABSTRACT

In this dissertation, mechanical properties of four middle ear tissues: tympanic membrane or eardrum, stapedial tendon, tensor tympani tendon and anterior malleolar ligament, were reported through experimental measurement and modeling analysis. The mechanical experiments with the aid of digital image correlation method were used to measure the stress-strain relationship, stress relaxation function, and ultimate or failure stress and strain of these middle ear tissues. The experimental results were further analyzed by finite element modeling and material modeling analysis with nonlinear hyperelastic models, the Ogden model and the modified Ogden model, to derive constitutive equations of investigated tissues. The viscoelastic properties of four middle ear tissues were reported for the first time in literature.

The geometric information of four middle ear tissues were also obtained through the image measuring technique and listed with statistic significances in Chapter 3. The mechanical properties of these middle ear tissues were then summarized and differences among them were explained based on their micro-structures and functions in Chapter 6.

Mechanical properties of four middle ear tissues were then employed in a published 3-dimensional finite element model of human ear with an accurate geometric configuration to investigate the transfer function of human middle ear in ligament related pathological conditions. The model predicted results were compared with temporal bone experimental data, and a good agreement between modeling results and experimental data were observed.

The major contribution of this study is to provide new and useful data on mechanical properties of middle ear tissues in literature. The results can be used for the theoretical analysis of human middle ear function under the normal or pathological conditions.

CHAPTER 1

INTRODUCTION

1.1 Structures and Functions of Human Ear

The human ear is composed of three parts – the outer ear, the middle ear, and the inner ear, as shown in Fig. 1.1. The outer ear includes the pinna (also called auricle) and the external ear canal. The middle ear mainly includes the tympanic membrane (TM) or eardrum, the ossicular chain (malleus, incus and stapes), ossicular associated ligaments and tendons, and the opening of the auditory tube (eustachian tube). The inner ear includes two principal portions: the vestibular and semicircular canals superoposteriorly and the cochlea inferoanteriorly.

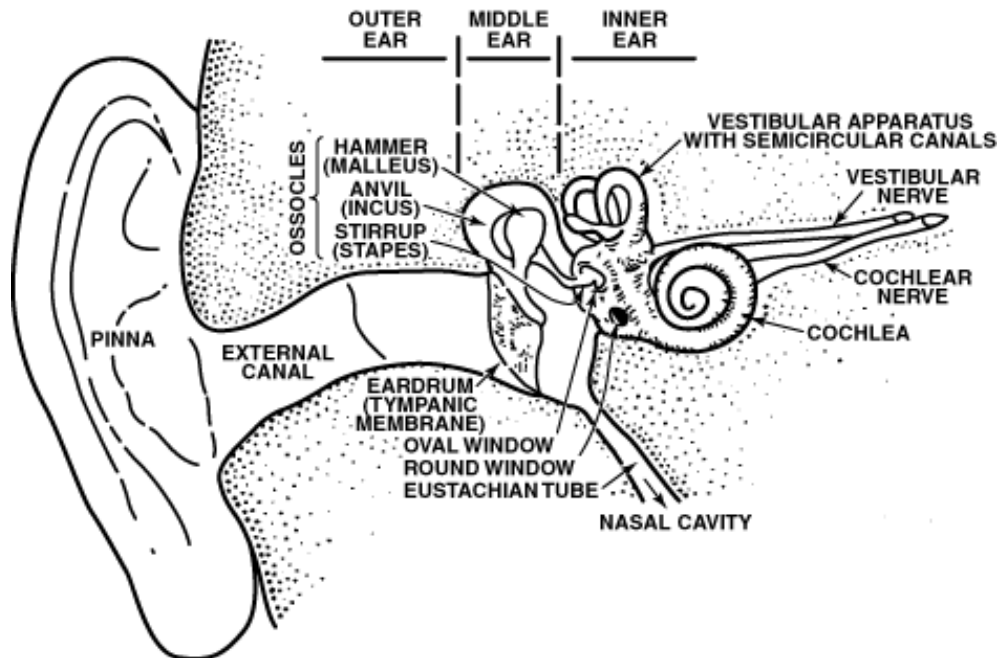


Figure 1.1 A schematic diagram of a human ear [Flanagan, 1965].

The outer ear collects sound waves and transmits vibrations of air into vibrations of the TM in the middle ear. The external ear canal amplifies sound waves with frequencies of approximately 3000 Hz, and the pinna provides protection for the middle ear in order to prevent damage to the eardrum ^[Flanagan, 1965].

The main function of the middle ear is to transform input sound waves into mechanical vibrations through the TM and three ossicular bones (malleus, incus and stapes). The malleus of middle ear has a long process called the manubrium which is attached to the mobile portion of the TM, the incus is the bridge between the malleus and stapes, and the stapes is the smallest named bone in the human body with the footplate contacting to the oval window of inner ear. The movement of the TM induces piston-like vibrations of ossicular bones. When the stapes footplate is pushed to and from the oval window, it causes oscillations of fluid within the cochlea (a portion of the inner ear) ^[Møller, 1974].

The middle ear also works as a lever system. It dampens distance but amplifies force: the amplitude of movement of the stapes footplate with each sound vibration is about 3/4 as much as the amplitude of the handle of the malleus, while the force of movement is increased by about 1.3 times ^[Geisler, 1998]. It can cause about 22 times as much pressure to be exerted on the fluid of the cochlea as is exerted by the sound wave against the TM, due to the force increase mentioned above and the difference between the surface areas of the TM and the stapes footplate ^[Guyton and Hall, 2000]. Therefore, the potential loss of energy caused by the sound wave passing from air into fluid is balanced. Some recent research on the mechanism of ossicular chain also shows that the ossicular chain serves as a

protective mechanism and achieved the optimal impedance for sound transmission through the middle ear [Kelly and Prendergast, 2001].

The middle ear cavity is an air space within the temporal bone which contains the ossicular chain that transmits sound wave from the TM to the inner ear. The cavity communicates with the nasopharynx by the Eustachian tube. The opening to the Eustachian tube lies on the anterior wall of the middle ear cavity. The Eustachian tube is a narrow trumpet-shaped canal, about 25 mm in length, extending from the anterior wall of the middle ear cavity to the lateral wall of the nasopharynx. It opens briefly during swallowing and in that way serves to equalize the air pressure in the middle ear cavity with the outside environment.

The cochlea of inner ear is concerned with hearing. The semicircular canals and the vestibule are the body's horizontal-vertical detectors necessary for balance. The cochlea is filled with liquid (cochlear fluid) and surrounded by rigid bony walls. Its cross-section shows three distinct chambers that run the entire length: the scala vestibuli, the scala tympani and the cochlear duct, or scala media. The basilar membrane separates the scala media from the scala tympani. Resting on the basilar membrane is the delicate and complex organ of Corti that contains several rows of tiny hair cells to which nerve fibers are attached. When the stapes footplate vibrates against the oval window, hydraulic pressure waves are transmitted rapidly down the scala vestibuli, causing the basilar membrane to vibrate up and down. This creates a shearing force between the basilar membrane and the tectorial membrane, causing the hair cell stereocilia to bend back and forth. This leads to internal changes within the hair cells that generate electrical signals. Auditory nerve fibers resting below the hair cells pass these signals on to the brain. The

impulse rate on the auditory nerve depends on both the intensity and frequency of the sound [Rossing, 1990; Wever & Lawrence, 1954; Anson & Donaldson, 1981]

1.2 Middle Ear Tissues

1.2.1 The Tympanic Membrane

The tympanic membrane (TM), also known as the eardrum, has an irregularly oval and conical shape, consisting of the pars tensa (lower major part) and the pars flaccida (upper small portion), as shown in Fig. 1.2. The apex of the cone is called umbo. Umbo is where the end of long process of malleus is connected. The diameter of the TM along the long process is approximately 9.0 to 10.2 mm, while the diameter perpendicular to the long process has a length about 8.5 to 9.0 mm [Donaldson *et al.*, 1992]. The angle formed by the TM and the floor of the ear canal is about 55° [Singh, 1980]. The height of the cone is about 2.0 mm, and the thickness of the TM is between 0.05 and 0.1 mm [Helmholtz, 1874 and Kirikae, 1960]. The surface area of the whole TM is $55.8 - 85.0 \text{ mm}^2$ [Wever & Lawrence, 1954 and von Békésy, 1949].

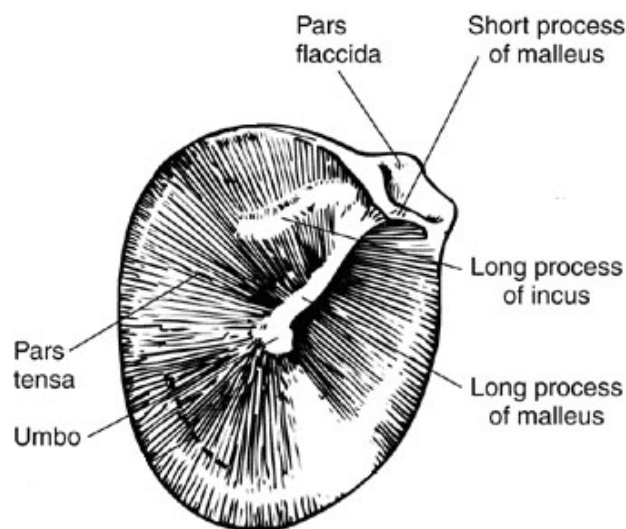


Figure 1.2 The tympanic membrane of a left human ear (lateral view).

The TM is a multi-layers fibrous connective tissue stretched across the ear canal [Wood, 1998], with two layers of fibers along the radial and circumferential directions in the pars tensa part [Lim, 1968 & 1970]. These two sets of fibers represent a majority of the stiff fibers appearing in the eardrum. The margin of the circumference of the membrane is a thickened fibrocartilaginous ring, which is called the tympanic annulus. The tympanic annulus is lacking superior to the short process of the malleus, thus it is incomplete [Singh, 1980].

1.2.2 The Ossicular Chain with Suspensory Ligaments and Tendons

The ossicular chain, which consists of three small bones (malleus, incus and stapes) as shown in Fig. 1.3, with suspensory ligaments or tendons (not shown) connecting to middle ear cavity wall, transmits sound energy from the TM to the oval window

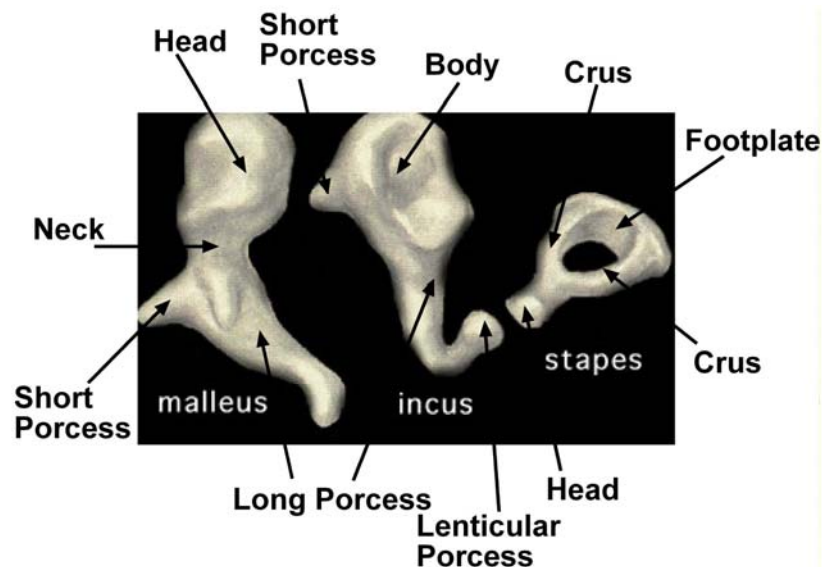


Figure 1.3 The ossicular chain.

The malleus is the bone on the lateral end of the ossicular chain. It has a head, neck, short process (lateral process) and long process. The malleus is held in place by three

middle ear ligaments (the anterior malleolar ligament, the lateral malleus ligament, and the superior malleus ligament) ^[Møller, 1974], one articulation (the incudomalleal joint), one middle ear tendon (the tensor tympani tendon) and the TM. The head is the largest part of the malleus. It articulates posteriorly with the incus. The head is attached to the roof of the middle ear cavity by the superior malleus ligament. The narrow part below the head is known as the neck. The short process and the long process are below the neck. The end of the short process serves as a point of attachment to the pars tensa of the tympanic membrane. The end of the long process is connected to the umbo of the tympanic membrane.

The incus is the biggest ossicle in the ossicular chain, linking the malleus and the stapes. It has a body, short process, long process and lenticular process. The short process points posteriorly. The long process lies approximately parallel to the manubrium and ends in the lenticular process. The end of the lenticular process connects with the head of stapes through the incudostapedial joint. The incus is held in place by two middle ear ligaments: the posterior incus ligament, which secures the short process to the posterior incudal recess, and the superior incus ligament ^[Møller, 1974].

The stapes is located at the medial end of the ossicular chain, and sits on the oval window of the inner ear. It is a stirrup-shaped bone consisting of a head, two crura and a base (footplate). The head is directed laterally and articulates with the lenticular process of incus. The stapedial muscle tendon is attached to the posterior crus. The footplate of the stapes is attached to the oval window by the annular ligament, or stapedial annulus. The size of the footplate varies individually. The length usually ranges from 2.64 to 3.36 mm, while the width from 0.7 to 1.66 mm ^[Wever and Lawrence, 1954].

The locations and relations of middle ear tissues mentioned above are shown in a middle ear model (Fig. 1.4).

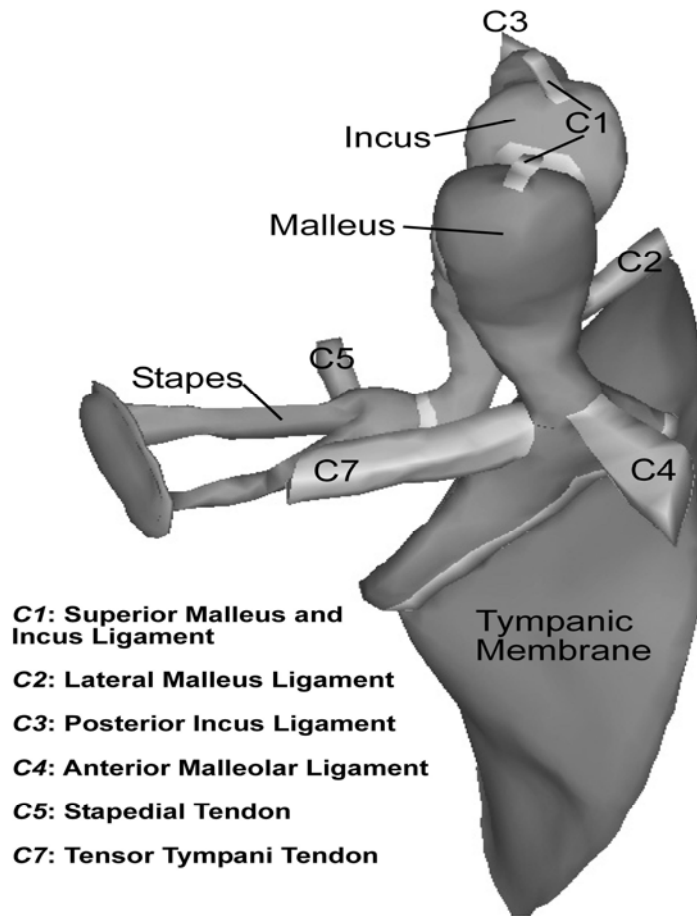


Figure 1.4 A human middle ear model (left ear).

1.3 Motivations and Objectives

Hearing loss is one of the common sensory impairments for people all over the world. According to the investigation by National Institute of Deafness and Communication Disorders (NIDCD), there are 28 million people with hearing loss in the United States. Hearing loss can be categorized as conductive hearing loss and sensorineural hearing loss. Conductive hearing loss is mainly due to the dysfunction of middle ear, such as trauma,

congenital abnormalities, otosclerosis, and most commonly, otitis media. The structures and properties of middle ear components are altered by these diseases, such as TM perforation, TM stiffening, and ligament calcification or detachment, etc. Therefore, understanding the relationship between the properties and functions of middle ear tissues is a fundamental hearing research which has not been well studied by researchers. Knowledge on mechanical properties of normal and pathological middle ear tissues, especially the TM and middle ear ligaments and tendons, is still poor and remains to be investigated. This study is proposed to derive mechanical properties of several middle ear tissues which are not available in literature. The motivations of this research are listed as follows:

- (1) Mechanical response of the TM to the sound stimulus from the ear canal initiates the transfer function of the middle ear ^[Funnel, 1982], which directly depends on the structure and properties of the TM. Unfortunately, there are not many data on viscoelastic properties of the TM in literature.
- (2) Studies have shown that middle ear ligaments and tendons are involved in normal function of the whole middle ear system, such as stapedial reflex which protects the inner ear against hazardous levels of noise ^[Love, 1978] and improves intelligibility of speech in the presence of background noise ^[Gauss, 1997]. However, no experimentally measured mechanical properties of middle ear ligaments and tendons are available in literature.
- (3) Mathematical models or numerical finite element (FE) models of human middle ear have been widely used for the study of middle ear function by researchers ^{[Wada, 1992; Beer, 1996; William, 1997; Prendergast, 1999; Ferris, 2000; Koike, 2002; Sun, 2002; Gan, 2002; Kelly, 2003;}

Ferrazzini, 2003 and Gan, 2004]. These models require geometry of middle ear components and mechanical properties of ear tissues. To the date, material properties of most middle ear tissues are obtained through cross-calibration process or assumption.

Based on the motivations proposed above, the objectives of this research are defined below:

- (1) Determine viscoelastic properties of the TM which are still not clear in literature.
- (2) Determine viscoelastic properties of three middle ear ligament and tendons (anterior malleolar ligament, stapedial tendon and tensor tympani tendon) which have never been published before.
- (3) Apply measured mechanical properties of middle ear tissues (TM and three middle ear ligament and tendons) into a finite element (FE) human ear model to study middle ear function through FE modeling analysis.
- (4) Upon finishing this study, a practical method which combines experimental measurement and theoretical analysis for deriving mechanical properties of middle ear tissues is developed, and the method is expected to be extended to the study of other soft tissues in tissue biomechanics.

1.4 Approaches

To incorporate mechanical experiments with the theoretical modeling analysis to determine mechanical properties of middle ear tissues, five approaches are listed here:

1. Three mechanical experiments are performed to measure viscoelastic properties of middle ear tissues: uniaxial tensile test; stress relaxation test and failure test.

The digital image correlation method is used to verify boundary effects on

experiments by computing the transverse strain distribution across the specimen and the average strain in the middle portion of the specimen during the uniaxial loading process.

2. Theoretical modeling analysis including material modeling and FE modeling are used to study constitutive behaviors of middle ear tissues during the loading process of uniaxial tensile test. To achieve this, microstructures of middle ear tissues are obtained first through the scanning electron microscopy (SEM). A nonlinear hyperelastic material model, the Ogden model or the modified Ogden model, is then used in FE modeling analysis or material modeling analysis to study the constitutive behavior of the tissue. The stress-strain relationships from the modeling are finally regressed with experimental data to derive the constitutive equation of the tissue.
3. Mechanical properties of the middle ear tissues are summarized and compared. The differences among those tissues are addressed and correlated to their structure and functions.
4. The mechanical properties of middle ear tissues obtained from this study are used in a published 3-dimensional FE human ear model to predict the transfer function of middle ear in the normal and middle ear ligament related pathological conditions.
5. The conclusions and future work are proposed at the end of this dissertation.

CHAPTER 2

BACKGROUND

2.1 Published Mechanical Properties of Human Tympanic Membrane

To date, there are four groups who published mechanical properties of the TM with different measurement methods and different results. A summary of their works is given in this section.

(1) In 1949, von Békésy ^[von Békésy, 1949] first measured the stiffness of the human cadaver TM from the bending test. He assumed that the eardrum of man had a thickness of about 0.05 mm (in the literature the value of 0.1 mm is often quoted) and was an unstretched membrane. For measurement of the natural elasticity of this membrane, a rectangle TM sample similar to that shown in Fig. 2.1 was cut out from the whole eardrum. The left side of the rectangle was left connected to the main part of the eardrum. The length of a hair was adjusted on a balance so that by pressing it down a maximum load of $L=1.96 \times 10^{-6}$ N was exerted. When this load was applied to the free end of the flap a displacement of $f = 5 \times 10^{-3}$ cm resulted. From the length of the strip $l = 0.2$ cm, the width $b = 5 \times 10^{-2}$ cm, and the thickness $h = 5 \times 10^{-3}$ cm, it is possible to calculate the elasticity coefficient E by means of the well-known formula

$$E = 4L / fb \times (l/h)^3 \quad (2.1)$$

The value obtained for this elasticity was $E = 2.0 \times 10^8$ dynes / cm², or 20 MPa.

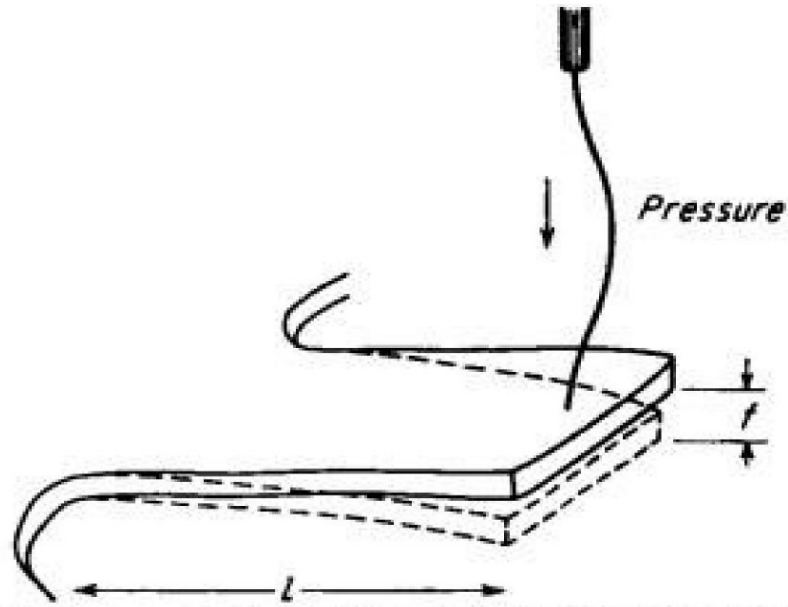


Figure 2.1 Arrangement for measurement of the elastic coefficient of human eardrum. A calibration hair was used to produce a known bending force on a tongue like piece cut from the eardrum [von Békésy, 1949].

(2) In 1960, Kirikae ^[Kirikae, 1960] measured the Young's modulus of a rectangular strip of fresh TM (length $l=10$ mm, width $b=1.5$ mm, thickness $h=0.075$ mm, and cross section area $\sigma = 1.25 \times 10^{-3} \text{ cm}^2$) excised from a male cadaver through the tension test. The TM strip was attached vertically to a horizontal vibrator (A) and stretched by a mass (M) as shown in Fig. 2.2. The vibrating frequency of A was 890 cycles / second (ν_0) in the experiment under reference. When the TM specimen (S) was attached to the A, the vibrating frequency changes to $\nu_0 + \Delta\nu_0$. A mass (m) was placed on the vibrator to change the vibrating frequency back into ν_0 . M was 300 mg and m was 18 mg. The Young's modulus of the TM is then calculated by the following formula:

$$E = (l \cdot w^2 \cdot m \cdot M) / (\sigma(M + m)) \quad (2.2)$$

where w is the natural angular velocity of the vibrator A, or $2\pi\nu_0$ ($\nu_0=890$ cycles / second).

By $M \gg m$

$$E \approx (l \cdot w^2 \cdot m) / \sigma \quad (2.3)$$

A Young's modulus of 40 MPa was calculated based on the thickness of the TM at 0.075 mm. Taking the thickness at 0.05 mm, as von Békésy did, would have resulted in a modulus of 60 MPa. These values are two or three times stiffer than von Békésy's (20 MPa). Kirikae reported that the difference in values between his and Békésy's seemed to be due to different experimental methods embracing both dynamical and static measurements.

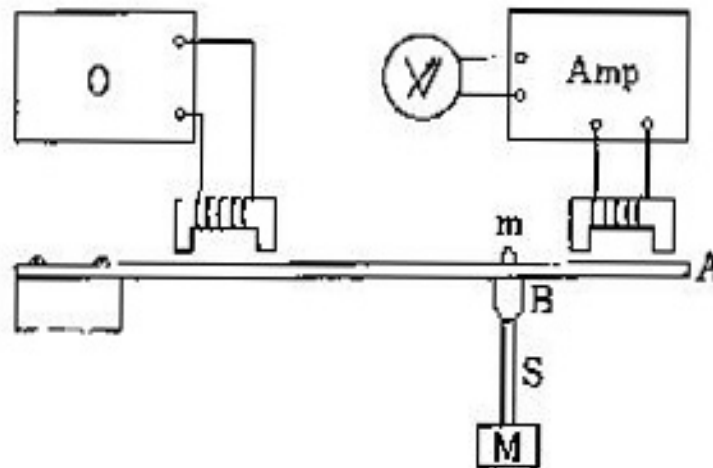


Fig. 2.2 Measuring apparatus of Young's modulus of human eardrum [Kirikae, 1960].

A: vibrator;
 S: test material or the TM specimen;
 M: a mass stretching the test material;
 m: a mass that makes no frequency difference of the vibrator before and after the test material is applied.

(3) In 1980, Decraemer ^[Decraemer, 1980] proposed a mechanical model to describe the “quasi-elastic” stress-strain relation for soft biological tissues based upon their fiber structured design. His model was based on three features:

- The specimen contained a large number (N) of fibers.
- Each fiber was assumed to be purely elastic (Young's modulus k) and was attributed the same average cross-section area S .
- The initial lengths l_i of these fibers were normally distributed around a mean value μ with a standard deviation s .

According to their initial length l_i , the fibers were more or less stretched when the total specimen (initial length l_0) was extended up to a length l . The corresponding elastic constitutive equation was proposed as

$$\sigma(l) = \frac{b}{\sqrt{2\pi}s} \int_{l_0}^l \frac{(l-l_i)}{l_i} e^{-(\mu-l_i)^2/2s^2} dl_i \quad (2.4)$$

where l is the extended length of specimen, b represents an effective Young's modulus of the specimen which equals $(NS/A)k$, and A is the cross-section area of the strip at rest. The "intensity" function $e^{-(\mu-l_i)^2/2s^2}$ differs only significantly from zero in the l_i interval $[\mu - (\text{a few times } s), \mu + (\text{a few times } s)]$. Therefore, one can approximate in the integral the factor $(l-l_i)/l_i$ by $(l-l_i)/\mu$. Splitting up the integral of equation (2.4) gives

$$\sigma(l) = \frac{b}{\sqrt{2\pi}s} \frac{l}{\mu} \int_{l_0}^l e^{-(\mu-l_i)^2/2s^2} dl_i - \frac{b}{\mu} \frac{1}{\sqrt{2\pi}s} \int_{l_0}^l l_i e^{-(\mu-l_i)^2/2s^2} dl_i \quad (2.5)$$

For values of $l > \mu + (\text{a few times } s)$ and the chosen value for l_0 (as $\mu - 4s$), the first term approaches $(bl)/\mu$, while the second approaches b . This means that the $\sigma(l)$ relation for large l values becomes linear

$$\sigma(l) \approx \frac{b}{\mu} l - b \quad \text{for } l > \mu + (\text{a few times } s) . \quad (2.6)$$

The model parameters (b, μ, s) were calculated to fit the experimental data (Fig. 2.3) of an uniaxial tensile test on a specimen of fresh human TM. The values for parameters $(b, \mu,$

s) derived numerically were in good accordance with experiments, therefore, a Young's modulus (b) of 23 MPa was obtained for the TM, which was in agreement with von Békésy's 20 MPa.

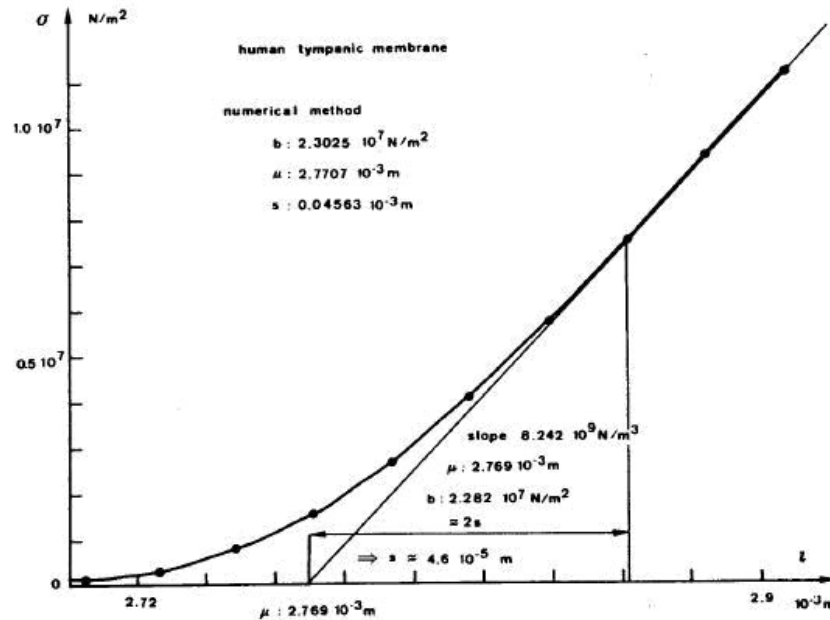


Figure 2.3 Stress-length relation of human eardrum [Decraemer, 1980].

(4) In 2005, Fay *et al.* [Fay *et al.*, 2005] proposed three approaches to estimate the elastic modulus of the TM. First, constitutive modeling was used to estimate an elastic modulus based on the known elastic modulus of collagen and experimentally observed fiber densities of the TM. From the stained cross-sections, the fibril density in the human TM appears to be 30-50%, this leads to an elastic modulus for a given fiber between 870 and 1450 MPa. The radial fiber packing near the outer edge of the TM is between 30% and 70%. Combining this with the estimate of the single fiber puts the fiber layer's elastic modulus at 260 – 1020 MPa in human TM. These values are much higher than the

previous data from von Békésy (20 MPa), Kirikae (40 MPa) and Decraemer (23 MPa). Fay explained this difference was probably due to the assumption in previous study that the TM was isotropic and uniform through its thickness.

Second, the experimental tension and bending test results of TM from literature ^[von Békésy, 1949; Kirikae, 1960; Decraemer, 1980] were re-interpreted using composite laminate theory (CLT). The idea is to build up a membrane's global properties by integrating the material properties through the thickness in an appropriate manner. (see ^[Tsai and Hahn, 1980] for a detailed explanation of CLT). The TM was assumed to be a four-layer composite. A required input to the composite model is the percentage of the total thickness taken up by each layer. By using 0.022 mm for the radial fiber layer and 0.015 mm for the circumferential fiber layer, the elastic modulus of the fiber layers in human TM is between 140 and 1430 MPa from re-interpreting von Békésy's bending test results, between 100 and 270 MPa from Kirikae's results, and between 60 and 160 MPa from Decraemer's results. All of them are higher than the previous data.

Third, dynamic measurements are used in conjunction with a composite shell model to estimate the material parameters. In this approach, the TM was acoustically driven with a tone generator, and the surface displacement was measured as a function of frequency at 58 locations along a line from the posterior to the anterior section of the TM (Fig. 2.4). The displacement pattern on TM has a wave-like appearance. The experimental wave number (by Spatial Fourier transforms) vs. frequency relationships were then found and compared with those computed from a composite shell model of the TM. By using isotropic fiber layer TM model, an elastic modulus of 30-90 MPa was suggested for the human TM, while by using orthotropic TM model, the results suggested that the elastic

modulus lied in the range of 100-400 MPa. The values from this approach are significantly higher than previous results.

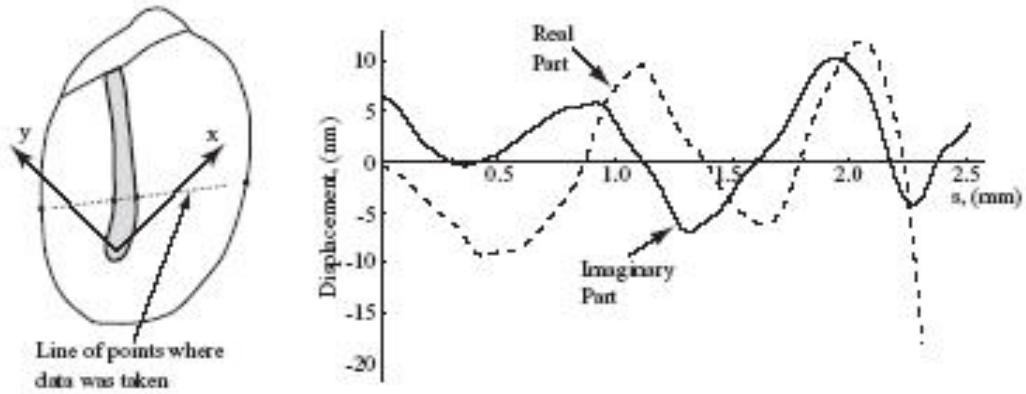


Figure 2.4 Line of points where vibration measurements were taken (left). Real and imaginary part of the vibration in the posterior section of the eardrum (right) [Fay *et al.*, 2005].

Table 2.1 summarizes the elastic modulus of the human TM published by above four groups. No conclusion can be made at this point on the final elastic modulus of the TM.

Table 2.1: Published elastic modulus of the tympanic membrane from experiments

Reference	Test type	Estimate modulus (MPa)
von Békésy (1949)	Bending	20
Kirikae (1960)	Dynamic Tension	40
Decraemer et. al. (1980)	Tension and Modeling	23
Fay et. al. (2005)	Dynamic Vibration	100 - 400

Comparing those published elastic moduli of the TM, one can see that the values vary from 20 to 400 MPa, and there is a lack of measurement or modeling on the viscoelastic behavior of the TM. Particularly, there is no description on variation of the elastic modulus of the TM with respect to the stress or strain at low stress levels from 0 to 1

MPa in previous works. The deficiency in knowledge about mechanical properties of the TM at the physiological condition not only affects understanding of middle ear mechanics for sound transmission or reconstruction of the TM (tympanoplasts), but also impedes development of finite element (FE) ear models for theoretical analysis of the middle ear transfer function.

In all published FE models of human ear, [Wada, 1992; Beer, 1996; William, 1997; Prendergast, 1999; Ferris, 2000; Koike, 2002; Sun, 2002; Gan, 2002; Kelly, 2003; Ferrazzini, 2003 and Gan, 2004], mechanical properties of the TM were either selected from limited published data or determined through the cross-calibration process. A single elastic modulus independent to the stress level was used by different FE modelers. These modulus values are summarized in Table 2.2. The accuracy of mechanical properties of the TM directly affects FE model-predicted results and limits medical applications of the model for normal and pathological ears.

Table 2.2: Published elastic modulus of the tympanic membrane used for finite element model of human middle ear

Reference	Elastic Modulus (MPa) Tympanic Membrane (TM)
Wada <i>et al.</i> (1992)	33.4
Beer <i>et al.</i> (1996)	32, 20
William <i>et al.</i> (1997)	50
Prendergast <i>et al.</i> (1999)	40, 20
Ferris <i>et al.</i> (2000)	40, 10
Koike <i>et al.</i> (2002)	33.4
Sun <i>et al.</i> (2002)	32, 20

Gan <i>et al.</i> (2002)	35, 20
Kelly <i>et al.</i> (2003)	40, 20
Ferrazzini (2003)	4, 1
Gan <i>et al.</i> (2004)	35, 20

Note: The first number in the TM column represents the pars tensa, the second number represents the pars flaccida, and single numbers represent one value for both pars tensa and pars flaccida.

2.2 Published Mechanical Properties of Middle Ear Ligaments and Tendons

Measurements on mechanical properties of human middle ear ligaments and tendons have never been reported. In published FE models of human ear, mechanical properties of middle ear ligaments and tendons were assumed through the cross-calibration process and a constant elastic modulus was normally used for the specific ligament or tendon in different FE models [Wada, 1992; Prendergast, 1999; Ferris, 2000; Koike, 2002; Sun, 2002; Gan, 2002; Kelly, 2003; Ferrazzini, 2003 and Gan, 2004]. These values are listed in Table 2.3. It is observed that a single value varying from 0.52 to 52 MPa was used for the stapedial tendon, from 2 to 70 MPa for the tensor tympani tendon, and from 2 to 21 MPa for the anterior malleolar ligament. The accuracy of mechanical properties of the ligaments and tendons used in FE modeling definitely affects model-predicted results and the applications of the model.

Table 2.3: Published elastic modulus of three middle ear ligament and tendons used for finite element model of human middle ear

Reference	Elastic Modulus (MPa)		
	<i>Stapedial Tendon</i>	<i>Tensor Tympani Tendon</i>	<i>Anterior Malleolar Ligament</i>
Wada <i>et al.</i> (1992)	0.52	2.6	21
Prendergast <i>et al.</i> (1999)	0.52	2.6	21
Ferris <i>et al.</i> (2000)	0.52	2.6	21
Koike <i>et al.</i> (2002)	0.52	2.6	21
Sun <i>et al.</i> (2002)	0.52	2.6	2.1
Gan <i>et al.</i> (2002)	0.52	2.6	2.1
Kelly <i>et al.</i> (2003)	0.52	2.6	21
Ferrazzini (2003)	6	2	2
Gan <i>et al.</i> (2004)	52	70	21

2.3 Fundamentals of Biomechanics

2.3.1 Mechanical Experiments

From the point of view of biomechanics, the properties of a tissue are known if its constitutive equation is known. The constitutive equation of a material can only be determined by experiments. A variety of mechanical tests has been reported to measure properties of soft tissues, such as uniaxial tensile [Fung, 1967], strip biaxial tension [Lanir, 1974], and shear tests [Gardiner, 2001]. Among them, the uniaxial tensile test is commonly used to characterize one-dimensional tensile properties of ligament tissues [Weiss, 2001] and was employed in this study to derive properties of middle ear tissues. For this purpose, a targeted specimen of rectangular shape was prepared and stretched in a testing machine.

The load and elongation were recorded for prescribing loading or stretching histories. From these records we can deduce the stress-strain relationship of the material under the uniaxial loading process.

It was emphasized by Fung in his “Biomechanics: Mechanical Properties of Living Tissues” book [Fung, 1993] that if a segment of a soft tissue was excised and tested in a tensile testing machine by imposing a cyclically varying strain, the stress response would show a hysteresis loop with each cycle, but the loop decreased with succeeding cycles, rapidly at first, then tending to a steady state after a number of cycles (Fig. 2.5 A). The existence of such an initial period of adjustment after a large disturbance seems common to all tissues and this process is defined as *preconditioning* [Fung, 1993]. The preconditioning is due to the change of the internal structure of the tissue, and only mechanical data of preconditioned specimens are presented in biomechanics.

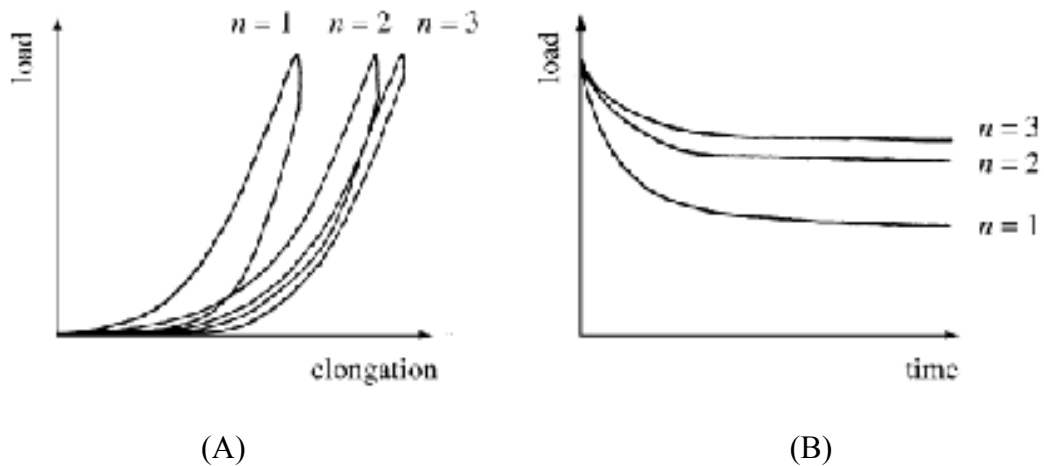


Figure 2.5 Preconditioning and stress relaxation of soft tissues [Fung, 1993].

Soft tissues usually show viscoelastic behavior in their physiological function range [Fung, 1993]. The features of hysteresis, relaxation and creep of tissues at low stress ranges

(“physiological”) are usually used to describe viscoelastic properties of materials. Figure 2.5 B shows typical stress relaxation curves of soft tissues. A step function of elongation was applied to the specimen at the beginning ($t=0$) with a constant displacement rate until a stretch was obtained. The length of the specimen was then held fixed and the change of tension with time was plotted. In this study, the hysteresis from the tensile test and stress relaxation function from the relaxation test were used to describe viscoelastic properties of middle ear tissue. Moreover, the strength of tissues can be determined from the failure test.

2.3.2 Computational Modeling

Experimental studies of soft tissue mechanics are often technically difficult, costly, and prone to error. The stress and strain fields within soft tissues are inhomogeneous, yet we are forced to measure these quantities between a small numbers of discrete points and assume they are homogenous. Other quantities such as pressure and contact area are extremely difficult to measure in an experimental setting. Also, parameterized studies require large numbers of animals or significant amounts of human tissues. This often results in prohibitively high costs and time requirements.

The emerging field of computational biomechanics offers a new set of tools for studies of solid and fluid biomechanics that can provide information that would otherwise be difficult or impossible to obtain from experiments. Advances in the fields of constitutive modeling, computational mechanics, numerical methods and computer science have led to the widespread application of numerical procedures for the analysis of mechanical system. For example, the finite element (FE) method has provided a

generalized procedure to analyze the stress/strain response of a structure [Weiss, 2001]. However, for the successful application of the FE method to studies of tissue mechanics, a detailed mathematical description of material behavior of the tissues is necessary. To develop such a material model, referred to in continuum mechanics terminology as a constitutive model, detailed experimental measurements of the material structure and mechanical behavior are needed.

A fundamental knowledge of mechanics is needed to understand the current state of research in computational modeling of soft tissues. Concepts in constitutive modeling and finite element method are briefly introduced in the following sections.

2.3.2.1 Constitutive Modeling

Constitutive equations are used to describe mechanical behaviors of materials through specification of the dependence of stress on kinematic variables such as the deformation gradient, rate of deformation, temperature, and pressure. They can be used to distinguish one material from another but must be defined such that they obey dimensional homogeneity and independence of choice of coordinate system. Constitutive relations must also obey the *Principle of Material Frame Indifference*, which states that constitutive equations must be invariant under changes of observer frame of reference. This principle ensures that rigid body motions will not change the stress in a material. The accurate description and prediction of the mechanical behavior of soft tissues by constitutive equations remains one of the challenges for computational modeling of ligaments and other soft tissues.

Specific steps are generally followed in the development of constitutive relations for a

material. The first step is to observe the material and classify it according to its behavior and composition. Examples of these classifications for a solid would include whether the material is elastic or viscoelastic, isotropic or anisotropic, linear or nonlinear, and homogeneous or heterogeneous. The second step is to choose an appropriate theoretical framework to develop a relationship between kinematic quantities and stress, and hyperelasticity is often utilized in the biomechanics field. The third step is to identify a specific constitutive equation. This step must take advantage of mathematical conditions such as observer independence to derive a relationship based on microstructural observations or experimental data. The fourth step is to perform experiments to determine values for the material parameters. The final step is independent validation of the model's predictive ability.

For an *elastic* material, the stress at any point can be defined solely as a function of the deformation gradient \mathbf{F} at that point. A change in stress arises only in response to a change in configuration, and the material is indifferent to the manner in which the change in configuration arises in space and time. For a *hyperelastic* material, the above definition applies, and in addition there is a scalar function from which the stress can be derived at each point \mathbf{X} . The scalar function is the stored energy or *strain energy function*, W , which can also be defined solely in terms of the deformation gradient:

$$W = \tilde{W}(\mathbf{F}) \quad (2.7)$$

The strain energy, W , must obey the *Principle of Material Frame Indifference*. Consequently, W may be expressed in the form

$$W = \tilde{W}(\mathbf{C}) \quad (2.8)$$

The second Piola-Kirchhoff stress is derived directly from the strain energy as

$$\mathbf{S} = 2 \frac{\partial W}{\partial \mathbf{C}} \quad (2.9)$$

Hyperelasticity provides a convenient framework for the formulation of constitutive equations for biological soft tissues because it allows for large deformations and anisotropy. Material symmetries will restrict the way in which the strain energy depends on \mathbf{C} . Specifically, any orthogonal transformation that is a member of the material symmetry group will leave its strain energy unaltered when applied to the material prior to deformation. For instance, if the material under consideration is *isotropic*, its symmetry group consists of the entire group of proper orthogonal transformations. For an isotropic material, W can depend on \mathbf{C} through only the three principle invariants of \mathbf{C} :

$$W = W(I_1, I_2, I_3) \quad (2.10)$$

where

$$I_1 = \text{tr } \mathbf{C}, I_2 = \frac{1}{2} [(\text{tr } \mathbf{C})^2 - \text{tr } \mathbf{C}^2], I_3 = \det \mathbf{C} \quad (2.11)$$

and “tr” denotes the trace of the tensor. The isotropic hyperelastic material reduces to linearized elasticity when appropriate assumptions regarding the magnitude of strains and rotations are made.

In literature, there are several hyperelastic constitutive models available for the modeling of isotropic materials, such as the Neo-Hookean, Mooney-Rivlin, Polynomial Form, Ogden Potential, Arruda-Boyce, Gent, and Yeoh models. Among them, the Ogden, Mooney-Rivlin and Yeoh models have been used to explain the stress–strain behavior of biological soft tissues, such as the skin, muscle and brain tissue, and the Ogden model was found more valid and useful for studying rubber-like biological soft tissue ^[Miller, 2002; Sarma, 2003 and Wu, 2003]. The strain energy potential of the Ogden model is given below:

$$\text{Ogden Potential Model: } W = \sum_{i=1}^N \frac{\mu_i}{\alpha_i} (\bar{\lambda}_1^{\alpha_i} + \bar{\lambda}_2^{\alpha_i} + \bar{\lambda}_3^{\alpha_i} - 3) + \sum_{k=1}^N \frac{1}{d_k} (J - 1)^{2k} \quad (2.12)$$

where:

N = material constant

μ_i, α_i, d_k = material constants

$\bar{\lambda}_i$'s ($i= 1, 2, 3$) are deviatoric principal stretches and $\bar{\lambda}_i = J^{-1/3} \lambda_i$, with λ_i 's being principal stretches and J the Jacobian determinant of the deformation gradient. The initial shear modulus, G , is given as

$$G = \frac{1}{2} \sum_{i=1}^N \alpha_i \mu_i \quad (2.13)$$

For an incompressible isotropic material ($J = \lambda_1 \lambda_2 \lambda_3 = 1$) in the uniaxial stress state, the first-order Ogden potential can be rewritten as

$$U = \frac{2\mu_1}{\alpha_1^2} (\lambda^{\alpha_1} + 2\lambda^{-0.5\alpha_1} - 3) \quad (2.14)$$

In this study, the non-linear hyperelastic model, the Ogden model (Eq. (2.14)), will be used to derive the constitutive equations of human middle ear tissues. The material parameters (μ_1 and α_1 in this study) of the Ogden model will be determined through the cross-correlation process between material modeling results and experimentally obtained stress-strain data of ear tissues.

2.3.2.2 Finite Element Method

Due to inhomogeneous material properties, complex three-dimensional geometry, and unique boundary/initial conditions such as in situ stress or residual stress of biological tissues, it is often difficult to combine the equations of motion with an appropriate

constitutive law to obtain closed-form mathematical solutions of the tissue. In that case, numerical solution techniques should be considered. The finite element (FE) method provides a powerful and commonly used methodology for the solution of complex problems in nonlinear solid and fluid biomechanics. In the FE method, a body is discretized into small finite elements of material volume, for which the material and physical properties are known. The appropriate boundary conditions and initial conditions, including applied loading and displacements, must also be specified for the forward problem to be well posed. The solution procedure involves the consideration of overall energy minimization and/or other fundamental physical balance laws to determine unknown field variables over the domain. From these variables, the stresses and strains (or other quantities of interest) can be determined throughout the body.

The FE method may be described as an analysis method for discrete systems. The domain of interest is divided into a finite number of discrete elements. A form is assumed for the variation of the unknown functions over each element. Usually a polynomial form is assumed, and these polynomials are defined in terms of other independent variables. In solid mechanics, the unknown variation of displacements over the element is described by these polynomials, referred to as *shape functions*, in terms of the other nodal displacements. These shape functions are called *isoparametric* if they are used to define both the variation of element geometry between nodal points as well as the variation of displacement over the element. The equilibrium equations are cast in integral (weak) form, with the shape functions and nodal displacement values replacing the continuous functions. The requirement of stationarity yields a system of equations that can be assembled element by element. Numerical integration is used to evaluate the integrals for

each element, and the result is a large (often nonlinear) system of simultaneous equations that can be solved for the nodal displacements that satisfy equilibrium.

In summary, steps in the analysis of a discrete system include the idealization of the system, establishment of equilibrium conditions, assemblage of the discrete element system into a set of simultaneous (possibly nonlinear) equations, and solution of these equations to determine the response of the state variables. These steps are the same whether the problem is steady-state or dynamic, linear or nonlinear, and regardless of the initial and boundary conditions. In contrast to other discretization methods, FE method has the ability to treat material inhomogeneities, complex boundary conditions, and complicated geometry in a systematic way.

For nonlinear elasticity, the weak form of the equilibrium equations can be obtained from the potential energy. The potential energy function, Π , is defined as the sum of the strain energy in the material (internal energy) and the energy due to externally applied body forces and surface tractions Π_{ext} . Both sources may be a function of the deformation map \mathbf{f} over the reference configuration \mathbf{R}_0 :

$$\Pi(\mathbf{f}) = \int_{R_0} \{W(\mathbf{X}, \mathbf{C}(\mathbf{f}(\mathbf{X})))\} dV + \Pi_{ext}(\mathbf{f}) \quad (2.15)$$

The first variation of Π with respect to the deformation \mathbf{F} in the direction \mathbf{V} yields the “Euler equations”. In the present case the Euler equations are simply a statement of the equilibrium equations in weak form. If these are transformed to the current configuration, with variations in configuration \mathbf{v} taken with respect to the current configuration:

$$D\Pi \cdot \mathbf{v} = \int_R \mathbf{T} : \nabla \mathbf{v} dV = \int_R \mathbf{b} \cdot \mathbf{v} dV + \int_S \bar{\mathbf{t}} \cdot \mathbf{v} da \quad (2.16)$$

Note that this is equivalent to the virtual work approach. $\mathbf{T} : \nabla \mathbf{v}$ represents the internal stresses, $\mathbf{b} \cdot \mathbf{v}$ is the body force, and $\bar{\mathbf{t}} \cdot \mathbf{v}$ is the surface traction. This equation is in general highly nonlinear.

Two solution procedures are commonly employed at this point. An “explicit time integration” provides the solution to the equations of motion by including all inertial effects and using the central difference method to integrate the equations forward in time. This approach is limited by the Courant stability criterion and requires extremely small time step size. It is appropriate for high-rate and impact problems. The second approach is to linearize the equations (2.16) about a known configuration. After introduction of the FE shape functions, it results in a system of linearized matrix equations:

$$(\mathbf{K}_{NL} + \mathbf{K}_L) \cdot \mathbf{Du} = \mathbf{F}_{ext} - \mathbf{F}_{int} \quad (2.17)$$

where \mathbf{K}_{NL} is the nonlinear stiffness, \mathbf{K}_L is the linear stiffness, \mathbf{Du} is the incremental displacement vector, and \mathbf{F}_{ext} and \mathbf{F}_{int} represent the external and internal forces respectively. This equation provides the starting point for an incremental-iterative solution strategy characterized by the Newton-Raphson method.

In this study, a commercial FEM software, ANSYS v.10.0 (ANSYS Inc., Canonsburg, PA), was employed to perform nonlinear structural analysis on a 3-dimensional FE model of investigated ear tissues. To build a FE model of the tissue, geometric information of the tissue is required, which can be obtained through image measuring techniques on the images taken for the ear tissue. The geometric domain of the tissue was then discretized into an assembly of finite elements.

In FE analysis, nonlinear structural behavior arises from a number of causes, which can be generally grouped into three principal categories: (1) changing status; (2)

geometric nonlinearities; and (3) material nonlinearities. In this study, only the material nonlinearities were considered for the FE analysis of ear tissues. Nonlinear stress-strain relationships of *hyperelastic* materials will cause a structure's stiffness to change at different load levels, which can be implemented in FE analysis by using appropriate pre-defined element types and material models in ANSYS.

There are several forms of strain energy potential associated with nonlinear hyperelastic material models defined in ANSYS, such as Neo-Hookean, Mooney-Rivlin, Polynomial Form, Ogden Potential, Arruda-Boyce, Gent, and Yeoh models. These models will work with following elements: SHELL181, PLANE182, PLANE183, SOLID185, SOLID186 , SOLID187, SOLSH190, SHELL208, and SHELL209. In this study, the Solid 185 element and the Ogden material model were used to calculate the nonlinear stress-strain behavior of middle ear tissues in tensile tests.

The procedure for performing a nonlinear static analysis consists of following tasks:

- Build the model,
- Set solution controls,
- Set additional solution options,
- Apply the loads, solve the analysis,
- Review the results.

Moreover, by using different element types and material models for different components of the tissue model, people can explore relationships between microstructures and properties of the tissue. The interaction between different components of the tissue would be included in the FE modeling analysis to gain insight into properties of the tissue in the microstructure level.

CHAPTER 3

METHODS

3.1 Mechanical Experiments

3.1.1 Machine Calibration

The material testing system (MTS, Model 100R, TestResources Inc.) with the SMT1-2.2 lbs capacity load cell (Interface Inc.) was used in this study to measure mechanical properties of middle ear tissues. Before the test, calibration of the load cell is required. The correction coefficient of the load cell should be determined through the standard weight. The detailed procedures of these two calibration processes are given in this section.

3.1.1.1. Load Cell Calibration

Step 1: Turn on the MTS machine and the computer connected to the machine.

Step 2: Run MtestWR.exe.

Step 3: Click the *CALIBRATE* button (Fig. 3.1) from the Main Menu.

Step 4: Click on *Load* Tab. Input “Ear Tissue” to the *Name*.

Step 5: Click *Clear All* button.

Step 6: Take a zero load reading by clicking *Set Pt*. Enter a load value of zero in the box adjacent to where the *Counts* reading appeared.

Step 7: Connect a standard scale with 50 grams to the load cell and click *Set Pt* and enter the load 0.4905 in the box adjacent the *Counts* reading.

Step 8: Repeat Step 7 with standards at 100, 150 and 300 grams, and enter the load of 0.981, 1.4715 and 2.943 N to the box as shown in Fig. 3.2.

Step 9: Enter the *Range* (10 N) and *Resolution* (1e-006) for the calibrated transducer.

Step 10: Select the *Direction of loading* as *Positive Position* for the tension.

Step 11: Click *Save* to save the calibration to a file named MTESTWR.CAL, residing in the program directory.

Step 12: Click *Exit* to return.

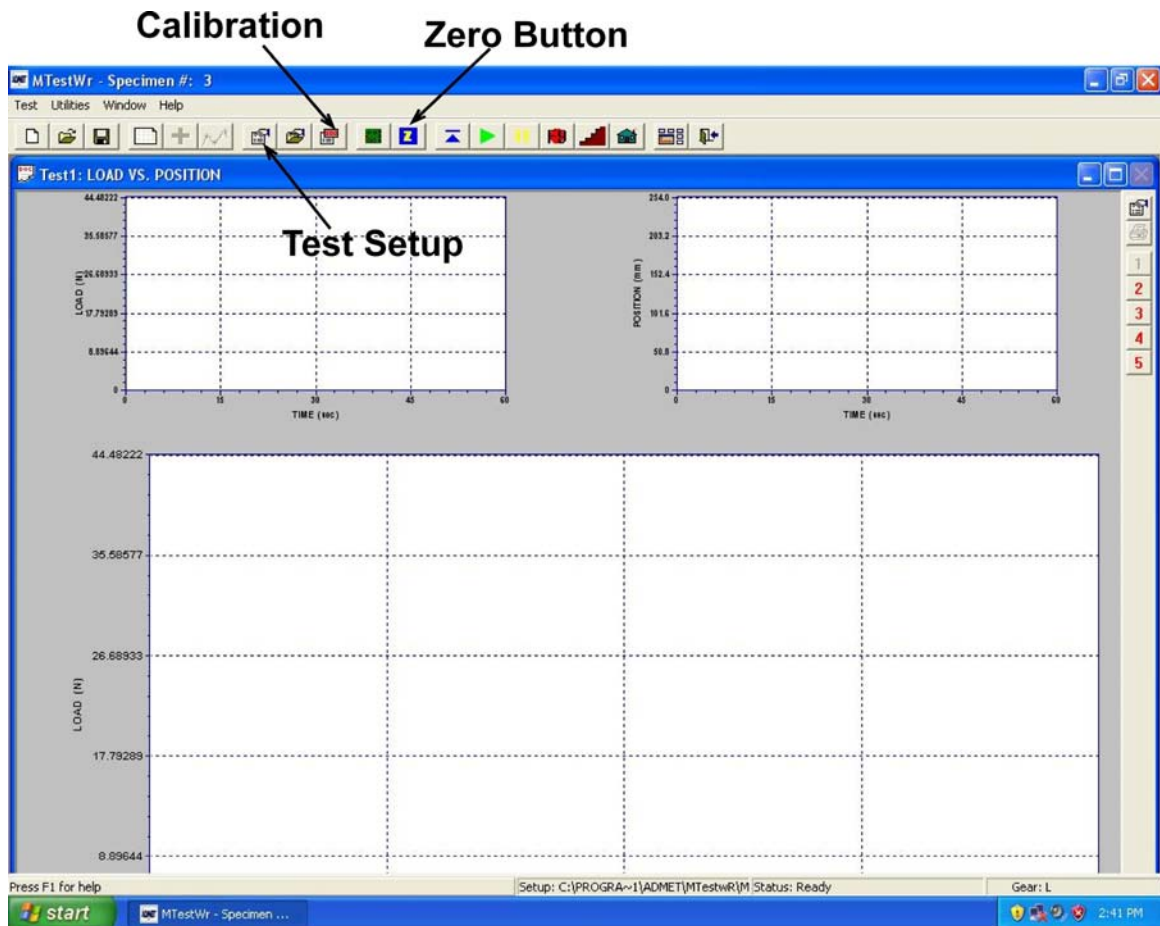


Figure 3.1 Main menu of the material testing system.

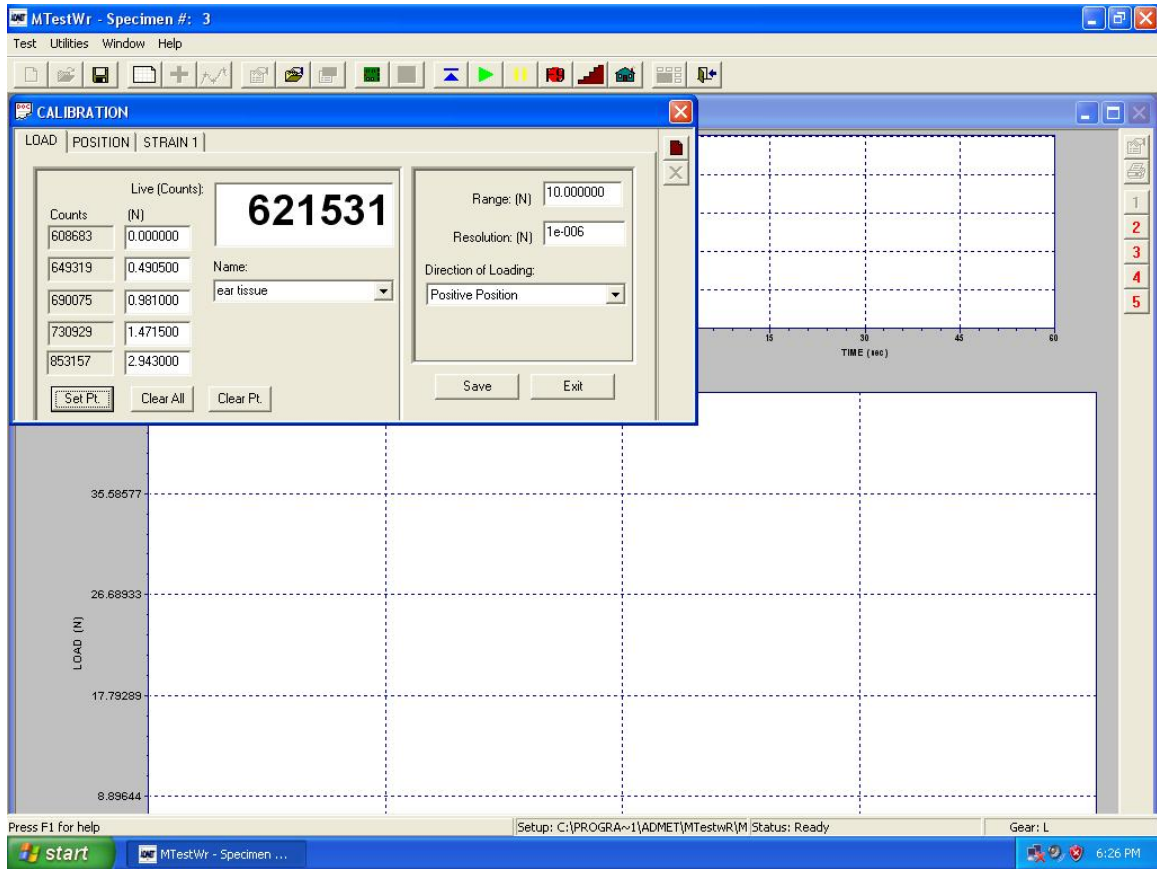


Figure 3.2 Calibration menu of the material testing system.

3.1.1.2. Correction Coefficient (k) Determination

Step 1: Return to the Main Menu.

Step 2: Press the *Zero* button (Z) (shown in Fig. 3.1) to initialize the zero load state.

Step 3: Connect a calibration weight of 1 gram (Denver Instrument Comp.) to the load cell.

Step 4: Record the load reading from the load cell (sampling size ≈ 6000).

Step 5: Save the loading data by the name of “1 gram”.

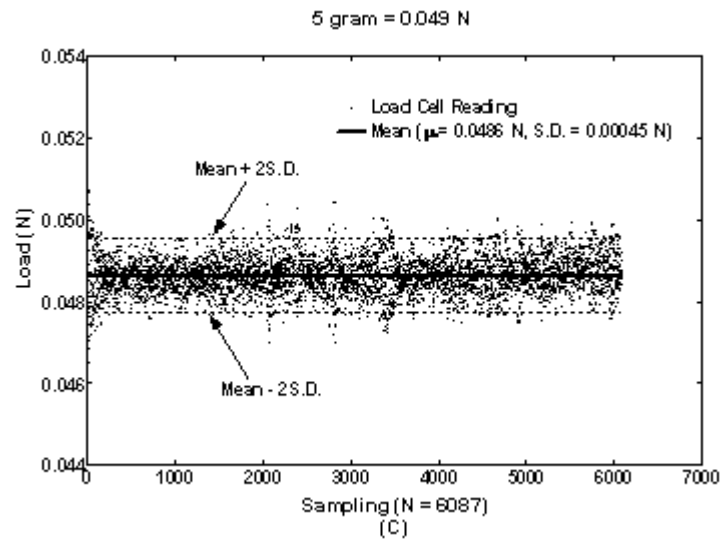
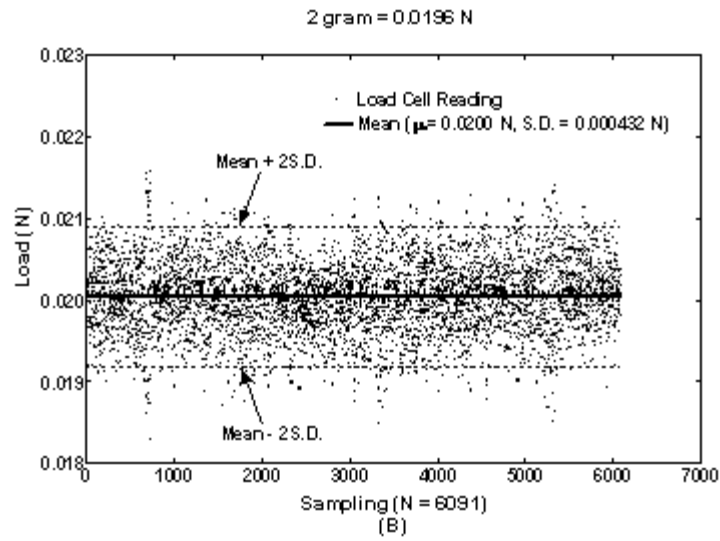
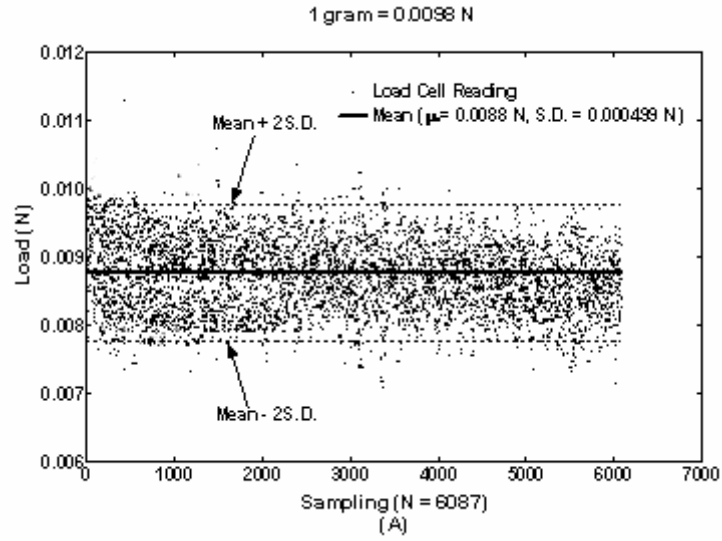
Step 6: Repeat step 4 to 6 with different calibration weights from 2 to 5, 20, 50, 100 and 300 gram and different names.

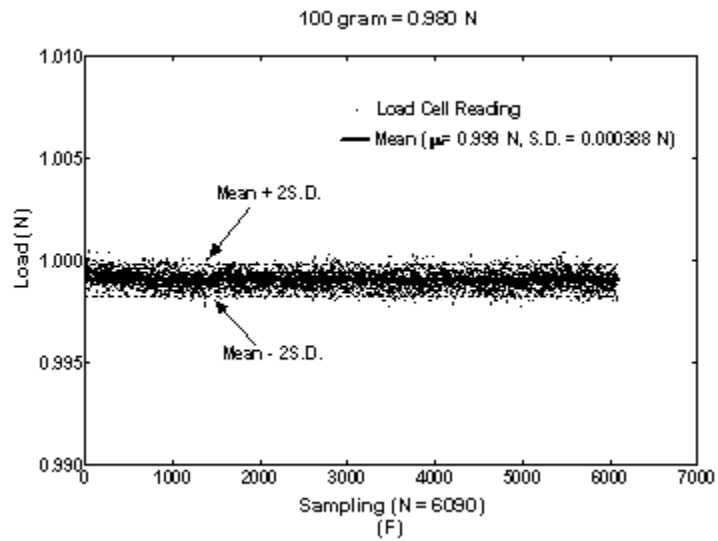
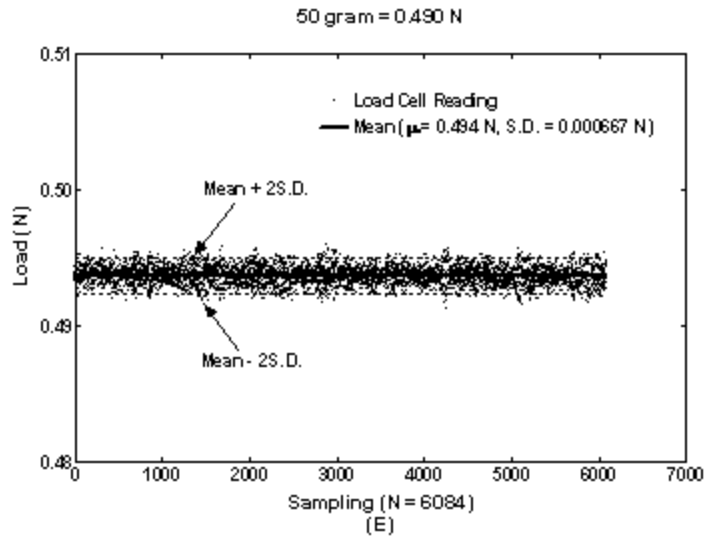
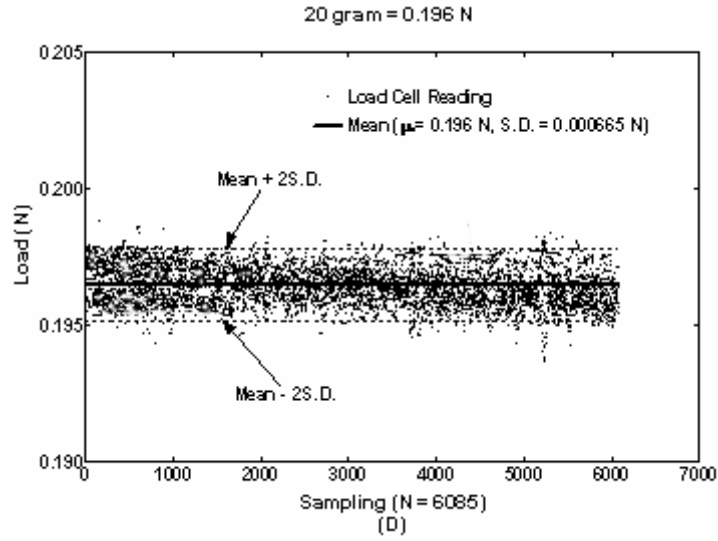
The recorded load data from the correction coefficient determination process were further analyzed to derive the mean load reading by the load cell at each standard weight with the standard deviation (S.D.). The results are listed in Table 3.1 and shown in Fig. 3.3 (A~G). The correction coefficient (k) of the load cell was then determined as 0.99007 as shown in Fig. 3.4, which was used to calibrate the results in later experiments.

Table 3.1: Experimental reading from the load cell on testing weight

Testing Weight (g)	Force (N)	Sample Size	Mean Reading (N)	S.D.	Mean + 2 S.D.	Mean - 2 S.D.
1	0.0098	6087	0.0088	0.000499	0.009798	0.007802
2	0.0196	6091	0.0200	0.000432	0.020864	0.019136
5	0.0490	6087	0.0486	0.000450	0.049500	0.047700
20	0.1960	6085	0.1960	0.000665	0.197330	0.194670
50	0.4900	6084	0.4940	0.000667	0.495334	0.492666
100	0.9800	6090	0.9990	0.000388	0.999776	0.998224
300	2.9400	6083	2.9670	0.000510	2.968020	2.965980

S.D. Standard Deviation





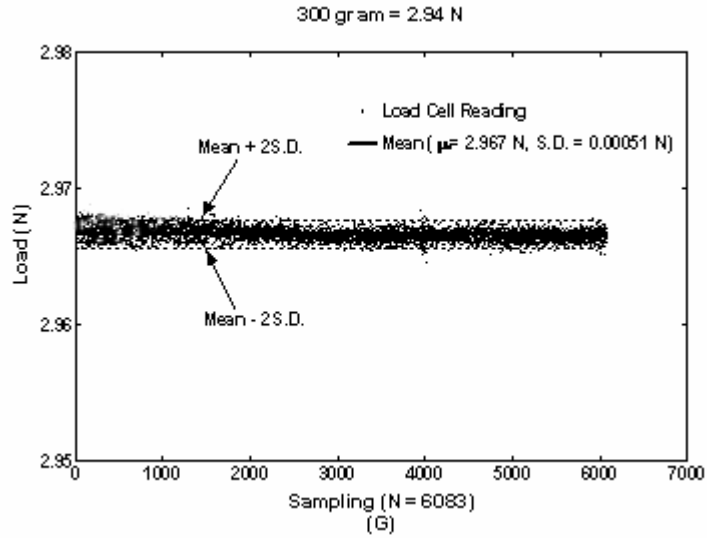


Figure 3.3 (A~G) Experimental load reading by the load cell at different weights.

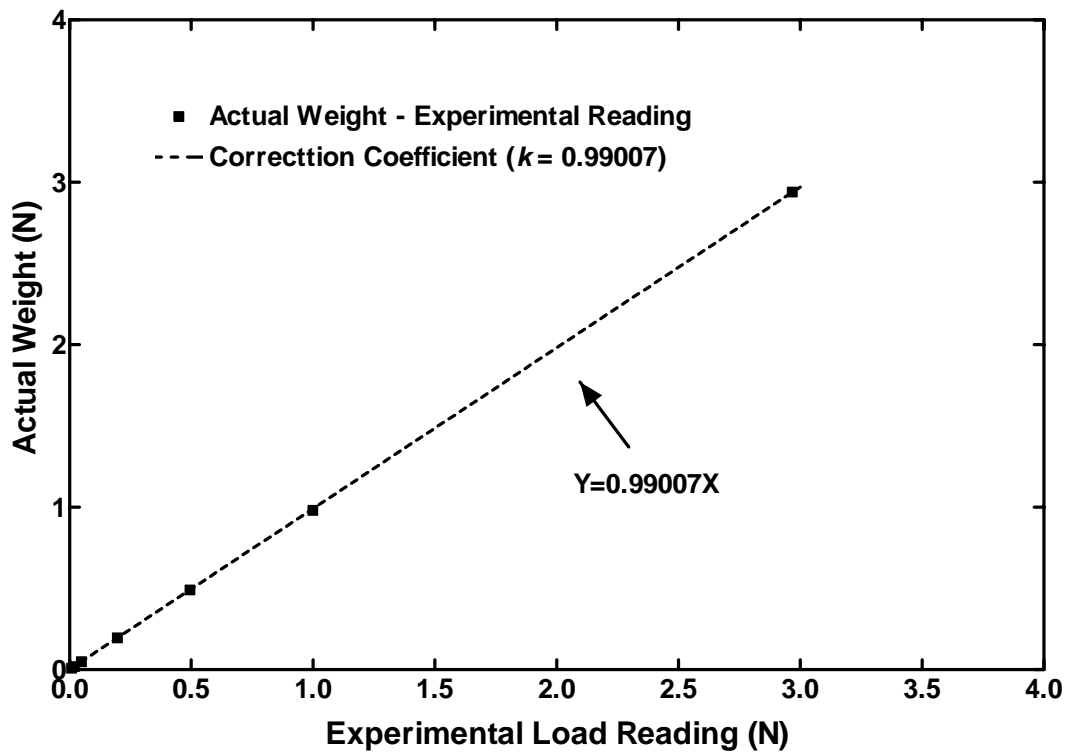


Figure 3.4 The correction coefficient (k) of the load cell.

3.1.2 Specimen Preparation

3.1.2.1 Tympanic Membrane (TM) Preparation

Eleven TM specimens were harvested from fresh or fresh frozen human temporal bones through the Willed Body Program at the University of Oklahoma Health Sciences Center. The donors' ages are from 51 to 92 years old, 5 males and 6 females. All the experiments were performed within 6 days after obtaining bones. To maintain soft tissue compliance, the bones were immersed in 1:10,000 Merthiolate in 0.9% saline solution at 5 °C until use ^[Gan, 2004]. The tympanic annulus of the TM was first separated from the bony ear canal, and then taken out with the malleus attached and placed in a normal saline solution. A rectangular strip was cut from the posterior site of the TM using a specially designed knife with two parallel blades with a distance at 2 mm, which is used to obtain the uniform width of the TM strip for the experiment each time. The strip, or specimen, had the tympanic annulus intact at both top and bottom sides to maintain the integrity of the membrane (Fig. 3.5 A and B). The specimen was treated as a flat rectangular strip for the experiment and the curvature of the TM was neglected in this study.

The specimen was then laid on the base of a microscope (Olympus SZX12) and fixed to the soft tissue mounting fixture at both annulus sides (top and bottom) using cyanoacrylate gel glue (Loctite). Briefly, the fixture has two metal plates for holding the specimen along the longitudinal direction. These two plates are connected by two plastic adapters so that the TM specimen can be mounted to the material testing system as a whole unit to avoid any damage on the tissue during the mounting process. After the

specimen was lined up with grips in the material testing system, plastic adapters were removed and the initial state was setup as shown in Fig. 3.5B.

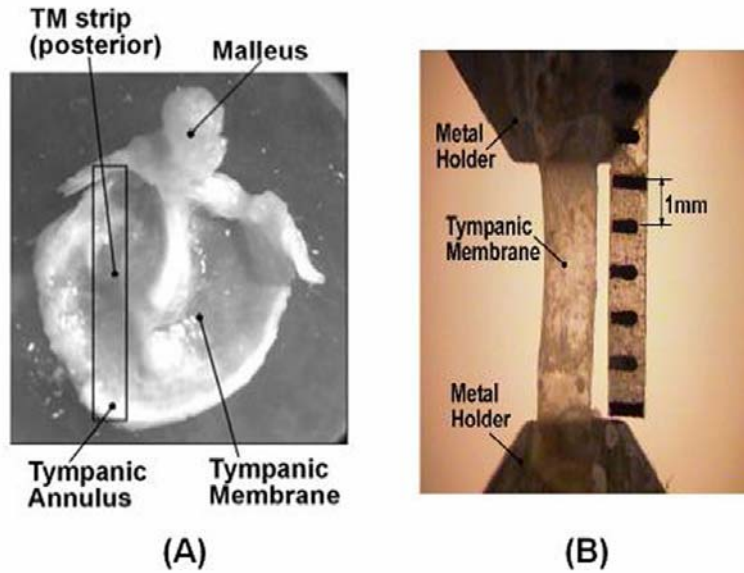


Figure 3.5 (A) The left ear TM harvested from a temporal bone with malleus and tympanic annulus attached. The TM strip was cut from the posterior site of the TM near the outer edge. (B) The TM specimen fixed at the mounting fixture along the longitudinal direction. A ruler was attached to the metal holder at the load cell side for dimension measurement.

A ruler was attached to the metal plate (or holder) at the load cell side for measurement of specimen dimensions. The still images of the specimen in front and side views were captured first using a digital CCD camera attached to a surgical microscope (OPMI 1-FC, Zeiss) for measuring the length, width and thickness of the specimen. During our experiments, initial dimensions of the specimen were first measured under the microscope using a caliper, and then measured again in computer using image analysis tools (e.g., Measuring Tools in Adobe Photoshop 7.0). The distance of 1 mm of the ruler in the image was used as a unit for dimensional calculation in the Measuring Tool of Adobe Photoshop 7.0. Due to individual differences of age, sex and health condition, the

dimensional variation exists for these TM specimens. The length range of specimens is from 5 to 8.5 mm, with an average of 6.44 mm and a standard deviation of 1.17 mm. The width range of specimens is from 1.5 to 2.5 mm, with an average of 1.97 mm and a standard deviation of 0.38 mm. The thickness ranged between 0.06 and 0.1 mm and the average thickness is 0.08 mm with a standard deviation of 0.01 mm.

3.1.2.2. Stapedial Tendon Preparation

Twelve stapedial tendon specimens were harvested from fresh-frozen human temporal bones (obtained from the same source as for the TM specimen mentioned above). The average age of donors was 71 (ranging from 51 to 92 yr, 6 male and 6 female). Experiments were performed within 6 days after harvesting the tissue. The stapedial tendon was prepared with the stapes and pyramidal eminence attached as shown in Fig. 3.6A. Two bony ends were attached to the mounting fixture under a microscope by a tiny drop of cyanoacrylate gel glue (Fig. 3.6B). Care was taken not to allow the glue reaching the tendon. The fixture has two pre-aligned metal plates to hold the specimen and the metal plates were connected by two plastic adapters and mounted to the material testing system as a whole unit. A ruler was attached to the plate as a reference for dimensional measurement. After the specimen was lined up with grips in the MTS, plastic adapters were removed and a preload of 0.001 N was applied to the specimen through the load cell to adjust the initial zero load state. The still images of the stapedial tendon in front and side views were captured at this state using a digital CCD camera. The length, width and thickness of the tendon were measured from these images through Measuring Tools in Adobe Photoshop 7.0 at the resolution of 0.01 mm.

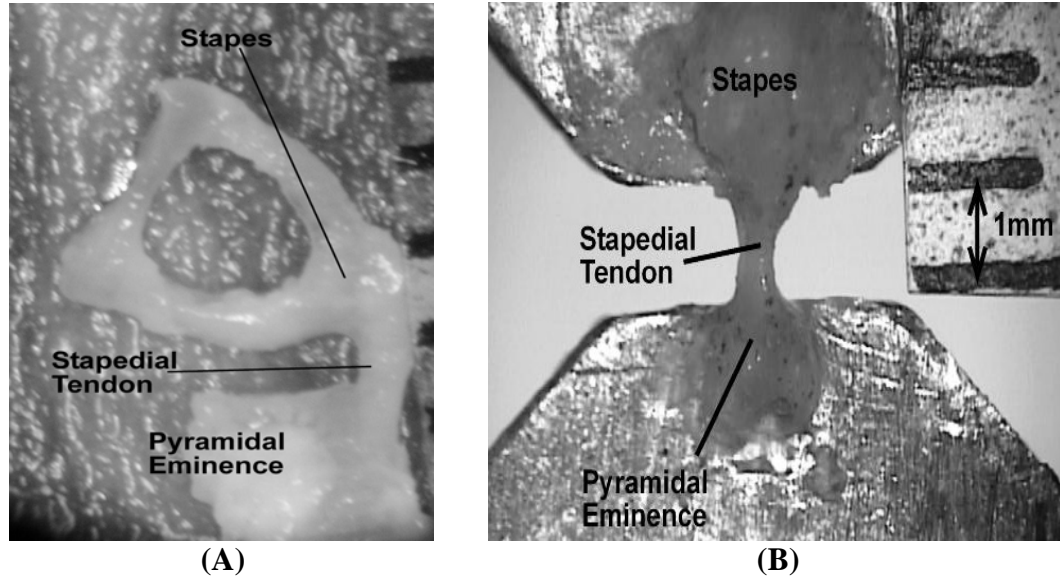


Fig. 3.6 (A) The stapedial tendon harvested from a human temporal bone with the stapes and pyramidal eminence connected. (B) The stapedial tendon specimen fixed at the mounting fixture along the longitudinal direction in a material testing system (MTS). A ruler was attached to the metal holder at the load cell side as a reference for dimension measurement.

Table 3.2 lists the dimensions of twelve individual stapedial tendon specimens with the mean and standard deviation (S.D.).

Table 3.2: Dimensions of stapedial tendon (ST) specimens (N=12)

	ST1	ST2	ST3	ST4	ST5	ST6	ST7	ST8	ST9	ST10	ST11	ST12	Mean	S.D.(±)
Length (mm)	0.87	0.89	1.12	1.10	1.02	0.95	1.00	1.08	1.06	0.90	0.86	1.00	0.99	0.09
Width (mm)	0.46	0.43	0.43	0.30	0.46	0.44	0.34	0.50	0.40	0.38	0.30	0.30	0.40	0.07
Thickness (mm)	0.40	0.37	0.62	0.41	0.40	0.32	0.36	0.52	0.37	0.26	0.30	0.37	0.39	0.10

3.1.2.3. Tensor Tympani Tendon Preparation

Ten specimens of the tensor tympani tendon were harvested from fresh frozen human temporal bones (obtained from the same source as above). The donors' ages were from 50 to 85 years old, 3 male and 7 female. The tensor tympani tendon was prepared with

the malleus and cochleariform attached as shown in Fig. 3.7A. Two bony ends were trimmed and attached to the mounting fixture at the ends under the microscope by cyanoacrylate glue. The fixtures hold the specimen along the longitudinal direction. Care was taken to avoid distortion of the specimen during this process. The metal plates were then connected by two plastic adapters and mounted to the material testing system as a whole unit. A ruler was attached to the metal plate at the load cell side as a dimensional reference (Fig. 3.7B). After the specimen was lined up with grips in the material testing system, plastic adapters were removed and a preload of 0.001 N was applied to setup the zero-load state of the specimen through the machine.

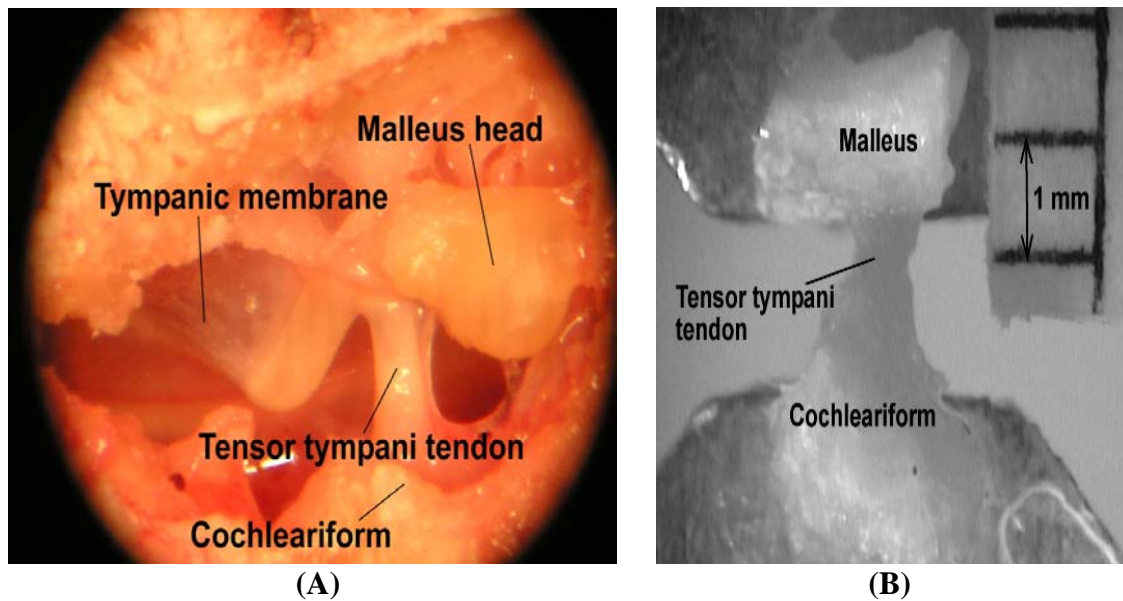


Figure 3.7 (A) The tensor tympani tendon in middle ear cavity connecting to the malleus head and cochleariform was viewed in a human cadaver temporal bone. (B) The tensor tympani tendon specimen was fixed at the mounting fixture along the longitudinal direction in material testing system (MTS). A ruler was attached to the metal holder at the load cell side as a dimensional reference.

The still images of the tendon in front and side views were captured at the initial state using a digital CCD camera. The tendon was distinguished from the bony ends by the

structural change identified under the microscope, and initial dimensions were measured through the Measuring Tools in Adobe Photoshop 7.0 at the resolution of 0.01 mm.

The length, width and thickness of the tensor tympani tendon specimens are given in Table 3.3, with the mean and standard deviation (S.D.).

Table 3.3: Dimensions of tensor tympani tendon (TTT) specimens (N=10)

	TTT 1	TTT 2	TTT 3	TTT 4	TTT 5	TTT 6	TTT 7	TTT 8	TTT 9	TTT 10	Mean	S.D. (±)
Length (mm)	1.23	1.27	1.58	1.44	1.59	1.79	1.51	1.25	1.39	1.45	1.45	0.18
Width (mm)	1.14	0.97	1.39	1.46	1.23	1.26	1.10	0.96	0.90	0.82	1.12	0.21
Thickness (mm)	0.50	0.57	1.00	1.05	1.58	1.05	0.47	0.88	1.10	0.67	0.84	0.43

3.1.2.4. Anterior Malleolar Ligament Preparation

Nine AML specimens were harvested from fresh-frozen human temporal bones. The average age of donors was 71 (ranging from 51 to 92 yr, 5 male and 4 female). Experiments were performed within 6 days after harvesting the tissue. The bones were immersed in 1:10,000 Merthiolate in 0.9% saline solution at 5 °C until use. The AML sample was prepared with two bony parts (the malleus and roof of epitympanum) at ends. By using the same mounting fixture and following the same procedure as we described before, two bony ends were attached to the mounting fixture under a microscope by a tiny drop of cyanoacrylate gel glue (Fig. 3.8). Care was taken not to allow the glue reaching the ligament. A ruler was attached to the top of the fixture as reference for dimension measurement. The AML was then installed and lined up with grips in the material testing system and a preload of 0.001 N was applied to the specimen through the load cell to adjust the zero load state.

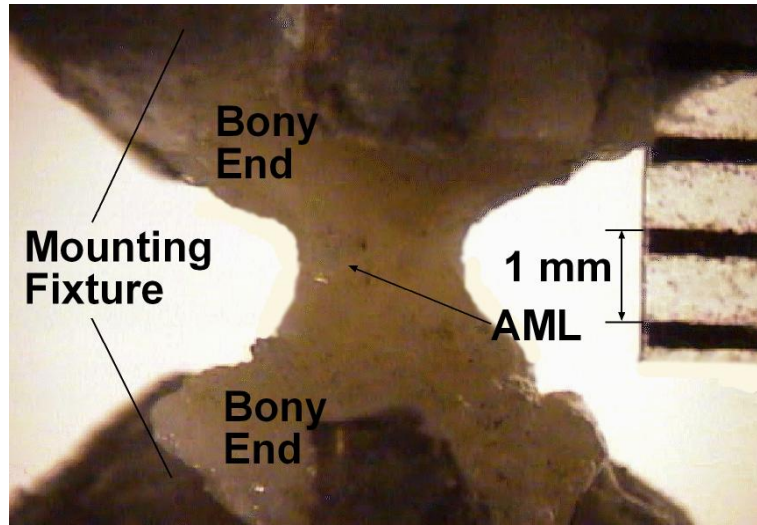


Fig. 3.8 The anterior malleolar ligament of the Human Middle Ear with two bony ends (the malleus and roof of epitympanum). A ruler was attached to the metal holder at the load cell side as a dimensional reference.

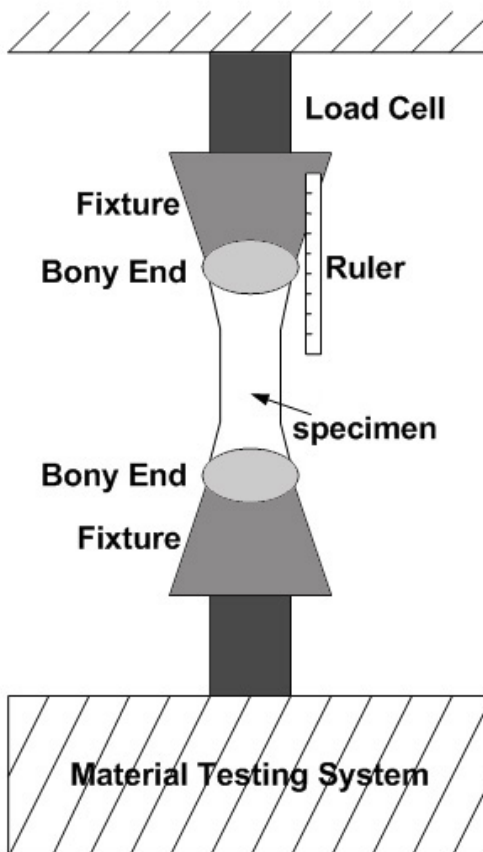
The still images of the ligament in front and side views were captured first using a digital CCD camera and the Measure Tool in Adobe photoshop 7.0 was used to measure the length, width and thickness of the specimen. Table 3.4 lists the dimensions measured from nine AML specimens with the mean and standard deviation (S.D.). Considering the variation of width along the length direction, the width was measured at three locations: top, middle and bottom part of the specimen.

Table 3.4: Dimensions of anterior malleolar ligament specimens (N=9)

	AML 1	AML 2	AML 3	AML 4	AML 5	AML 6	AML 7	AML 8	AML 9	Mean	S.D.(±)
Length (mm)	2.05	2.38	1.66	1.71	2.20	1.76	1.45	1.46	1.77	1.83	0.32
Width (top) (mm)	1.70	2.21	1.45	1.50	1.68	1.64	2.11	1.56	1.52	1.71	0.27
Width (middle) (mm)	1.20	1.90	1.11	1.10	1.08	1.25	1.77	1.21	1.22	1.32	0.30
Width (bottom) (mm)	1.50	2.10	1.31	1.35	1.35	1.43	1.80	1.40	1.01	1.47	0.31
Thickness (mm)	0.81	1.54	1.30	1.10	1.02	1.41	1.27	1.14	1.19	1.20	0.22

3.1.3 Experimental Protocols

The material testing system with the SMT1-2.2 lbs capacity load cell was used to measure the load-deformation relation, stress relaxation function and failure or ultimate stress and strain of the TM, stapedial tendon, tensor tympani tendon and anterior malleolar ligament. The schematic figure and picture of the experiment setup are given in Fig. 3.9 (A, B). The load was applied to the bottom part of the specimen by means of elongation, and the top part of the specimen was fixed. Images of the deformation process for each specimen on each test were recorded simultaneously using a digital CCD camera attached to a surgical microscope with a frame rate of 30 frames /sec.



(A)



(B)

Figure 3.9 The experimental setup.

It is well known that the steady state of biological soft tissues is only reached after preconditioning [Fung, 1993], a process that stress-strain curves are gradually stabilized during repeated cyclings of the specimen. In this study, the MTS machine was programmed to perform five cycles of uniaxial elongation at the elongation rate of 0.5 mm/sec for the TM and 0.1 mm/sec for ligament and tendons, and the elongation length of 10% of the original length for both TM and ligament and tendons. Five cycles of load-displacement curves of a TM specimen recorded in MTS are shown in Fig. 3.10, in which the first three cycles are pointed out. Cycle curves were decreasing during repeated loading-unloading process, and a steady state was generally observed after the third

cycle. The same phenomena were observed for the stapedial tendon, tensor tympani tendon and anterior malleolar ligament, as shown in Figs. 3.11, 3.12 and 3.13. The hysteresis was also observed for all these tissues with the unloading curve lagging the loading curve as being pointed in Fig. 3.13.

After preconditioning, the specimen was subjected to the uniaxial tensile, stress relaxation and failure tests. At the end of uniaxial tensile or stress relaxation test, the specimen was returned to the initial state and waited 2-3 minutes for recovery from previous deformation. The MTS machine and CCD camera were electronically synchronized so that the load and deformation data on images could be correlated simultaneously. The MTS grip-to-grip displacement and the images of deformation were collected to compute strains and assess the boundary effect. The protocols for three tests in MTS are listed as follows:

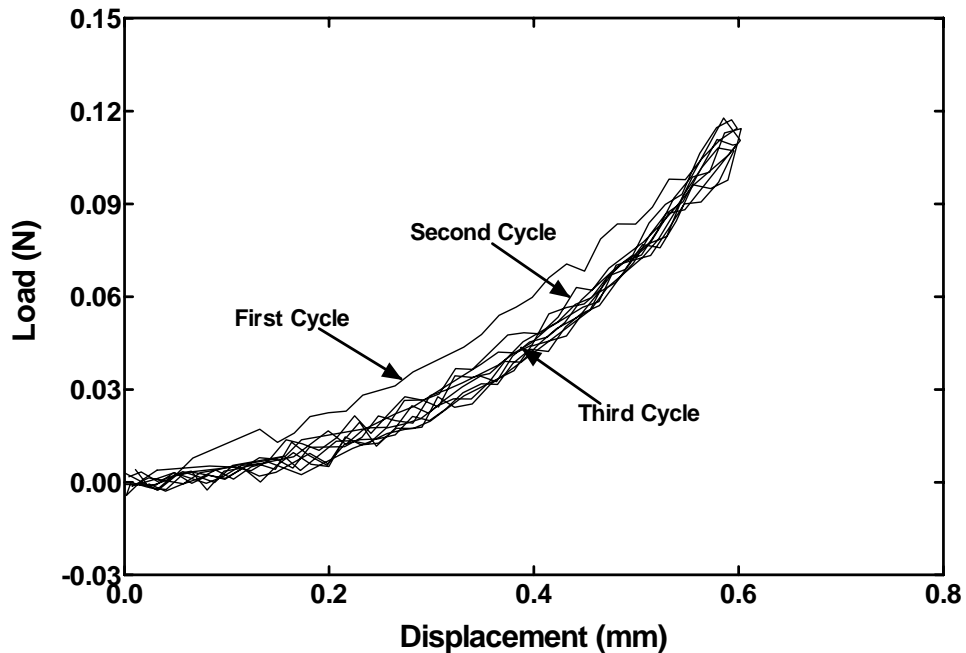


Figure 3.10 Preconditioning of the TM specimen.

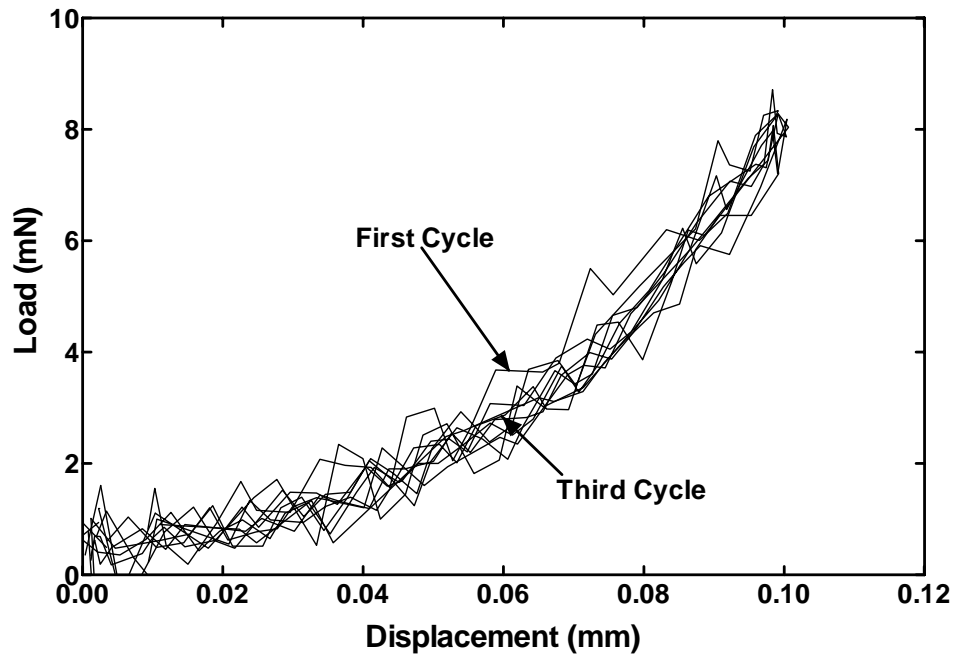


Figure 3.11 Preconditioning of the stapedia tendon specimen.

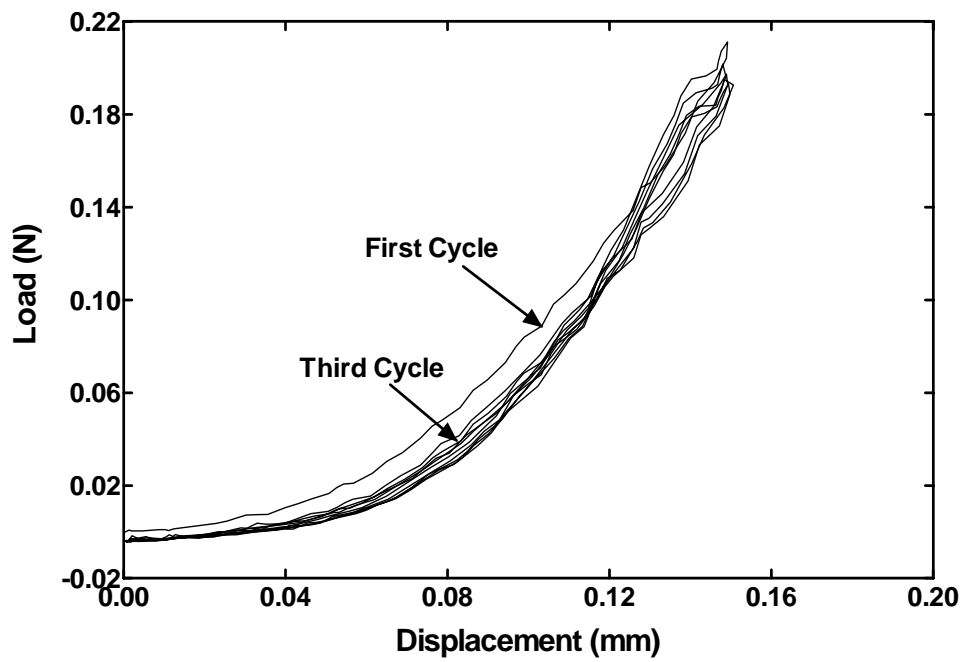


Figure 3.12 Preconditioning of the tensor tympani tendon specimen.

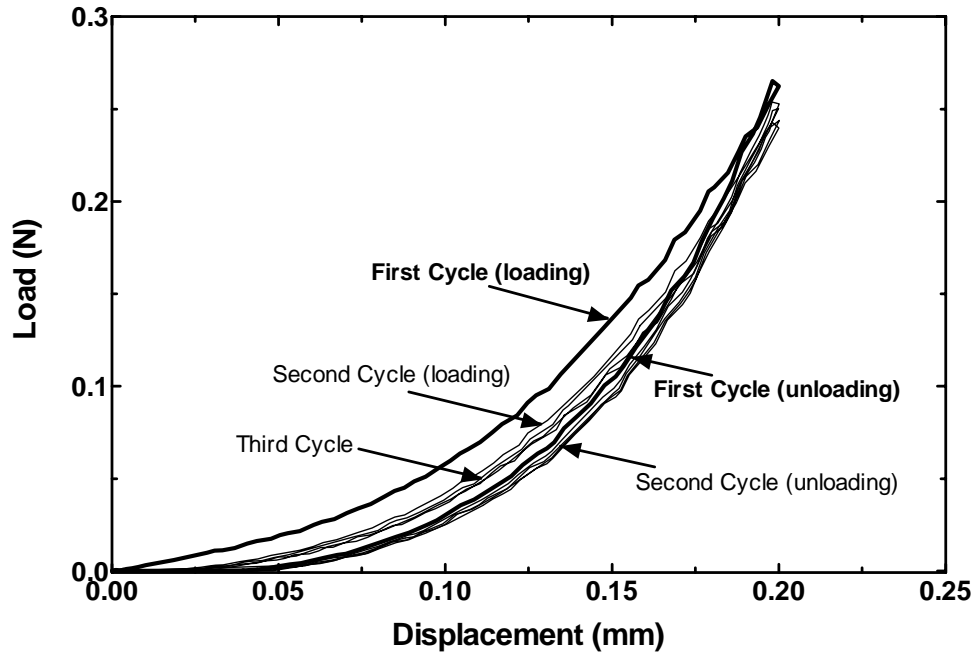


Figure 3.13 Preconditioning of the anterior malleolar ligament specimen.

3.1.3.1. Uniaxial Tensile Test

The elongation rate was set at 0.1 mm / sec, and the elongation length (Δl) was 15% of the original length for the TM and 40% of the original length for the ligament and tendons. Three parameters: load, deformation and time, were recorded by the MTS software (MTestWRTM, TestResources, MN) with a resolution level of 10^{-6} for the load (N). These data were further used to calculate the stress and strain as well as the Young's modulus of the tissue.

3.1.3.2. Stress Relaxation Test

The stress relaxation test was performed to gain insight into viscoelastic properties of the tissue. An approximate step function of elongation was applied to the specimen at the beginning ($t = 0$) with an elongation rate of 1.8 mm / sec. The corresponding stresses

which include the initial stress response σ_0 and the relaxed stress $\sigma(t)$ were recorded over a period of time until the rate of loading change was less than 0.1%/sec, or fully relaxed. In this study, the elongation length of the specimen for the relaxation test was the same value used for the uniaxial tensile test. When a fully relaxation was observed, the MTS data recording program was stopped manually and the specimen was returned to the initial unstressed state for the next test (failure test).

3.1.3.3. Failure Test

To determine the mechanical strength of the tissue, we performed the failure test on all tissue specimens. The elongation rate was set at 0.1 mm / sec for the TM and 0.02 mm / sec for the ligament and tendons. The specimen was extended till it's broken. The load and deformation data were recorded by MTS, and the entire failure process was recorded using the CCD camera. The breaking site of each specimen was observed.

Note that all specimens were maintained in their physiological condition by spraying normal saline solution on the side of the tissue opposite to the camera during the test.

3.2 Digital Image Correlation (DIC) Method

The digital image correlation (DIC) method was employed in this study to verify the boundary effect on mechanical testing of the specimen with a dimension of 1 or 2 mm. In DIC analysis, the tensile strain distribution across the specimen and the average strain are calculated based on images of specimen recorded during the uniaxial loading process.

3.2.1 DIC Algorithm

Digital image correlation (DIC), a non-contact method for measuring the surface displacement or strain distribution in solid materials, has been developed since 1980s [Peters, 1982; Sutton, 1983; Vendroux, 1998 and Lu, 2000], and was extended into soft tissues in this study. The DIC method relies on the existence of a distinct grayscale pattern in a region composed of a subset of pixels around a location where deformations are computed. In general, the DIC method is performed between two images. One is the reference or undeformed image, and the other is the deformed image. Typically, a grid of nodes is located in the reference image, and the deformation mapping is calculated at each of these nodes. The fundamental level of the calculation is at the node level, so the following development of the algorithm is for each node. Three steps are employed to achieve the DIC algorithm: displacement mapping, bicubic spline interpolation, and least squares correlation.

3.2.1.1. Displacement Mapping

Consider a two-dimensional deformation. A subset of points around a node is mapped from the reference image to the deformed image. Each of these subset points is located in the reference image at (x, y) and is mapped to the deformed image at location (\tilde{x}, \tilde{y}) using

$$\begin{aligned}\tilde{x} &= x + U(x, y) \\ \tilde{y} &= y + V(x, y)\end{aligned}\tag{3.1}$$

with U and V being the displacement components of each subset point. The new assumption that U and V can be approximated by a second-order Taylor series expansion around point (x_0, y_0) leads to the mapping functions

$$\begin{aligned}
\tilde{x} &= x_0 + U_0 + U_x \Delta x + U_y \Delta y + \frac{1}{2} U_{xx} \Delta x^2 + \frac{1}{2} U_{yy} \Delta y^2 + U_{xy} \Delta x \Delta y \\
\tilde{y} &= y_0 + V_0 + V_x \Delta x + V_y \Delta y + \frac{1}{2} V_{xx} \Delta x^2 + \frac{1}{2} V_{yy} \Delta y^2 + V_{xy} \Delta x \Delta y
\end{aligned} \tag{3.2}$$

where $\Delta x = x - x_0$ and $\Delta y = y - y_0$.

3.2.1.2. Bicubic Spline Interpolation

The bicubic spline interpolation implements a third-order polynomial that allows both gray-scale values and C^2 continuous gradients to be determined at any location in the gray-scale image fields. Bicubic spline interpolation is a piecewise interpolation scheme in which a set of coefficients are determined for each rectangular patch. Both the reference and the deformed images are interpolated to allow the nodes to be located anywhere in the image fields. The grayscale value at any location in the interpolated region of the reference image can be calculated using the bicubic equation as

$$g(x, y) = \sum_{m=0}^3 \sum_{n=0}^3 \alpha_{mn} x^m y^n \tag{3.3}$$

3.2.1.3. Least Squares Correlation

A least square correlation coefficient is used to determine the optimum values for the mapping parameters. Let S represent all the points in the subset, and let S_p represent any single point in the subset. This correlation coefficient is defined as

$$C = \frac{\sum_{S_p \in S} \{g(S_p) - h(S_p, P)\}^2}{\sum_{S_p \in S} g^2(S_p)} \tag{3.4}$$

The summations are performed over all the points in the subset region. From the equation, the range of values for C is $[0, \infty)$, where the minimum is reached when the differences between g and h are minimized. The set of P that minimizes the correlation

3.2.2 DIC Implementation for Ear Tissues

In this section, we will use the TM specimen to show how to implement the DIC method to analyze our experimental data. The DIC method was employed to calculate the normal strain of the TM specimen based on images simultaneously recorded during the uniaxial tensile test. All the images were first digitized using Adobe Premiere 6.5 and output as sequential images at a constant time interval, starting from time $t = 0$ to the end of a loading process. The first image ($t = 0$) was used as a reference and the consecutive images (more than 20) were used as deformed states. All the images were transformed from the color format (true color, 24 bit) into the grayscale (256 level, 8 bit) format before being read into the DIC software package WinDIC_LS 2.0 (provided by Prof. H. Lu at Oklahoma State University).

Figure 3.14 shows the reference and three consecutive images selected from a TM specimen. As shown in this figure, horizontal and vertical lines were first identified and drawn in a relatively large area around the center of the specimen in the reference image using the DIC software. A grid of nodes (3×11) was then generated along these lines and the deformation was calculated at each node by tracing these nodes through three procedures of the DIC algorithm introduced before. The length of each vertical line in the reference image was used as the original length (L_0), and the length of corresponding lines in deformed images was measured as the deformed length (L). The normal strain ε

in the vertical direction was calculated by $\varepsilon = \frac{L - L_0}{L_0}$. The strain across the transverse direction at 11 nodes and the average strain was then obtained and synchronized with the stress measured by the load cell in MTS to derive the strain distribution across the specimen and the stress-strain relationship of the specimen during the uniaxial loading process. The stress-strain relationship of the specimen based on DIC analysis was further compared with that obtained from the MTS recorded results to evaluate the boundary effect of the experiment.

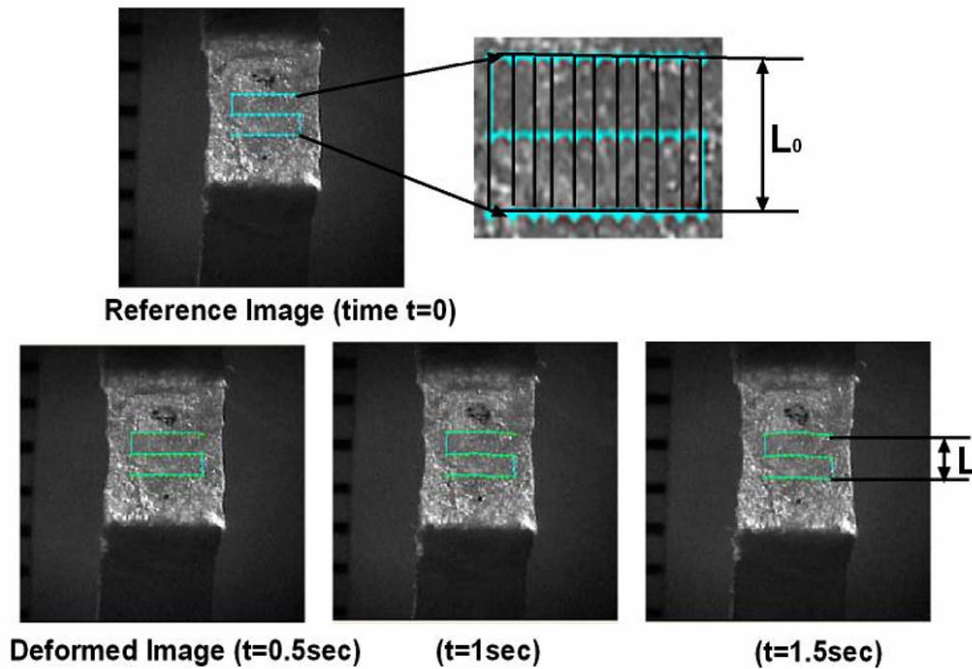


Figure 3.14 Illustration of the digital image correlation (DIC) method for calculating the strain distribution of the TM specimen under the uniaxial loading process.

The illustrations of the DIC method on middle ear ligament and tendons (stapedial tendon, tensor tympani tendon and anterior malleolar ligament) are given in Figs. 3.15 ~3.17, with the same procedures as used for the TM to obtain the strain distribution across the ligament specimen and the average strain in the middle portion of the ligament

or tendon. Note the dimensions of ligament or tendons are smaller than the TM, therefore, fewer nodes were generated for the DIC analysis of the ligament or tendons.

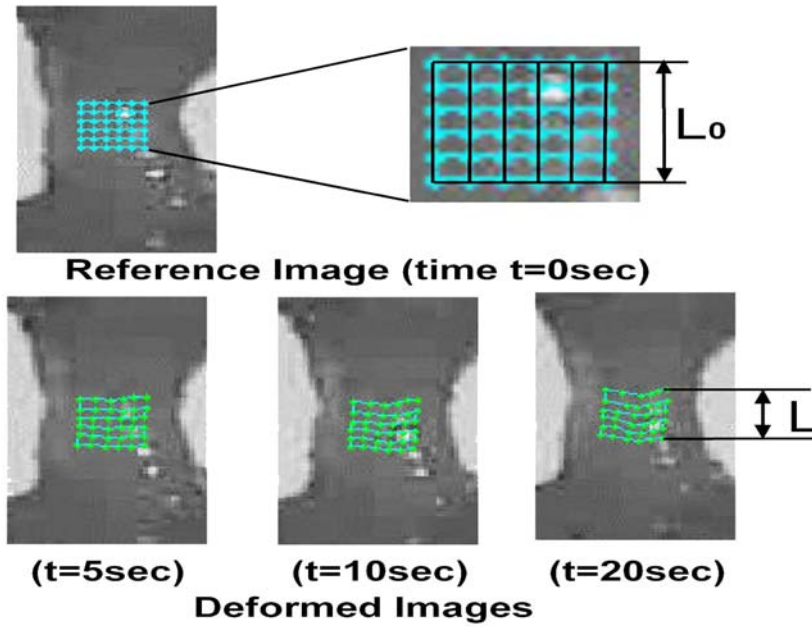


Figure 3.15 Illustration of the digital image correlation (DIC) method for calculating the strain distribution of the stapedial tendon specimen under the loading process.

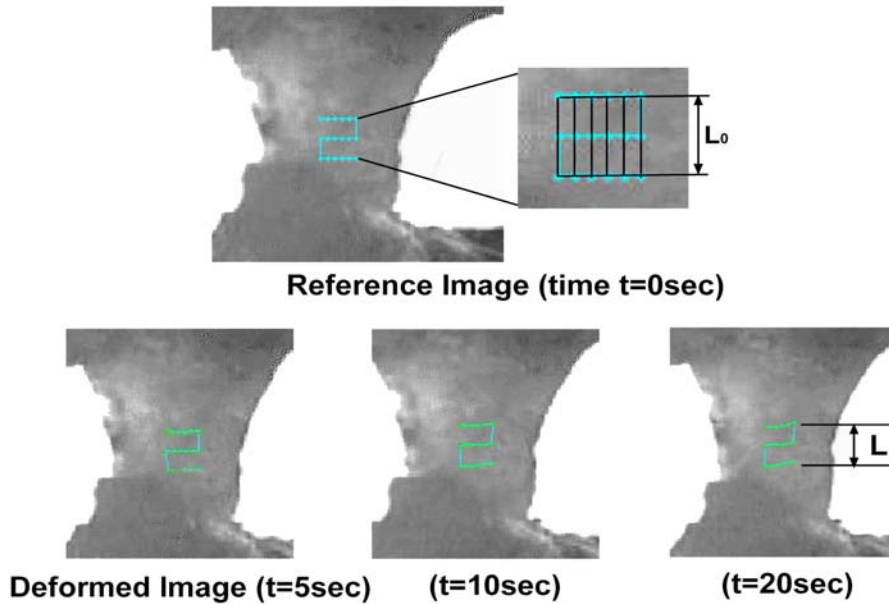


Figure 3.16 Illustration of the digital image correlation (DIC) method for calculating the strain distribution of the tensor tympani tendon specimen under the loading process.

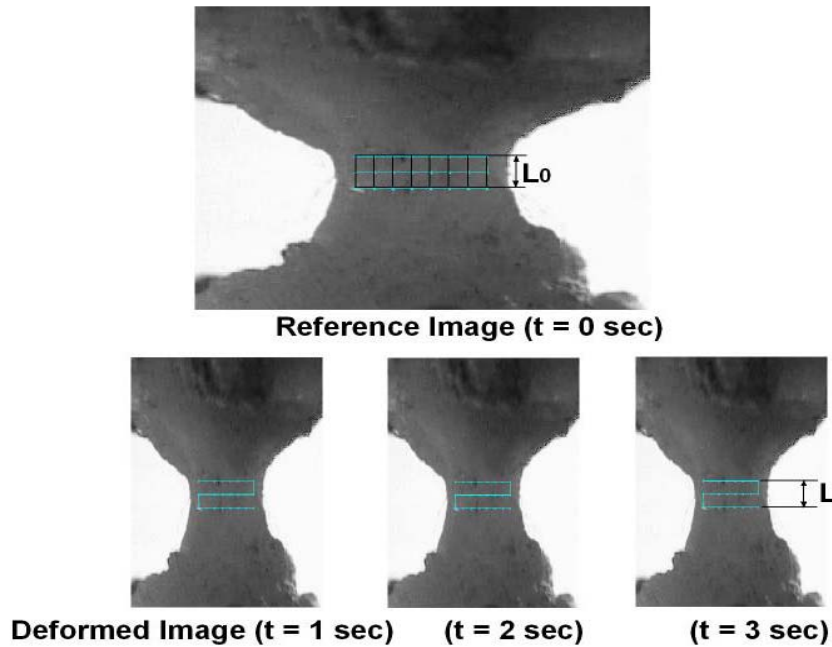


Figure 3.17 Illustration of the digital image correlation (DIC) method for calculating the strain distribution of the anterior malleolar ligament specimen under the loading process.

3.3 Modeling Analysis

The experimental data measured by the MTS were post processed to obtain: the stress-strain relationship and Young's modulus-stress or strain relationships of the tissue. The loading values directly recorded by the load cell were multiplied by the correction coefficient $k=0.99007$ before further analysis. In this study, we applied several different approaches (constitutive modeling or FE modeling) to investigate mechanical properties of different middle ear tissues (TM, stapedial tendon, tensor tympani tendon and anterior malleolar ligament), which are given one by one in details as follows.

3.3.1 Analysis on Tympanic Membrane

The TM specimen was assumed as an isotropic, non-linear viscoelastic material based on the observation of loading-deformation curves recorded in preconditioning and

uniaxial tensile test. The raw data were treated using a hyperelastic material model for elasticity analysis. There are several non-linear material models available for analysis on mechanical properties of biological tissues, such as the Ogden, Mooney-Rivlin and Yeoh models. Sarma *et al.*^[Sarma, 2003] have tried these models to explain the stress-strain behavior of the smooth muscle tissue and concluded that the Ogden model was more valid and useful for studying rubber-like biological soft tissues. In literature, the Ogden model has been well used to predict the behavior of several non-linear and viscoelastic biological tissues such as the skin and brain tissue ^[Miller, 2002 and Wu, 2003], and was used to analyze experimental data of the TM.

For the uniaxial elongation, the Ogden model is generally expressed as

$$\sigma = \frac{2\mu_1}{\alpha_1} [(1 + \varepsilon)^{\alpha_1 - 1} - (1 + \varepsilon)^{-(0.5\alpha_1 + 1)}] \quad (3.5)$$

where σ is the normal stress, ε is the strain, and μ_1 and α_1 are material constants ^[Wang, 2002]. In this study, we used the stretch ratio λ , the ratio of the deformed length to the original length, to describe the strain and $\varepsilon = \lambda - 1$, thus, Eq. (3.5) becomes

$$\sigma = \frac{2\mu_1}{\alpha_1} [\lambda^{(\alpha_1 - 1)} - \lambda^{-(0.5\alpha_1 + 1)}] \quad (3.6)$$

Differentiating Eq. (3.6) with respect to λ , we have

$$\frac{d\sigma}{d\lambda} = \frac{2\mu_1}{\alpha_1} [(\alpha_1 - 1)\lambda^{\alpha_1 - 2} + (\alpha_1 / 2 + 1)\lambda^{-(0.5\alpha_1 + 2)}] \quad (3.7)$$

which shows the relationship between the tangent modulus or Young's modulus $\frac{d\sigma}{d\lambda}$ and stretch ratio λ .

Two material constants μ_1 and α_1 of the tissue were derived from stress-strain loading curves obtained in the uniaxial tensile test using MATLAB v.7.0 through the data iteration process, i.e., given experimental data and a user-defined function (Eq. (3.6) in this section), find coefficients that best fit the function to the data in a least-squares sense. The constitutive equation of the TM in the Ogden form was then represented by substituting μ_1 and α_1 into Eq. (3.6), and the Young's modulus of the TM with respect to the strain were determined from Eq. (3.7).

Note that Eqs. (3.6) and (3.7) are based on the strain energy potential of the Ogden model and the Young's modulus of the tissue is described as a function of the strain. To derive the relationship between the Young's modulus and stress, the Young's modulus-stress curve of the TM was plotted from experimental data following the equation

$$\frac{d\sigma}{d\lambda} = k(\sigma + b) \quad (3.8)$$

Then, integration gave the stress-strain relationship as

$$\sigma + b = ce^{k\lambda} \quad (3.9)$$

The integration constants c could be determined by finding one point on the curve, say $\sigma = \sigma^*$ when $\lambda = \lambda^*$. Then

$$\sigma = (\sigma^* + b)e^{k(\lambda - \lambda^*)} - b \quad (3.10)$$

This process has been well accepted for the study of soft tissue biomechanics [Fung, 1993].

3.3.2 Analysis on Stapedial Tendon

The data recorded by the MTS during uniaxial tensile tests were analyzed to obtain stress-strain relationship, or constitutive equation, of the stapedial tendon by using the

same hyperelastic Ogden model (Eq. (3.6)) and following the same procedures as for the TM.

Material constants μ_1 and α_1 were derived from the mean stress-strain loading curve of 12 specimens using the least-squares-fit process in MATLAB v.7.0. Based on experimental data and Eq.(3.6), the coefficients that best fit the equation to the data were determined. The constitutive equation of the stapedial tendon was then expressed by substituting μ_1 and α_1 into Eq. (3.6).

3.3.3 Analysis on Tensor Tympani Tendon

In addition to using the same data analysis procedures mentioned above for the tensor tympani tendon, finite element (FE) modeling analysis was used to study relationship between the structure and behavior of the tensor tympani tendon in this study.

Based on a parallel-bundled fibrous microstructure of the tensor tympani tendon (Fig. 3.18A) observed under the scanning electron microscope (SEM, Model: DSM960, Zeiss) with 3000x magnification in Samuel Roberts Noble Electron Microscopy Lab at University of Oklahoma, five 3-dimensional FE models of the tensor tympani tendon with different fiber to ground substance ratio were created in ANSYS v.10.0 (ANSYS Inc., Canonsburg, PA) as shown in Fig. 3.18 B~F. Note that only X-Y plane models were shown in these figures for a better illustration. The length, width and thickness of each model were 1.45, 1.12 and 0.84 mm respectively based on the mean value of specimen dimensions listed in Table 3.3. The volume ratio of collagen fiber to ground substance, k , was varied from 2.3 (fiber density 70%) to 3.0 (fiber density 75%), 4.0 (fiber density 80%), 5.7 (fiber density 85%) and 9.0 (fiber density 90%) respectively. Each model was

meshed by eight-node hexahedral solid elements (Solid185) with a total of 4860 elements and 5880 nodes.

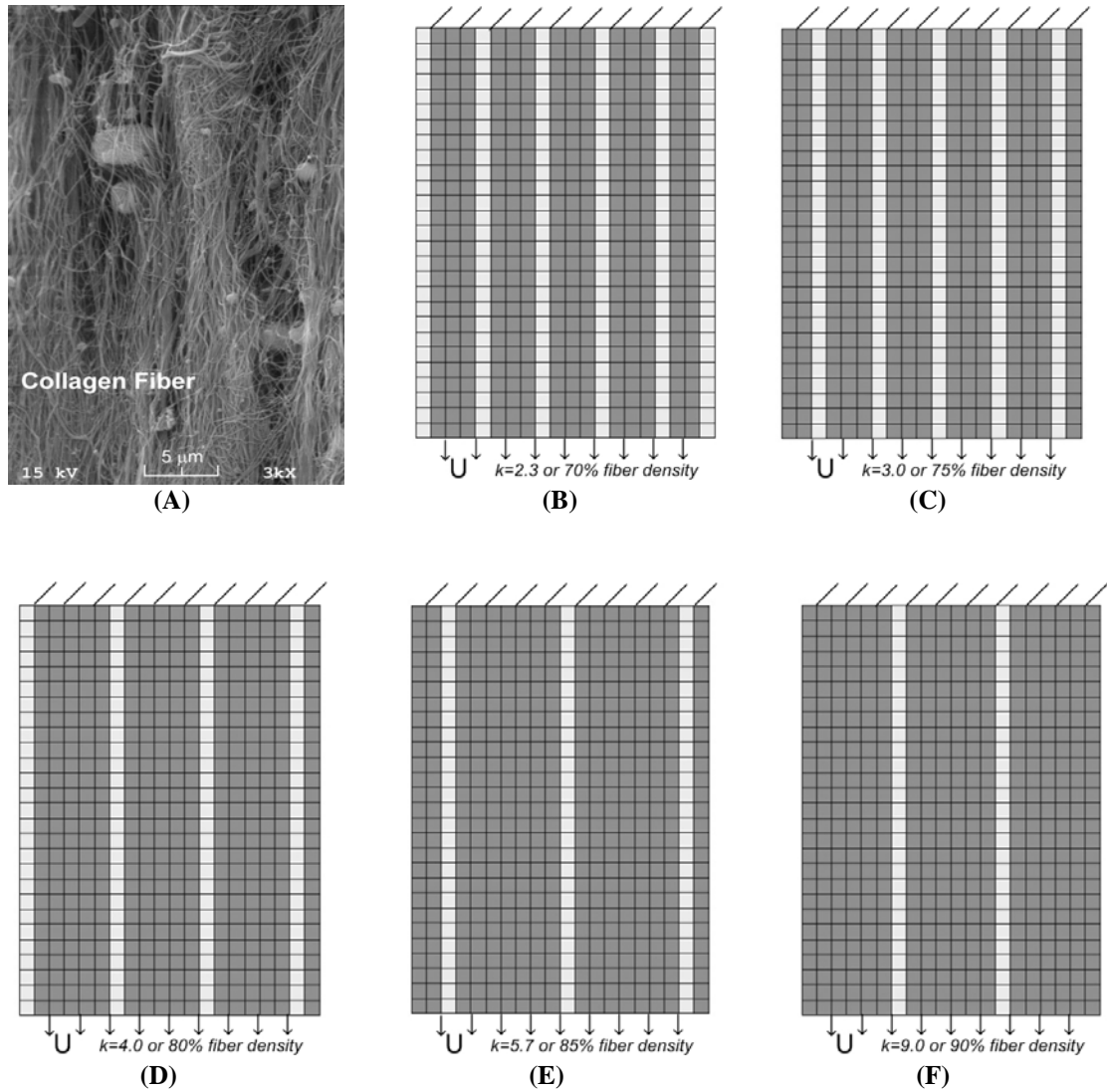


Figure 3.18 (A) SEM picture of the tensor tympani tendon at 3000x magnification. (B~F) Five FE models of the tensor tympani tendon with different collagen fiber-ground substance ratio (k) or fiber density.

Since the Ogden model was used in data analysis of raw experimental data, it was selected in FE analysis. The tensor tympani tendon was assumed as isotropic material with fibers oriented along the Y axis. A Poisson ratio (ν) of 0.495 was used in the FE

modeling because an ideal Poisson ratio of 0.5 for incompressible material could bring numerical difficulties for the commercial FE solver. The first-order Ogden model (Eq. (3.6)) was used in this modeling work. The initial Young's modulus of the fiber along Y direction for incompressible materials ($\nu = 0.5$) was expressed as

$$E_{Y0} = 2(1 + \nu)G = 3G = 3\alpha_1\mu_1 \quad (3.11)$$

The initial modulus along X and Z directions are assumed as 1/10 of E_{Y0} due to the transverse properties of the fibrous tendon [Weiss, 2001]. The ground substance was assumed to be isotropic material with a uniform initial Young's modulus of 10 kPa based on the lowest stiffness of soft tissues such as fat (4.8 kPa) published by Wellman *et al.* [Wellman, 1999]. Boundary and loading conditions were applied through nodes on top and bottom surfaces of the model. For the uniaxial tensile test, all the nodes on top surface were fixed, and all the nodes on bottom surface were elongated by 0.6 mm. The elongation was accomplished by 120 substeps to reach the maximum of loading.

Nonlinear structural analysis was carried out on five FE models of the tensor tympani tendon to calculate the force and deformation of the tendon during the elongation. The nominal stress and strain along the fiber direction at each substep were derived. Meanwhile, the material constants (μ_1 and α_1) in the Ogden form for the tensor tympani tendon were derived again from FE analysis. The FE simulated stress-strain curves of the tendon with different microstructure configurations (fiber to ground substance ratio) were compared with experimental results. The relationship between the structure and properties of the tensor tympani tendon was then determined.

3.3.4 Analysis on Anterior Malleolar Ligament

The scanning electron microscope (SEM) picture of the AML at 5000x magnification prepared by Samuel Roberts Noble Electron Microscopy Lab at University of Oklahoma is shown in Fig. 3.19. A parallel-bundled (coiled) collagen fibrous microstructure of the AML was observed. The mechanical behavior of the AML is expected to be described by a unidirectional fiber reinforced composite model.

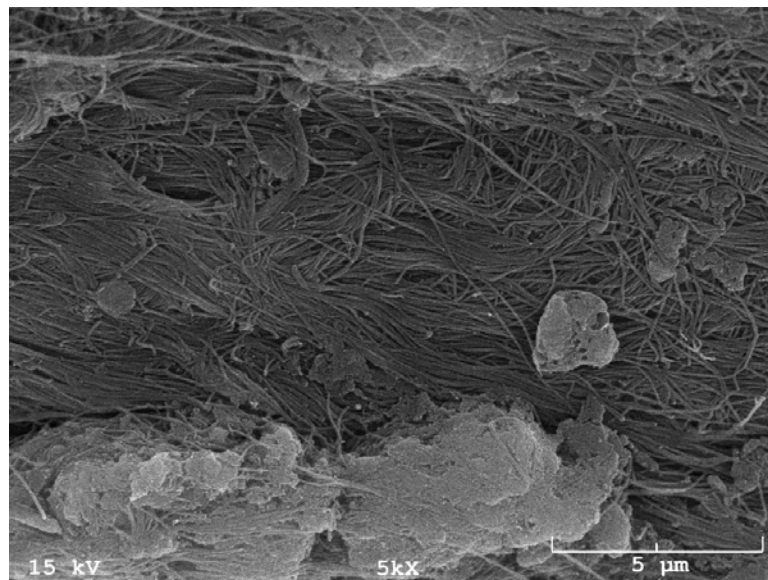


Figure 3.19 Microstructure of the anterior malleolar ligament under SEM (5000x).

In this study, instead of using the Ogden hyperelastic model which was used for the TM and other two tendons introduced above, we used a transversely isotropic model which consists of a first-order Ogden model augmented by a I_4 -type reinforcing term proposed by Ogden in 2003 [Ogden, 2003]. The strain energy potential of the model, U , is described as

$$U = \frac{2\mu_1}{\alpha_1^2} (\lambda_1^{\alpha_1} + \lambda_2^{\alpha_1} + \lambda_3^{\alpha_1} - 3) + \frac{2k\mu_1}{\beta^2} (I_4^{\beta/2} + 2I_4^{-\beta/4} - 3), \quad \lambda_1\lambda_2\lambda_3 = 1 \quad (3.12)$$

where $\lambda_1, \lambda_2, \lambda_3$ are principal stretches of the incompressible material and $\lambda_1\lambda_2\lambda_3 = 1$. I_4 coincides with the square of material stretch in the fiber direction. In Eq. (3.12), μ_1 is the infinitesimal shear modulus of the material in a natural configuration, and α_1 and β are temperature dependent material parameters. Parameter k is a coefficient (> 0) which counts for the increase of material stiffness in the fiber direction. The case with $k=0$ represents the isotropic Ogden model which has been well used to model soft tissues such as the tympanic membrane, brain tissue, and skin [Cheng, 2007a; Miller, 2002 and Wu, 2003].

The Cauchy stress tensor $\boldsymbol{\sigma}$ is then derived from the strain energy function U (Eq. (3.12)) as

$$\boldsymbol{\sigma} = \sum_{i=1}^3 (\lambda_i \frac{\partial U}{\partial \lambda_i} - p) \mathbf{v}^{(i)} \otimes \mathbf{v}^{(i)}, \quad (3.13)$$

where $\mathbf{v}^{(i)}$ are eigenvalues of the left stretch tensor \mathbf{V} , p is the Lagrange multiplier associated with the incompressibility constraint, and \otimes denotes the tensor product.

Assuming that fibers of the AML are aligned along the X_2 -axis of a given Cartesian coordinate system (X_1, X_2, X_3) and the uniaxial loading is applied along the fiber direction (X_2 -axis), the stretch in the loading direction would be $\lambda \equiv \lambda_2$, and the nonzero

stress component of $\boldsymbol{\sigma}$ is $\sigma = \sigma_{22}$. Thus, $\lambda_1 = \lambda_3 = \lambda^{-1/2}$, $p = \frac{2\mu_1\lambda^{-\alpha_1/2}}{\alpha_1}$, $I_4 = \lambda^2$, and

$$U = \frac{2\mu_1}{\alpha_1^2} (\lambda^{\alpha_1} + 2\lambda^{-\alpha_1/2} - 3) + \frac{2k\mu_1}{\beta^2} (\lambda^\beta + 2\lambda^{-\beta/2} - 3) \quad (3.14)$$

$$\sigma = \frac{2\mu_1}{\alpha_1} (\lambda^{\alpha_1-1} - \lambda^{-0.5\alpha_1-1}) + \frac{2k\mu_1}{\beta} (\lambda^{\beta-1} - \lambda^{-0.5\beta-1}) \quad (3.15)$$

Eq. (3.15) represents the stress (σ) ~ stretch (λ) relationship or constitutive equation of the AML expressed with material parameters of μ_1, α_1, β and k .

Differentiating Eq. (3.15) with respect to λ , we have the tangent modulus or Young's modulus ($\frac{d\sigma}{d\lambda}$) of the material:

$$\frac{d\sigma}{d\lambda} = \frac{2\mu_1}{\alpha_1} [(\alpha_1 - 1)\lambda^{\alpha_1-2} + (\frac{\alpha_1}{2} + 1)\lambda^{-(0.5\alpha_1+2)}] + \frac{2k\mu_1}{\beta} [(\beta - 1)\lambda^{\beta-2} + (\frac{\beta}{2} + 1)\lambda^{-(0.5\beta+2)}] \quad (3.16)$$

Three material parameters (μ_1, α_1, β) in this study were determined as k value changed from 0 to 5, 10 and 20 through iterative regression processes in MATLAB (v.7.0). Briefly, given experimental stress-stretch data and a user-defined function (Eq. (3.15) in this study), we find the material parameters that best fit the function to the data in a least-squares sense. Constitutive equation of the AML was then obtained by substituting the material parameters into Eq. (3.15). The Young's modulus of the specimen was obtained from Eq. (3.16) and plotted against the stress to derive the Young's modulus-stress relationship of the AML.

CHAPTER 4

RESULTS OF THE TYMPANIC MEMBRANE

Mechanical properties of the human tympanic membrane (TM) were obtained through the methods introduced in Chapter 3 and presented here. The results have recently been published in *Annals of Biomedical Engineering* [Cheng *et al.*, 2007a].

4.1 Mechanical Properties of the Tympanic Membrane

Figure 4.1 shows stress-stretch ratio curves obtained from the uniaxial tensile test on three TM specimens after preconditioning, with raw data as well as smooth curves derived from the Ogden model. The correlation coefficients of model fitting for each specimen on Fig. 4.1A, 4.1B, and 4.1C are: 0.9968, 0.9979, and 0.9982 respectively, which show adequate accuracy of using the Ogden model to fit the experimental data. The hysteresis phenomenon is observed for all of them. Mechanical properties of the TM presented in this section are all from the loading curve. Variations among individual TM specimens resulted from differences of age, sex, health and sample dimensions are also shown in Fig. 4.1.

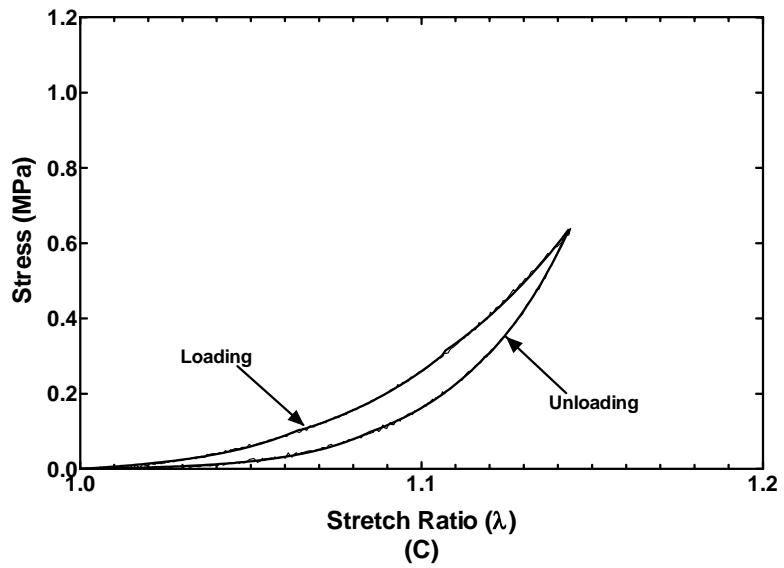
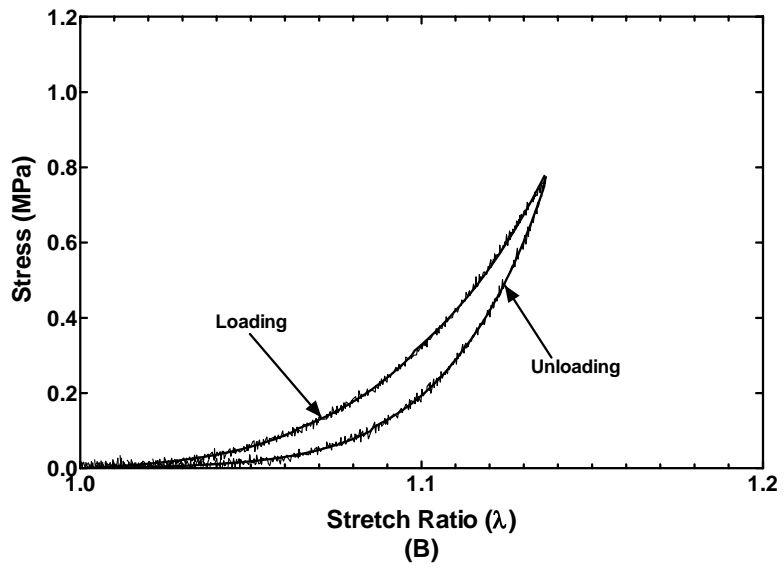
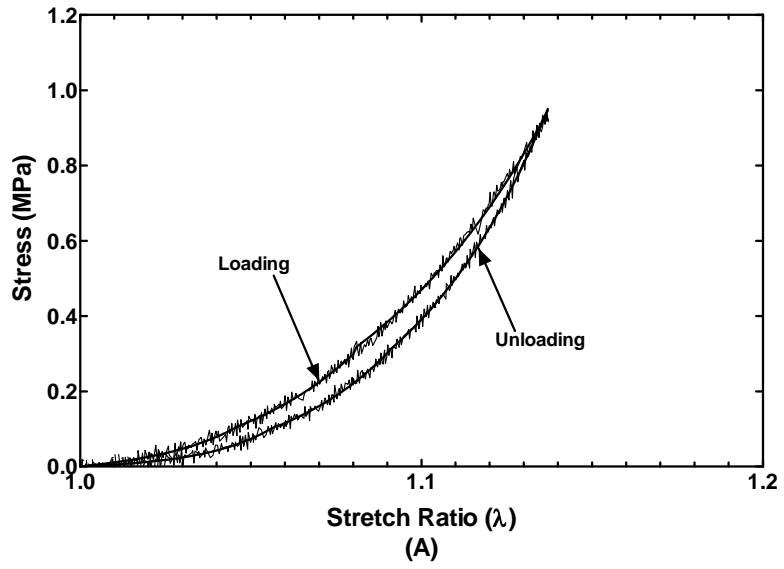
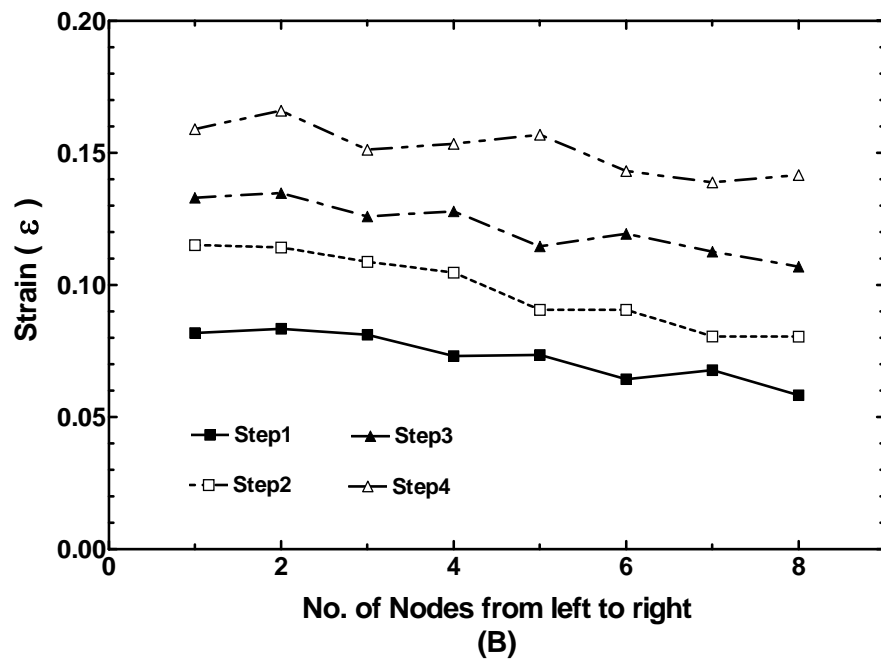
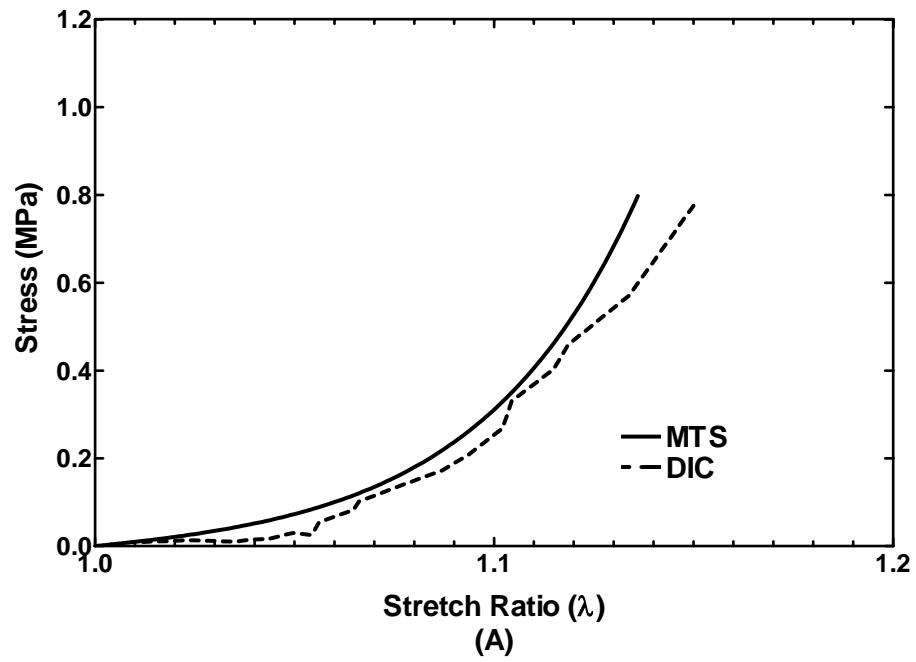


Figure 4.1 Stress-stretch ratio curves of three TM specimens obtained from uniaxial tensile tests after preconditioning. The wave-like lines were original stress-stretch ratio curves recorded in MTS. The smooth lines were obtained after the Ogden model fitting process. The hysteresis was seen on each specimen with the unloading curve lower than the loading curve (pointed by arrows).

Comparisons of stress-stretch ratio curves of two TM specimens directly obtained from the uniaxial tensile test (solid lines) and that derived from the DIC method (broken lines) are shown in Fig. 4.2A and 4.2C respectively. The transverse strain distribution across TM specimens from the DIC analysis are shown in Fig. 4.2B and 4.2D as well. In Fig. 4.2B and D, the x-axis represents the location of nodes (from left to right) along the middle horizontal line in Fig. 3.14, and the y-axis is the normal strain ε calculated at these nodes. The normal strains from four steps with a constant time interval are shown in each figure. The results show that the transverse strain is relatively uniform across the membrane, and the stress-strain curve of the TM obtained from MTS and DIC agrees with each other. Therefore, the boundary effect which might be introduced by the small size of the specimen was limited in our experiments.



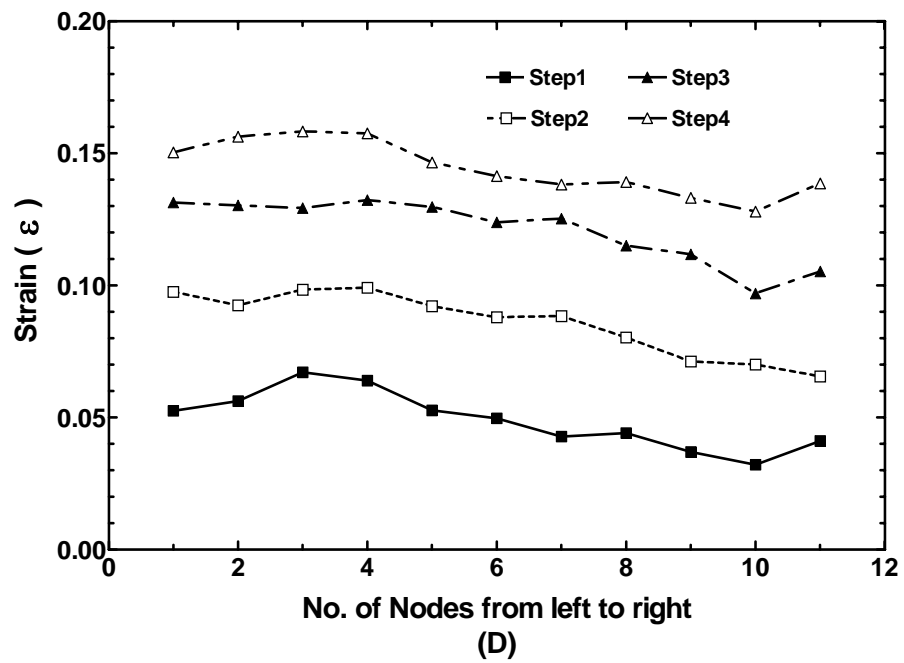
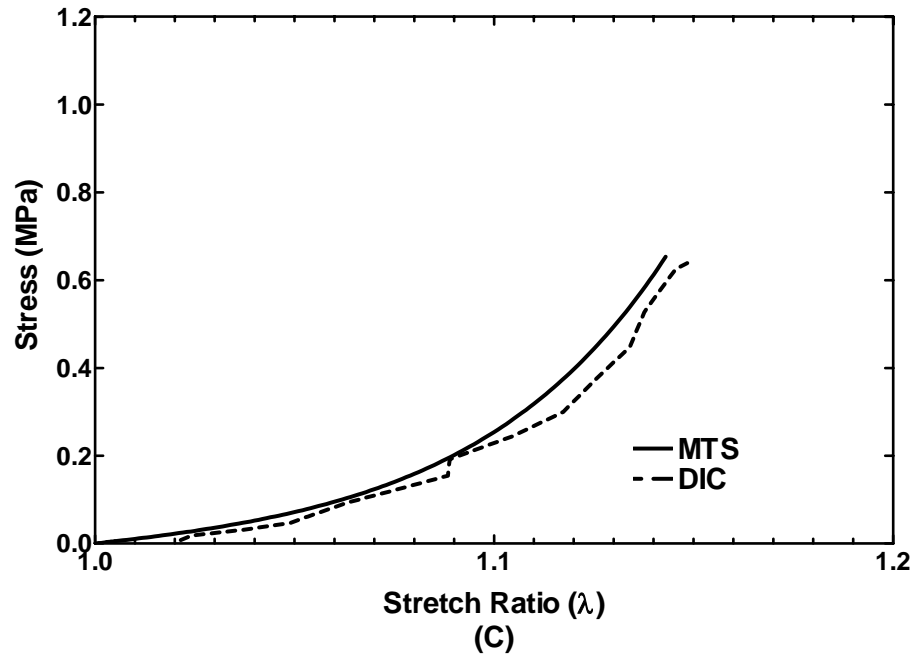
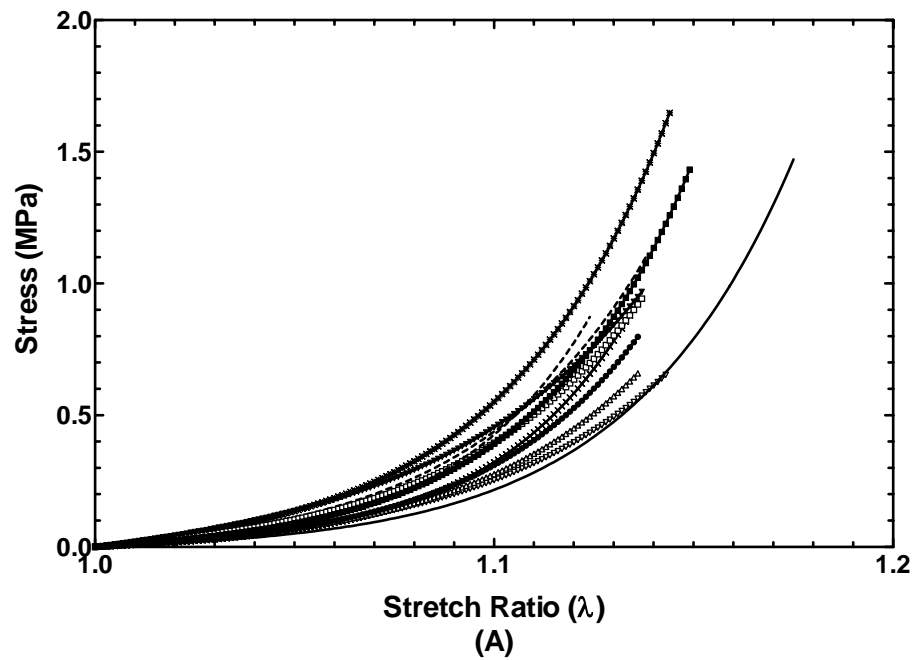


Figure 4.2 (A, C) Comparison of stress-stretch ratio curves of two TM specimens obtained from the MTS measurement (solid lines) and DIC analysis (broken lines). (B, D) Transverse strain distribution across the TM specimen calculated from DIC analysis at four time steps.

Figure 4.3A shows stress-stretch ratio relationships of eleven TM specimens under the loading process of the uniaxial tensile test. As can be seen in this figure, most TM specimens are stretched up to λ of 1.15, while a few are either stretched longer or shorter than λ of 1.15 or 15% elongation of the original length. Figure 4.3B displays the mean and standard deviation for these stress-stretch ratio curves. It is clearly seen that the absolute standard deviation increases with the increasing stress, while the relative standard deviation remains the same at 0.25. The stress-stretch curve is relatively flat at the beginning of the loading and becomes stiff as the stress or stretch ratio increases.



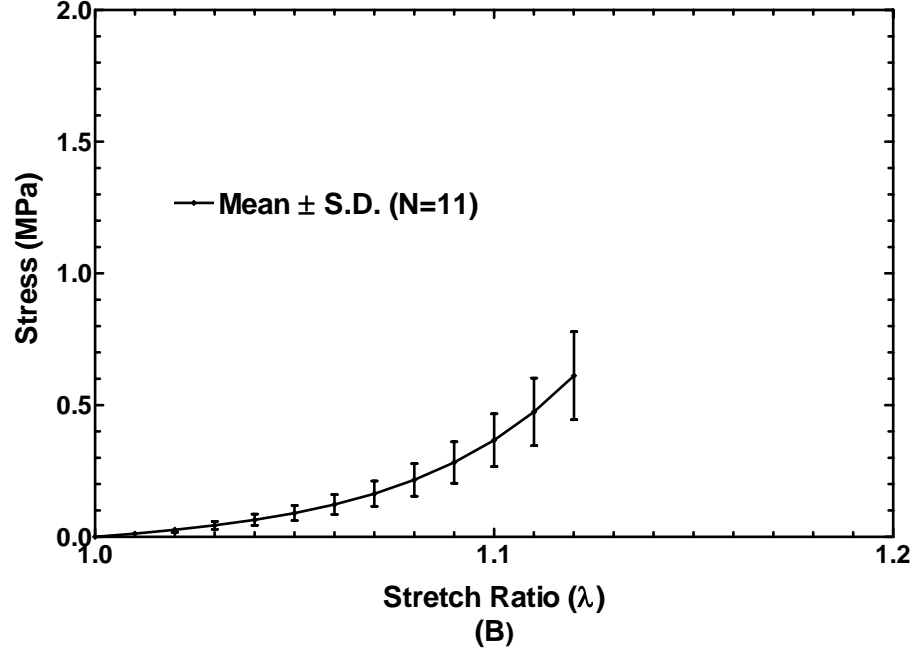


Figure 4.3 (A) Stress-stretch ratio curves of eleven TM specimens under uniaxial loading tests. The stretch ratio λ was around 1.15 and the strain rate was 0.1 mm/sec. (B) The mean value of stress-stretch ratio relationship of eleven TM specimens with standard deviation (S.D.) bars.

An important biomechanics study of ear tissues is to derive the constitutive equation of the tissue based on experimentally measured stress-strain curves. Using Eq. (3.6), the constitutive equation of the TM in the Ogden form can be derived by determining two material constants, μ_1 and α_1 . Through the data iteration process, we have $\mu_1 = 0.46$ MPa and $\alpha_1 = 26.76$ (mean value from eleven specimens). Therefore, the constitutive equation of the TM in the Ogden form is derived as

$$\sigma = 0.03(\lambda^{25.76} - \lambda^{-14.38}) \quad (0 \leq \sigma \leq 1.0 \text{ MPa}, 1 \leq \lambda \leq 1.15) \quad (4.1)$$

Meanwhile, based on Eq. (3.7), the Young's modulus-strain relationship of the TM in the Ogden form is derived as

$$\frac{d\sigma}{d\lambda} = 0.88\lambda^{24.76} + 0.49\lambda^{-15.38} \quad (0 \leq \sigma \leq 1.0 \text{ MPa}, 1 \leq \lambda \leq 1.15) \quad (4.2)$$

It was noted that the behavior of the TM was different at different stress levels. Therefore, following Eq. (3.8), the Young's modulus-stress relationship of the TM was derived over three stress ranges: 0~0.1, 0.1~0.3, and 0.3~1.0 MPa. Figure 4.4A shows Young's modulus-stress relationships for eleven individual TMs and Fig. 4.4B represents the mean and standard deviation. As shown in Fig. 4.4, the modulus $\frac{d\sigma}{d\lambda}$ is linearly increased with the stress σ . Through a two degrees polynomial curve fitting process, the Young's modulus-stress relationship of the TM in the form of Eq. (3.8) is derived over three stress ranges as

$$\begin{aligned}\frac{d\sigma}{d\lambda} &= 32.16\sigma + 0.398 & (0 \leq \sigma < 0.1 \text{ MPa}) \\ \frac{d\sigma}{d\lambda} &= 29.75\sigma + 0.645 & (0.1 \leq \sigma \leq 0.3 \text{ MPa}) \\ \frac{d\sigma}{d\lambda} &= 17.65\sigma + 4.274 & (0.3 < \sigma \leq 1.0 \text{ MPa})\end{aligned}\tag{4.3}$$

Eq. (4.3) suggests that the Young's modulus of the TM increases faster at a low stress level than that at a high stress level. There is no significant difference on the modulus at stress levels 0 ~ 0.1 MPa and 0.1 ~ 0.3 MPa.

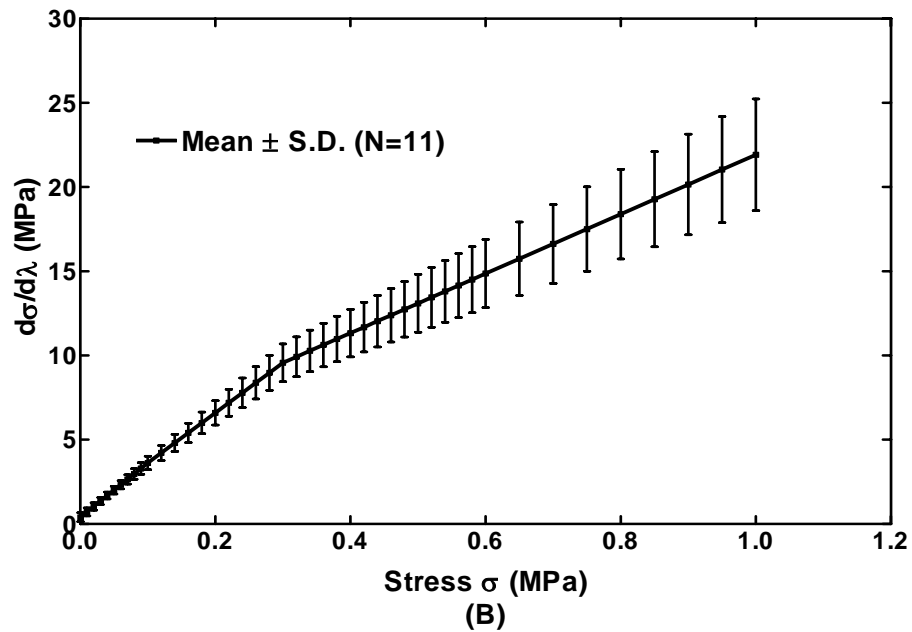
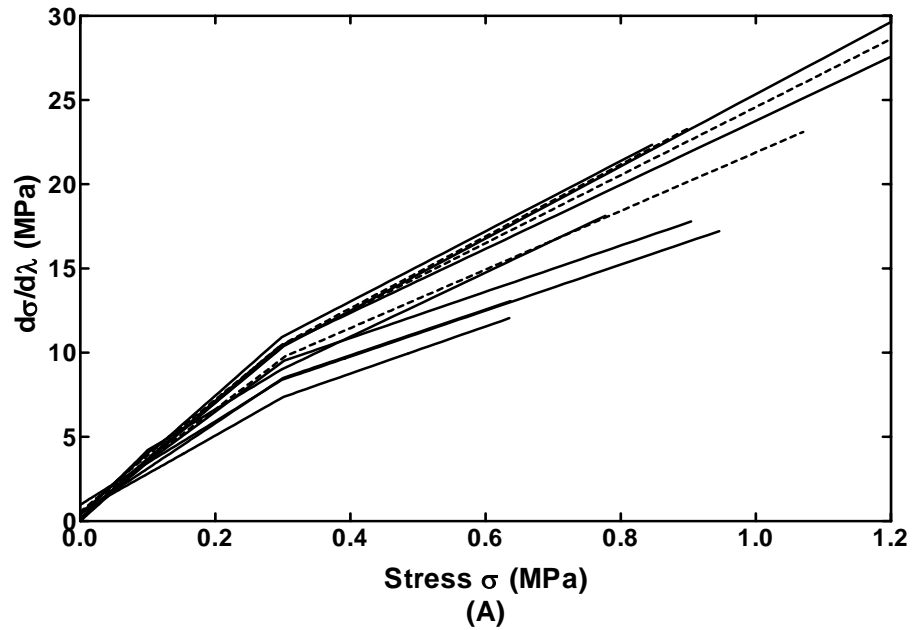


Figure 4.4 (A) Young's modulus-stress curves of eleven TM specimens under uniaxial loading tests obtained from three stress ranges: 0~0.1, 0.1~0.3 and 0.3~1 MPa. (B) The mean value of Young's modulus-stress curves of eleven TM specimens with standard deviation (S.D.) bars over three stress ranges as in (A).

Integration of Eq. (4.3) gives another form of the constitutive equation of the TM as

$$\begin{aligned}
 \sigma &= 0.01e^{32.16(\lambda-1)} - 0.01 & (0 \leq \sigma < 0.1 \text{ MPa}) \\
 \sigma &= 0.14e^{29.75(\lambda-1.06)} - 0.02 & (0.1 \leq \sigma \leq 0.3 \text{ MPa}) \\
 \sigma &= 0.61e^{17.65(\lambda-1.1)} - 0.24 & (0.3 < \sigma \leq 1.0 \text{ MPa})
 \end{aligned} \tag{4.4}$$

The integration constants are determined by the initial stress-strain value, i.e. $\sigma = 0$ when $\lambda = 1$. Eq. (4.4) shows that the constitutive equation of the TM could be represented by different exponential functions at different stress ranges.

Figure 4.5 shows the stress relaxation behavior of the TM obtained from nine specimens (two of eleven TM specimens do not have relaxation results). The normalized stress relaxation function $G(t)$ in y-axis is defined as the ratio between the stress $\sigma(t)$ at time t and the initial stress σ_0 . The initial strain rate used for this study is 1.8 mm/sec, 18 times of the strain rate used in the uniaxial tensile test. The mean initial stress σ_0 for nine specimens is 1.02 MPa. The stress $\sigma(t)$ decreases with time and finally it reaches a relatively stable state after 120 seconds. The mean normalized relaxation function $G(t)$ with standard deviation is shown in Fig. 4.5 as well. It is found that the stress relaxation of the TM is fast at the beginning. Within 1 sec, 10% of the stress is relaxed; at 5 sec, 20% of the stress is relaxed; after 50 sec, the stress relaxation gradually tends stable and finally, on average, 35% of the stress is totally relaxed. The mean stress after total relaxation is 0.64 MPa. The change of the stress with time under the constant stretch indicates that the human TM is a typical viscoelastic material. However, the viscoelastic property in response to acoustic excitation needs future study on dynamic behavior of the TM.

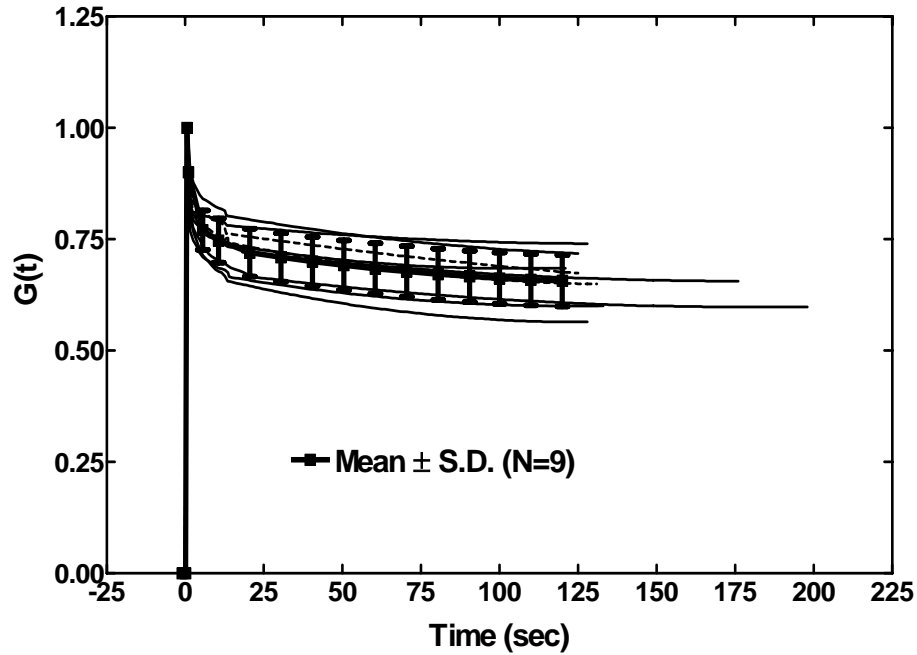


Figure 4.5 Normalized stress relaxation function $G(t)$ of nine TM specimens from stress relaxation tests. The solid line shows the mean value of $G(t)$ with standard deviation (S.D.) bars.

Table 4.1 lists the ultimate stress or failure stress and stretch ratio for eleven TM specimens with the standard deviation (S.D.). The mean failure stress is 1.66 MPa, while the mean failure stretch ratio is 1.23. The breaking location of TM specimens is in the midsubstance as observed for all specimens.

Table 4.1: Ultimate stress and stretch ratio of TM specimens (N=11)

	TM1	TM2	TM3	TM4	TM5	TM6	TM7	TM8	TM9	TM10	TM11	Mean	S.D.(±)
Failure Stress (MPa)	2.27	1.14	2.35	2.89	1.08	1.01	1.10	1.40	0.93	2.03	2.07	1.66	0.67
Failure Stretch Ratio λ	1.26	1.17	1.28	1.24	1.19	1.25	1.16	1.32	1.18	1.19	1.35	1.23	0.06

S.D. Standard Deviation

4.2 Discussion on the Results

In this study, mechanical experiments were carried out on TM samples harvested from fresh cadaver temporal bones. The experimental results were analyzed using the hyperelastic Ogden model and it was the first time of using digital image correlation method to measure the deformation of ear tissues. Two forms of the constitutive equation and the Young's modulus-stress or strain relationship of the TM at low stress levels (0~1 MPa) were derived in Eqs. (4.1) ~ (4.4). It is generally accepted that the representation of empirical data is a non-unique process in practice [Fung, 1993]. Therefore, both Eq. (4.1) and Eq. (4.4) can be used to describe the behavior of the TM equally well even though they have different expressions due to different approaches.

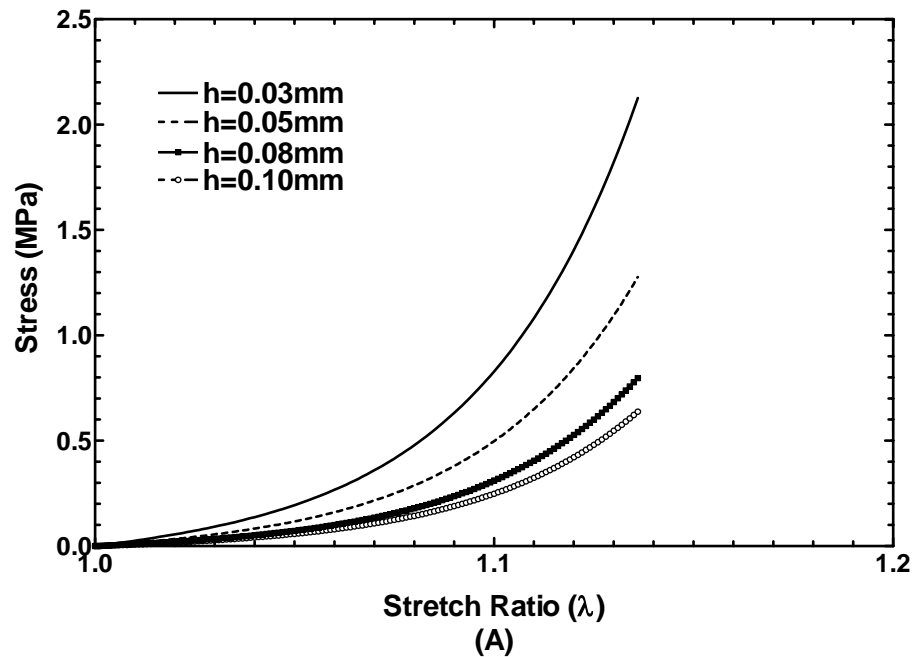
The previously published Young's modulus of the TM is a single value of elastic property ranging from 20 to 400 MPa (20 MPa by von Békésy from beam-bending test, 40 MPa by Kirikae from dynamic tension vibration test, 23 MPa by Decraemer *et al.* from uniaxial tensile test and 30 ~ 90 or 100 ~ 400 MPa by Fay *et al.* from two modeling correlation methods). The Young's modulus obtained in this study varies from 0.4 to 22 MPa over the stress range from 0 to 1 MPa and associates with the constitutive equation of the tissue. The variation of the Young's modulus within a low stress range from 0 to 1 MPa, constitutive equations and the failure stress and strain of the TM obtained in this study are first time reported in literature. The results provide a better understanding of mechanical properties of the TM over low and high stress levels. Our studies also show that the published Young's modulus data of the TM were measured at higher stress levels from 6 to 12 MPa (Decraemer *et al.*). The results presented in this study may help to

investigate the dynamic behavior of the TM and to understand whether the pre-stress exists in the TM structure, an interesting topic in ear tissue biomechanics.

The hysteresis phenomenon was observed in TM specimens during the loading and unloading process as shown in Fig. 4.1. The stress relaxation functions of TM specimens were obtained and displayed in Fig. 4.5. These results show that the TM is a typical viscoelastic material with the constitutive properties related to the stress and strain history. The hysteresis or the lag of unloading curves to loading curves indicates the loss of internal energy and entropy of the specimen during the deformation. Therefore, the loading process may be more meaningful for describing the behavior of the tissue. In this study, only loading curves in uniaxial tensile tests were analyzed for mechanical properties of the TM. It is expected that analysis on unloading curves can result in similar straight lines as those in Fig. 4.4, but with different slopes.

For the tensile test on biological soft tissues with small dimensions, it is important to verify the boundary effect on measurement of the sample deformation. In this study, digital image correlation method was applied to calculate the axial strain distribution on the TM specimen. The uniform strain distribution across the membrane from DIC analysis (Fig. 4.2B and 4.2D) and the agreement between stress-strain curves of TM specimens obtained by two methods (Fig. 4.2A and 4.2C) provide a standard for accepting experimental data. All the experimental results from uniaxial tensile tests have been double checked using DIC method for final acceptance. It is expected that digital image correlation method, as a useful tool for studying mechanical properties of the TM, may be extended to other ear tissues.

To estimate the error induced by measurement of the specimen thickness in this study, different thickness values were assumed for one TM specimen to calculate its stress-strain relationship and Young's modulus-stress relationship. When the thickness is varied from 0.03 to 0.05, 0.08 and 0.1 mm, the corresponding stress-stretch ratio curves are shown in Fig. 4.6A and Young's modulus-stress relationships are shown in Fig. 4.6B. As seen in Fig. 4.6A, stress-stretch ratio curves are affected by the thickness, but Young's modulus-stress curves only have slight differences as shown in Fig. 4.6B. The Young's modulus of the TM with four different thickness values at the stress level of 0.5 MPa are calculated as: 14.6, 13.7, 13.1 and 13.0 MPa, decreasing slightly with the thickness increasing. The maximum variance is less than 1.6 MPa. This indicates that the Young's modulus of the TM reported in this paper is reliable.



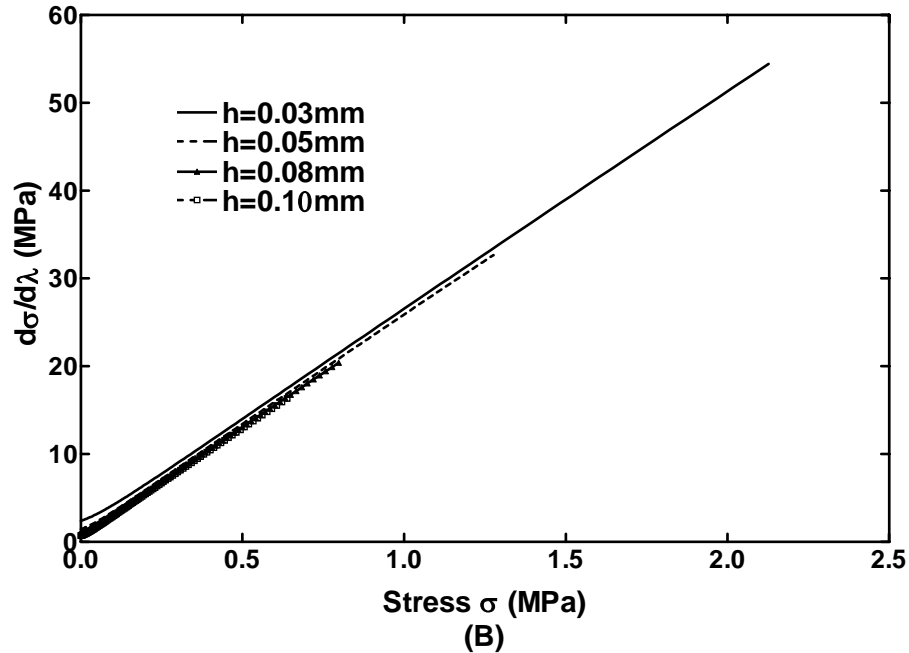


Figure 4.6 Effect of TM thickness on stress-stretch ratio curves and Young's modulus-stress curves. The thickness (h) was changed from 0.03 to 0.05, 0.08 and 0.1 mm.

In this study, the specimens were harvested from the posterior site of the TM and uniaxial tensile tests were performed along the superior-inferior or longitudinal direction of specimens. The TM was considered as an isotropic and homogeneous material for macro-mechanics study. However, the human TM is a multi-layer structure with collagen fibers along radial and circumferential directions ^[Lim, 1970]. The ultrastructure of the TM should be considered in mechanical measurements. Therefore, two future studies maybe performed following the present work. First, the finite element modeling and analysis technique will be used to simulate the ultrastructure of the TM and derive the stress-strain relationship of the TM under the uniaxial tensile test. In the meantime, specimens may be harvested from different locations such as the inferior or anterior site of the TM. The relationship between mechanical properties and the structure of the TM will be finally derived. Second, nanoindentation techniques will be conducted in TM samples to

measure mechanical properties of the TM at the micro- or nano-scale level. Research collaborations with Oklahoma State University are currently conducted in this direction.

In summary, the results obtained in this study indicate that the human TM is a typical viscoelastic material. The constitutive equation or stress-strain relationship of the TM and Young's modulus-stress or strain relationship are derived at the stress range of 0~1 MPa. The data provided in this study add useful information for ear biomechanics on both experimental measurement and theoretical analysis of ear tissues.

CHAPTER 5

RESULTS OF TENDONS AND LIGAMENT

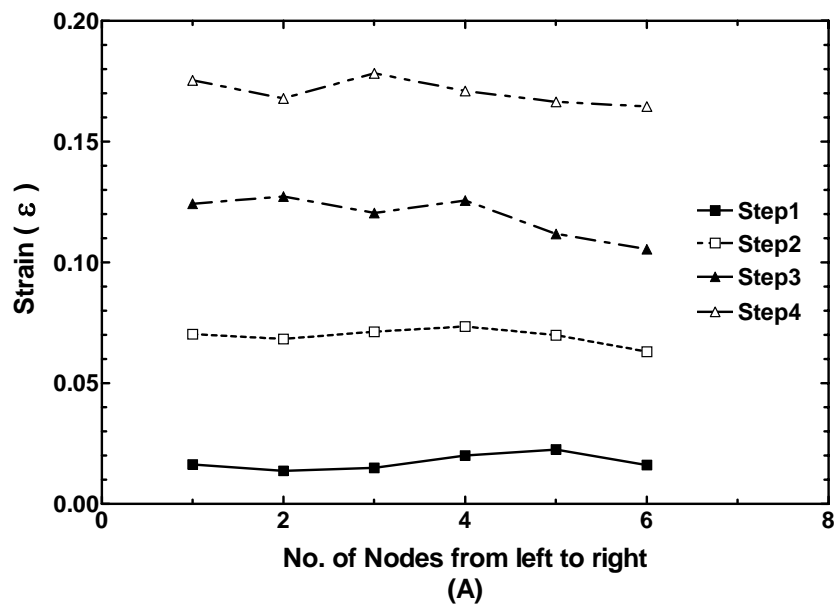
Mechanical properties of the stapedial tendon, tensor tympani tendon and anterior malleolar ligament were obtained from experimental measurement and modeling analysis. The results are given in the following sections with the discussion on each tissue. The results of the stapedial tendon and tensor tympani tendon are in press with Transactions of the ASME - Journal of Biomechanical Engineering [Cheng and Gan, 2007b] and Medical Engineering & Physics [Cheng and Gan, 2007c]. The manuscript of the anterior malleolar ligament was submitted to Biomechanics and Modeling in Mechanobiology [Cheng and Gan, 2007d] and is under review.

5.1 Stapedial Tendon

5.1.1 Mechanical Properties of the Stapedial Tendon

Fig. 5.1A showed the transverse strain distribution across a stapedial tendon specimen from the DIC analysis at four steps with a constant time interval, and Fig. 5.1B showed the comparison of the stress-stretch loading curve measured from the MTS (solid line) and derived from the DIC method (broken line). The relatively uniform strain distribution across the specimen at each step (Fig. 5.1A) indicated that the boundary effect was

limited in the experiment. The stress-strain curve of the stapedial tendon obtained from the MTS and DIC generally agreed with each other (Fig. 5.1B). However, there is some deviation observed above 25% stretch (or 1.25), which may be caused by sensitivity level of the DIC method for large deformation. In MTS test, the specimen was treated as a whole unit and the grip to grip displacement was used for strain calculation. The results from DIC were relied on local micro-deformation in the tissue, which may have different response at large deformation.



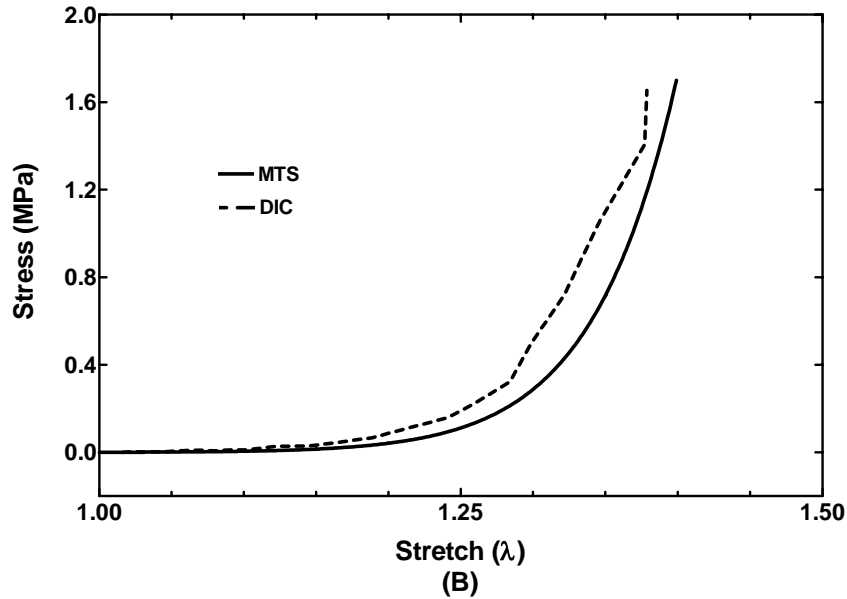


Figure 5.1 (A) Transverse strain distribution across the tendon specimen calculated from DIC analysis at four time steps. The time interval for each step is 5 sec. (B) Comparison of stress-stretch loading curves of a stapedial tendon specimen obtained from MTS experiment (solid line) and DIC analysis (broken line).

Figure 5.2 showed stress-stretch curves of a stapedial tendon specimen with raw experimental data as well as the smoothed data fitted into the Ogden model. The correlation coefficient of model fitting for this specimen was 0.99, and the mean correlation coefficient for all specimens was 0.98 with standard deviation of 0.03. This indicated that the Ogden model fitted the experimental data well for the stapedial tendon. The hysteresis phenomenon was also shown in Fig. 5.2 by different traces of loading and unloading curves.

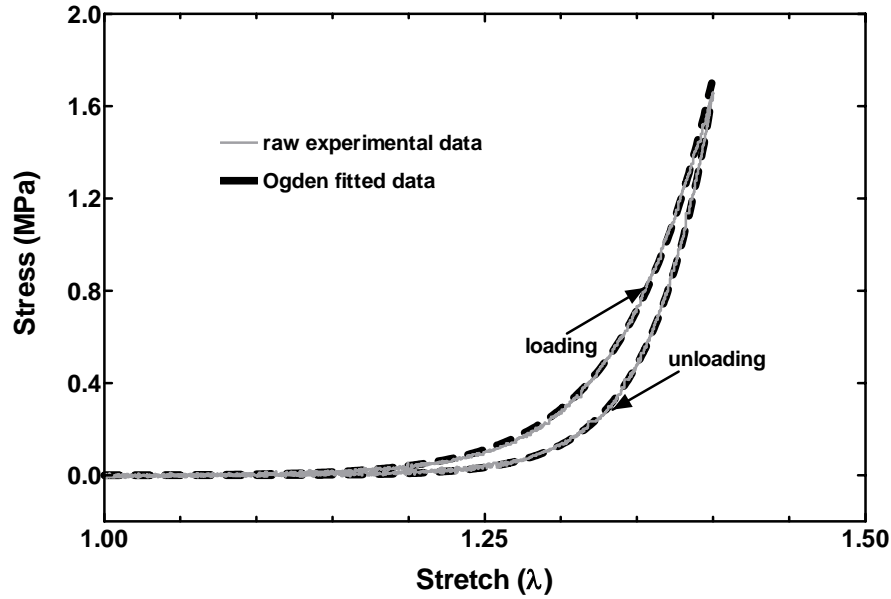


Figure 5.2 Stress-stretch curves of a stapedal tendon specimen obtained from the uniaxial tensile test. The wave-like lines were the original stress-stretch curve recorded in MTS. The smooth lines were obtained after the Ogden model fitting process. A hysteresis loop was observed for the stapedal tendon.

Figure 5.3A showed stress-stretch curves of twelve stapedal tendon specimens under the loading process of uniaxial tensile tests, and Fig. 5.3B displayed the mean curve with standard deviation. The standard deviation was increasing with the increasing stress, but the relative standard deviation remained the same at 0.50, which indicated that the variation between individual specimens was not changing with the stress level. It was also seen that the stress increased slowly at the beginning. The stress-stretch curve was almost flat when the stretch ratio was less than 1.2, and became stiffer when the stretch ratio continued increasing.

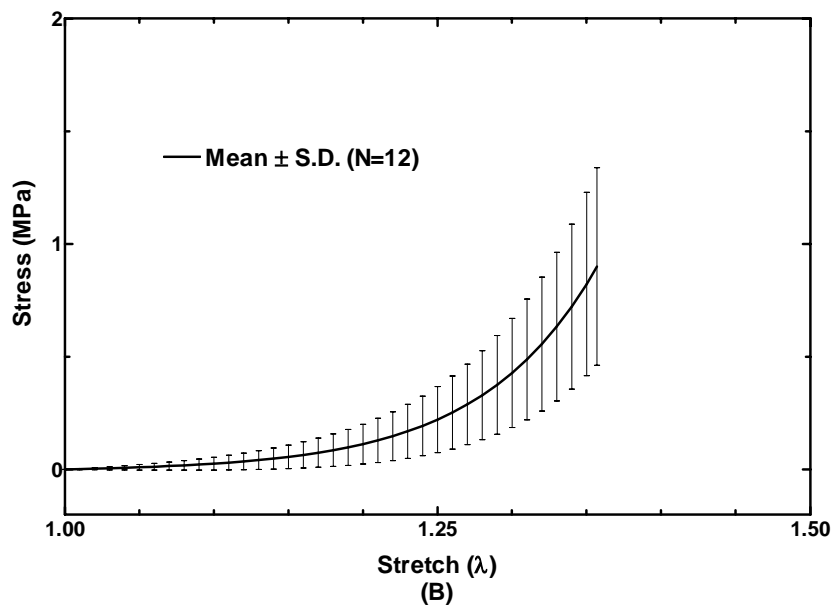
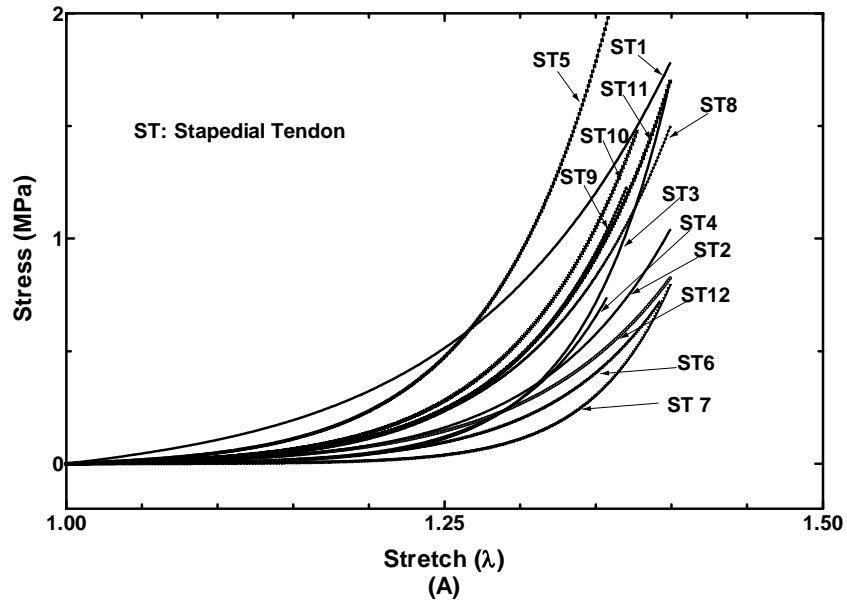


Figure 5.3 (A) Stress-stretch curves of twelve stapedial tendon (ST) specimens under uniaxial loading processes. The maximum stretch ratio λ was around 1.4 and the displacement rate was 0.01 mm/sec. (B) The mean curve of stress-stretch relationships obtained from twelve stapedial tendon specimens with standard deviation (S.D.) bars.

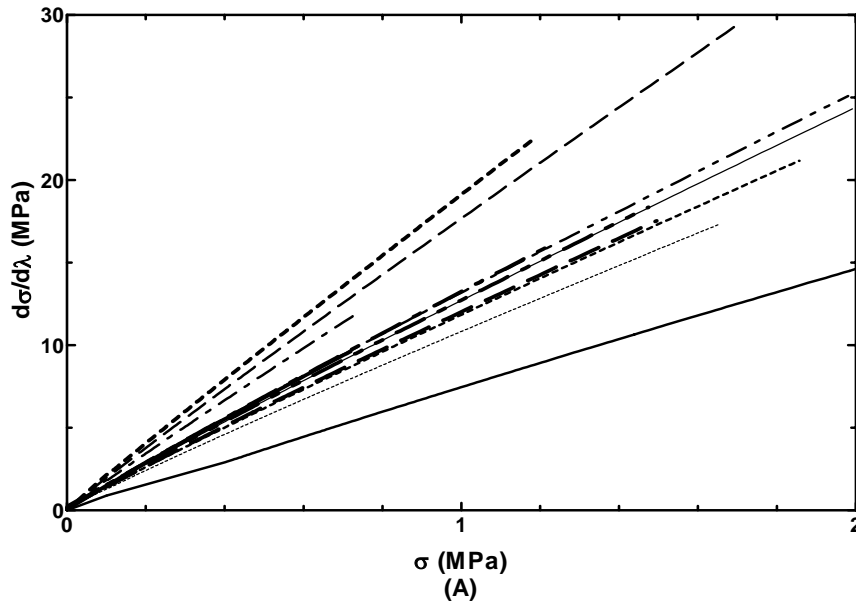
The constitutive equation of the stapedial tendon was derived based on MTS measured stress-strain curves (mean curve in Fig. 5.3B) after fitting into the Ogden

model. Two material constants were determined as $\mu_1=0.05$ MPa and $\alpha_1=17.40$ when the stretch ratio was less than 1.4. The constitutive equation was then derived as:

$$\sigma = 5.8 \times 10^{-3} (\lambda^{16.40} - \lambda^{-9.70}) \quad \text{for } 1.0 \leq \lambda < 1.4, 0 \leq \sigma \leq 1.45 \text{ MPa} \quad (5.1)$$

Using Eqs 3.6 and 3.7 in Chapter 3, the Young's modulus ($d\sigma/d\lambda$) and stress (σ) relationships for these stapelial tendon specimens were derived and shown in Fig. 5.4. The Young's modulus is linearly increased with the stress (Fig. 5.4A) and the standard deviation increases as the stress increases (Fig. 5.4B). The Young's modulus-stress relationship of the stapelial tendon was represented by a straight line as:

$$d\sigma/d\lambda = 11.93\sigma + 0.35 \quad \text{for } 0 \leq \sigma \leq 1.5 \text{ MPa}, 1 \leq \lambda \leq 1.4 \quad (5.2)$$



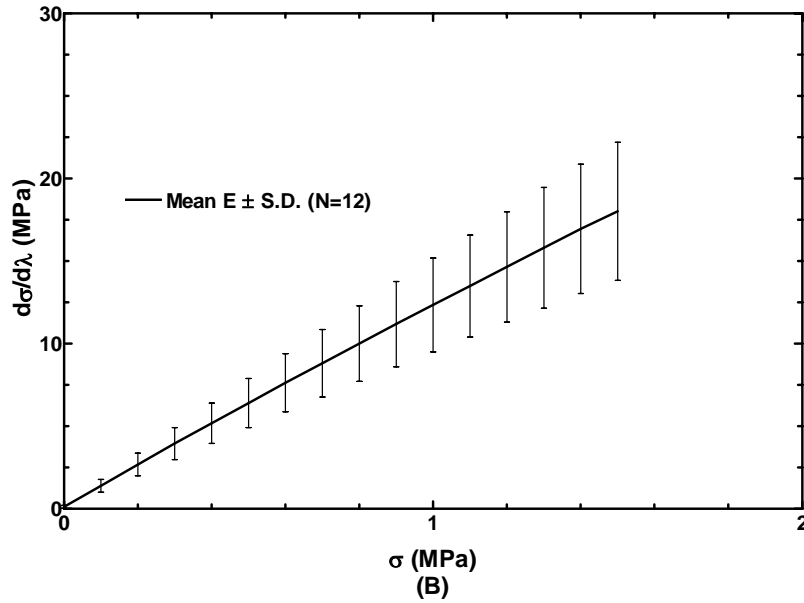


Figure 5.4 (A) Young's modulus-stress curves of twelve stapelial tendon specimens under uniaxial loading tests. (B) The mean value of Young's modulus-stress curves of twelve stapelial tendon specimens with standard deviation (S.D.) bars.

Figure 5.5A showed the stress relaxation behavior of the stapelial tendon obtained from nine specimens. The normalized stress relaxation function $G(t)$ was defined as the ratio between the stress $\sigma(t)$ at time t and initial stress σ_0 . The $\sigma(t)$ or $G(t)$ decreased with time and finally reached a stable state at 120 sec, or the rate of stress change was less than 0.1% / sec. The stress was then considered as fully relaxed. The mean normalized relaxation function with standard deviation was shown in Fig. 5.5B. The mean initial stress was 2.62 MPa. After fully relaxation, on average, 45% of the initial stress was totally relaxed. The mean stress after total relaxation is 1.44 MPa

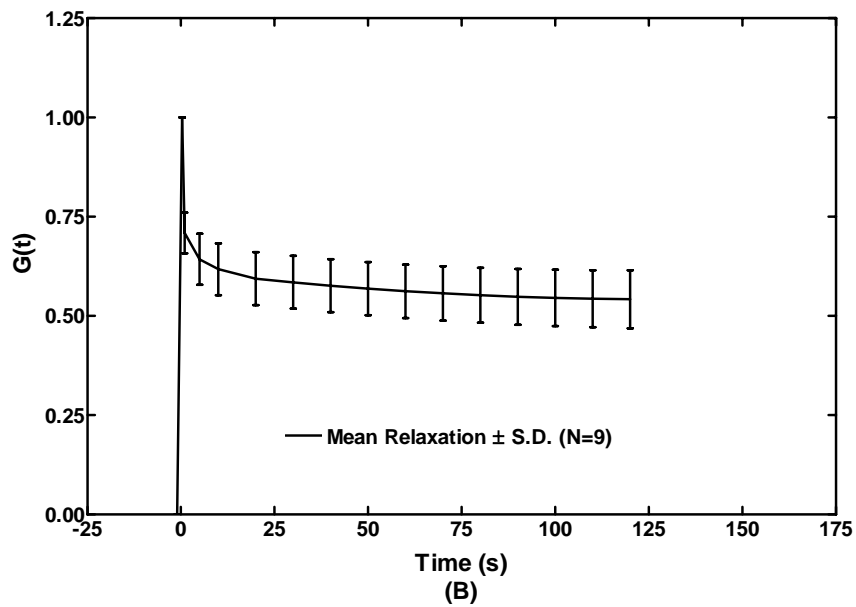
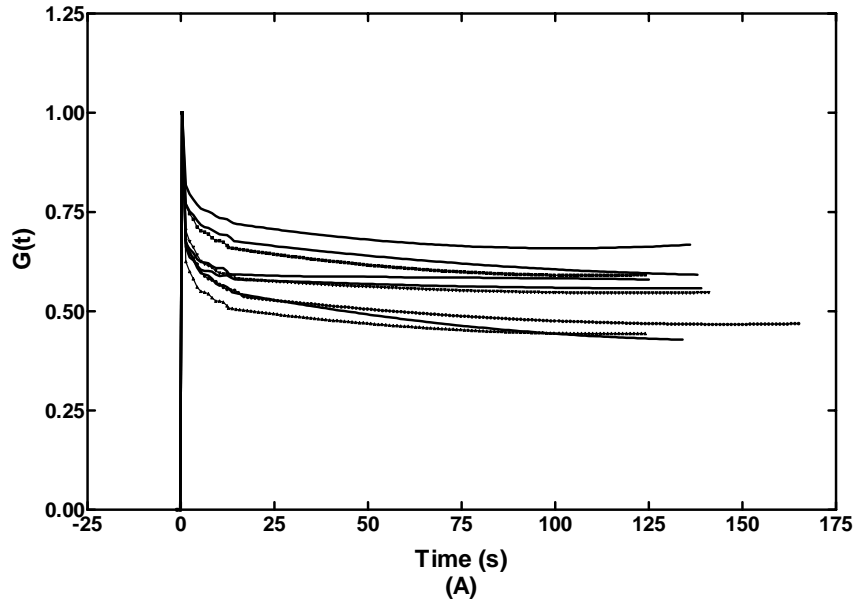


Figure 5.5 (A) Normalized stress relaxation function $G(t)$ obtained from nine stapedial tendon specimens in stress relaxation tests. (B) The mean curve of $G(t)$ of twelve tendon specimens with standard deviation (S.D.) bars.

Table 5.1 listed the ultimate stress and stretch ratio for eleven stapedial tendon specimens (one specimen was damaged before the failure test). The breaking location of all specimens occurred about midsubstance.

Table 5.1: Ultimate stress and stretch of stapedial tendon (ST) specimens

	ST 1	ST 2	ST 3	ST 4	ST 5	ST 6	ST 7	ST 8	ST 9	ST 10	ST 11	Mean	S.D. (\pm)
Ultimate Stress (MPa)	5.43	3.59	2.06	7.32	2.34	7.39	2.70	2.08	3.31	4.76	3.44	4.04	1.95
Ultimate Stretch λ	1.80	1.67	1.45	1.55	1.72	1.78	1.62	1.51	1.58	1.59	1.85	1.65	0.13

S.D. Standard Deviation

5.1.2 Discussion on Stapedial Tendon Results

In this study, mechanical experiments were carried out on stapedial tendon specimens of human cadaver ears in MTS. The DIC method was used to assess the boundary effect on experimental data. The grip-to-grip strain of the tissue measured from experiments, which agreed with the strain calculated from the DIC method, was further used to derive the constitutive equation of the stapedial tendon.

The nonlinear stress-strain relationship of the stapedial tendon shown in Fig. 5.3 will result in stress-dependent elastic modulus for the tendon. The modulus would increase as the stress increases, which is the typical mechanical behavior of soft tissues. Therefore, the data reported in this study can be used to improve FE models of human middle ear. A varying modulus of the stapedial tendon at different stress levels may be used to simulate the middle ear response to the change of ear physiological condition such as the otitis media with effusion.

Compared with large ligaments or tendons such as the human medial collateral ligament (MCL) [Weiss, 2002], the stapedial tendon is much softer. The stress in stapedial tendon was 0.025 MPa under the stretch of 1.1, while it was 24 MPa (about 1000 times) under the same stretch in MCL. The difference between these two tissues may be related to their functions. The stapedial tendon works as one of suspensory elements in middle

ear to maintain the stability of ossicular chain in response to sound pressure, while the MCL primarily provides restraint to valgus stress at knee during walking.

5.2 Tensor Tympani Tendon

5.2.1 Mechanical Properties of the Tensor Tympani Tendon

The transverse strain distribution across a tensor tympani tendon specimen from the DIC analysis at four steps is shown in Fig. 5.6A. The relatively uniform strain distribution across the specimen indicated that the boundary effect that might be introduced by small dimension of the tissue is limited. Comparison between the stress-stretch loading curve of a tensor tympani tendon specimen directly from the uniaxial tensile test (solid line) and that from the DIC method (broken line) is shown in Fig. 5.6B. The results from two approaches are in good agreement up to the stretch ratio of 1.25. However, there is some deviation observed above 35% stretch (or $\lambda = 1.35$), which was probably caused by the same reason as we mentioned above for the stapedial tendon, i.e., the sensitivity level of the DIC method for large deformation.. All the results reported in this paper were checked through this process to ensure accuracy of the strain used in data analysis.

Figure 5.7A shows stress-stretch curves of ten specimens under loading process. Most specimens were stretched up to λ of 1.4. Figure 7B displays the mean and S.D. It is clearly seen that the absolute S.D. increases with the stress, while the relative S.D. remains the same at 0.12. The stress response of the tendon is almost flat at low strain level, but it stiffens rapidly after the stretch ratio λ increases above 1.2

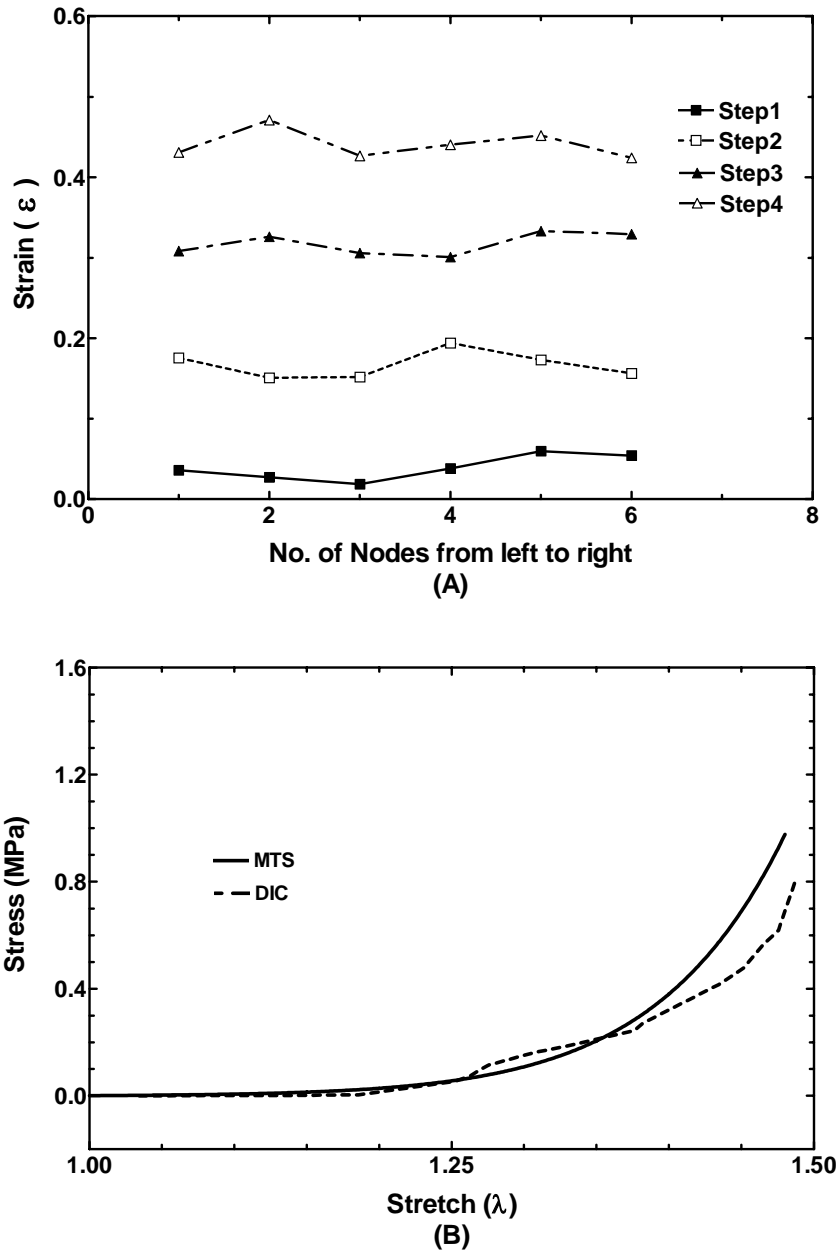


Figure 5.6 (A) Transverse strain distribution across the tensor tympani tendon specimen calculated from DIC analysis at four time steps. (B) Comparison of the stress-stretch curve of a tensor tympani tendon specimen obtained from DIC analysis (broken line) and MTS measurement (solid line).

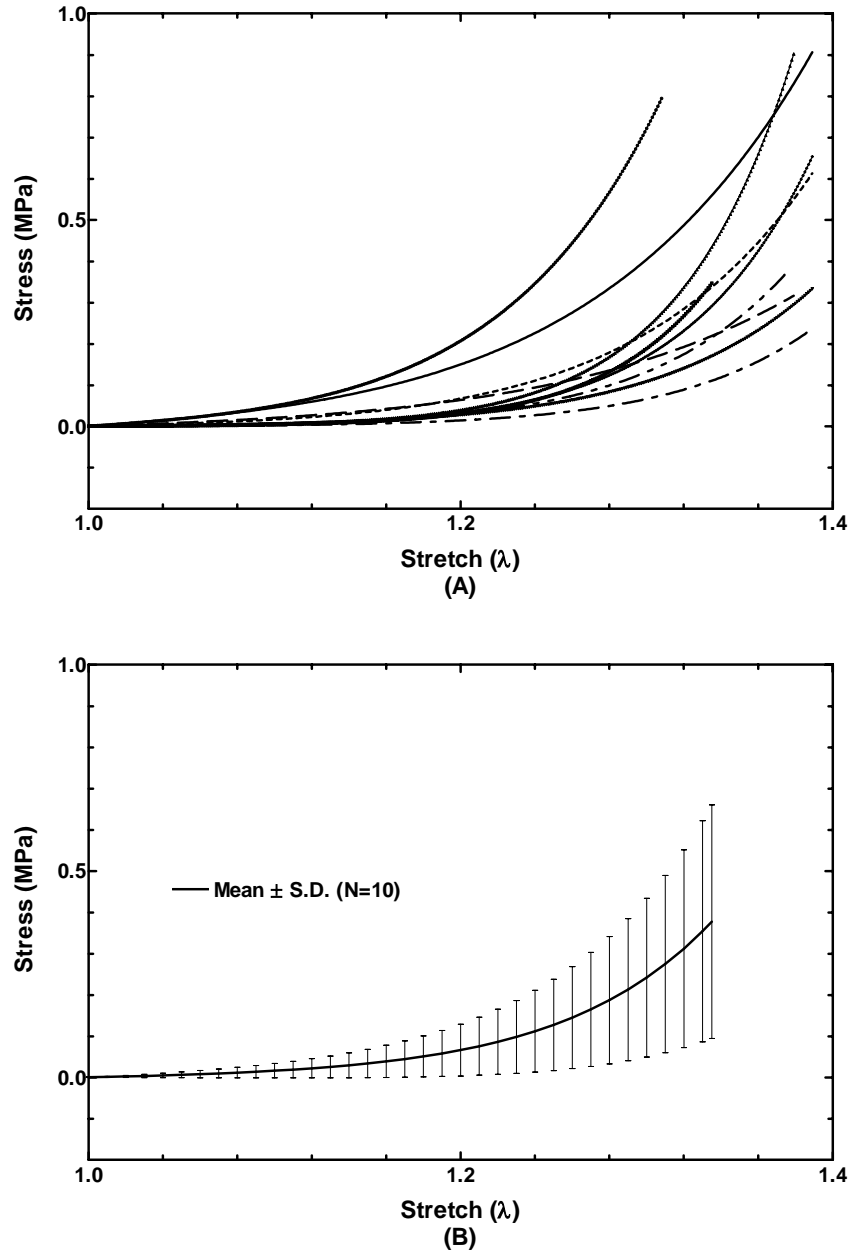


Figure 5.7 (A) Stress-stretch curves of ten tensor tympani tendon specimens under uniaxial loading processes. The maximum stretch ratio λ was around 1.4 and the elongation rate was 0.01 mm/sec. (B) The mean value of stress-stretch relationships of ten tensor tympani tendon specimens with standard deviation (S.D.) bars.

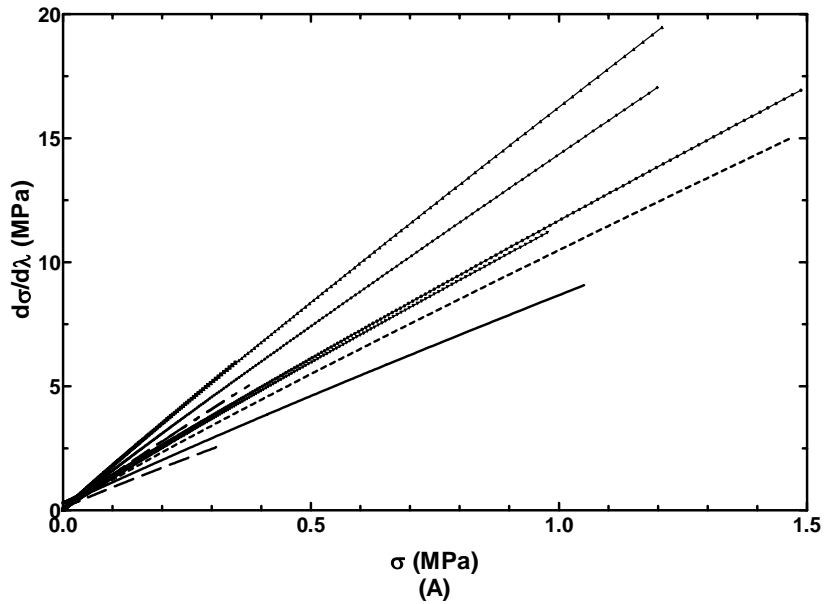
Through the data iteration process, two material constants, μ_1 and α_1 , were determined as $\mu_1 = 0.01$ MPa and $\alpha_1 = 23.52$ using the mean experimental data of Fig. 5.7.

Therefore, the constitutive equation of the tensor tympani tendon in the Ogden form is derived as

$$\sigma = 8.5 \times 10^{-4} (\lambda^{22.52} - \lambda^{-12.76}) \quad \text{for } 0 \leq \sigma \leq 1.0 \text{ MPa}, 1 \leq \lambda < 1.4 \quad (5.3)$$

The Young's modulus of each tensor tympani tendon derived from Eq. (3.7) is plotted against the stress derived from Eq. (3.6) as shown in Fig. 5.8A. The mean Young's modulus and stress with S.D. is shown in Fig. 5.8B. It is clearly seen that the Young's modulus of the tensor tympani tendon is linearly increasing with the stress, the value varies from 0.14 to 12.34 MPa when the stress increases from 0 to 1 MPa. The Young's modulus-stress relationship of the tensor tympani tendon is thus expressed as

$$\frac{d\sigma}{d\lambda} = 12.08\sigma + 0.26 \quad \text{for } 0 \leq \sigma \leq 1.0 \text{ MPa}, 1 \leq \lambda \leq 1.4 \quad (5.4)$$



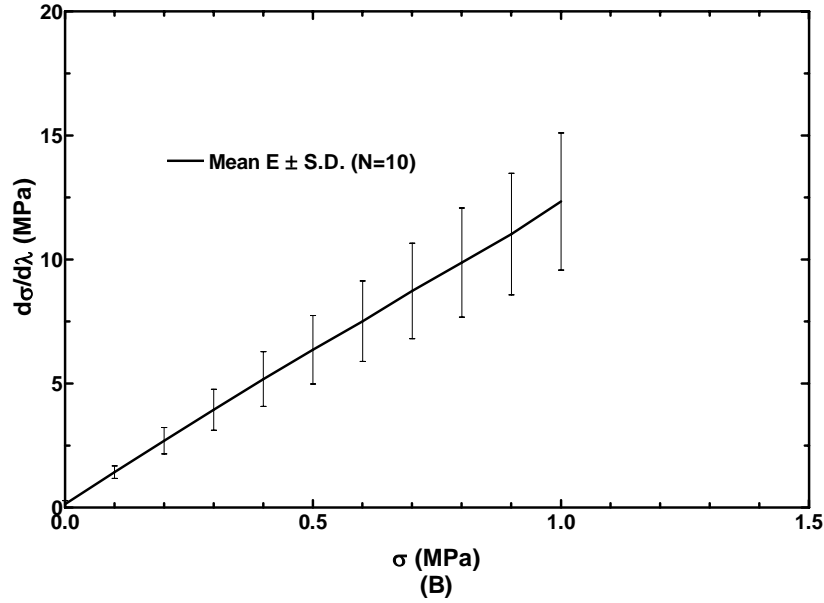


Figure 5.8 (A) Young's modulus-stress curves of ten tensor tympani tendon specimens under uniaxial loading processes. (B) The mean value of Young's modulus-stress curves of ten tensor tympani tendon specimens with standard deviation (S.D.) bars.

Figure 5.9A shows normalized stress relaxation functions of ten tendon specimens. The stress $\sigma(t)$ decreases with time and finally reaches a stable state after 120 seconds. The normalized stress relaxation function $G(t)$ is defined as the ratio between stress $\sigma(t)$ and the initial stress σ_0 . The mean normalized stress relaxation function $G(t)$ with S.D. is shown in Fig. 5.9B. The mean initial stress for ten specimens is 1.33 MPa. Within one second, 21% of the stress is relaxed; after 5 second, 27% of the stress is relaxed; and finally after 120 second, 37% of the stress is totally relaxed. The mean stress after total relaxation is 0.84 MPa.

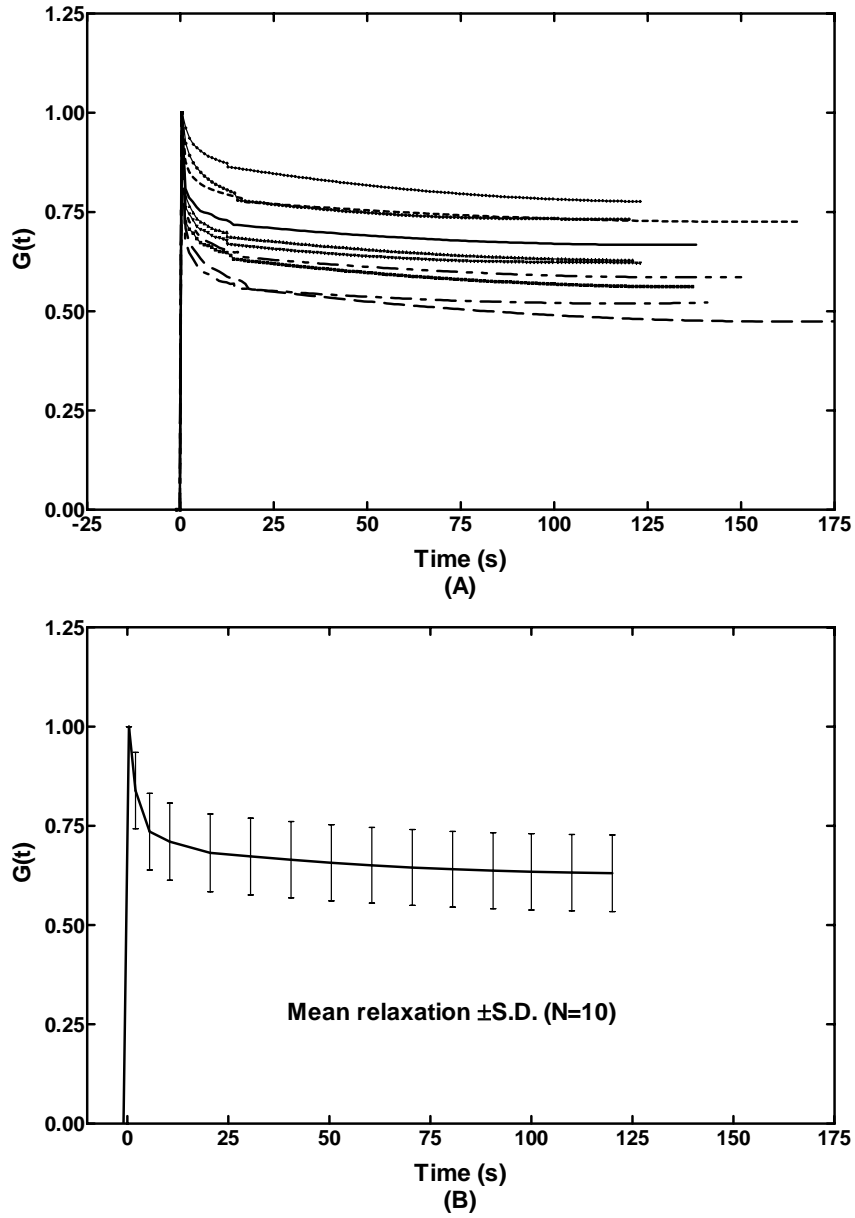


Figure 5.9 (A) Normalized stress relaxation functions $G(t)$ of ten tensor tympani tendon specimens from stress relaxation tests. (B) The mean value of $G(t)$ of ten tensor tympani tendon specimens with standard deviation (S.D.) bars.

Table 5.2 lists the failure stress and stretch of ten tensor tympani tendon specimens. The mean failure stress is 2.25 MPa with S.D. of 1.47 MPa, which shows the strength variation among tested individual specimens. The breaking location of all specimens occurred in their midsubstance.

Table 5.2: Ultimate stress and stretch of tensor tympani tendon (TTT) specimens

	TTT 1	TTT 2	TTT 3	TTT 4	TTT 5	TTT 6	TTT 7	TTT 8	TTT 9	TTT 10	Mean	S.D.(±)
Failure Stress (MPa)	1.61	2.06	0.98	0.58	1.55	1.81	2.65	2.98	2.38	5.88	2.25	1.47
Failure Stretch λ	1.53	1.59	1.70	1.59	1.88	1.71	1.57	1.74	1.65	1.69	1.66	0.10

S.D. Standard Deviation

5.2.2 Finite Element Modeling Results

The stress-stretch ratio relationships of five FE tensor tympani tendon models are compared with the mean stress-stretch ratio relationship of the tendon from experiments as shown in Fig. 5.10. The material constants from FE analysis are listed in Table 5.3. It is clearly seen that the FE model #3 with the fiber density of 80% has the closest behavior as that from experiments. The material constants of the FE model #3, $\mu_1 = 0.007$ MPa and $\alpha_1 = 20$, are also close to the values obtained from experimental data.

Table 5.3: Material constants of tensor tympani tendon obtained from FE models

Model #	Fiber/substance ratio k	Fiber Density	μ_1 (MPa)	α_1
1	2.3	70%	0.008	25
2	3.0	75%	0.007	32
3	4.0	80%	0.007	20
4	5.7	85%	0.006	19
5	9.0	90%	0.005	23

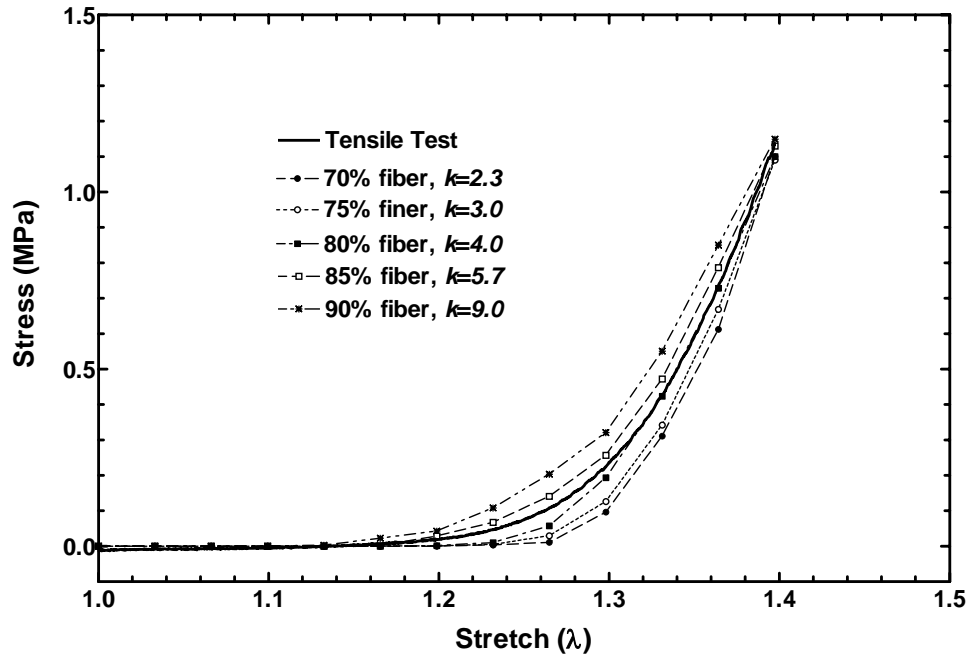


Figure 5.10 Comparison between stress-stretch curves of the tensor tympani tendon obtained from FE models and the mean curve measured from ten tendon specimens in uniaxial tensile tests. The broken lines with symbols representing modeling results from 5 FE tendon models. The solid line without symbols represents the experimental mean curve.

5.2.3 Discussion on Tensor Tympani Tendon Results

In this study, mechanical experiments were performed in tensor tympani tendon specimens. Digital image correlation method was applied to test the boundary effect on experiments. The experimental data were analyzed using the hyperelastic Ogden model to derive the stress-strain relationship (Fig. 5.7) and Young's modulus-stress relationship (Fig. 5.8). The constitutive equation (Eq. (5.3)) shows nonlinear elastic properties of the tensor tympani tendon for the first time in literature.

In stress relaxation test, an elongation rate of 1.8 mm/sec was used to elongate the specimen of about 0.6 mm (based on average specimen length and 40% elongation). This elongation rate is 180 times faster than the elongation rate used in tensile test (0.01

mm/sec) and can be considered as a sufficiently high rate of loading. The initial stress in specimen was imposed within 0.3 sec, which provided a reasonable approximation of the tensile stress instantaneously generated in the tissue ^[Fung, 1993]. However, compared with the ideal step function of stretching, the relaxation function obtained in this study would be slightly lower than that from ideality.

The SEM picture of a tensor tympani tendon specimen (Fig. 3.18A) shows that the tendon is mainly composed of collagen fibers which are embedded into ground substance matrix. However, it is difficult to calculate the fiber density of the tendon based on the picture. Therefore, five FE models of the tissue with varying fiber density were created to explore the relationship between the structure and properties of the tendon. The results in Fig. 5.10 suggest that the stress-strain curve shifts up when the fiber density increases. This indicates that the Young's modulus increases with the collagen fiber density and mechanical properties of the tendon are related to the composition of the tissue structure. Note that collagen fibrils of the tendon was assumed straight and uniformly distributed in FE model. In real cases, collagen fibrils could be crimped. The interaction between collagen fibers and ground substances would also contribute to elastic response of the tissue, which was not included in current study. In our future studies, a more accurate fiber structure of the tendon will be developed and the interaction between fibers and ground substances will be included.

In summary, the results obtained in this study indicate that the tensor tympani tendon is a viscoelastic material with nonlinear stress-strain relationship. The constitutive equation or stress-strain relationship of the tendon is dependent on stress or strain level. The hyperelastic Ogden model provides a good representation for non-linear behavior of

the tendon. The data reported in this paper add useful information to ear tissue biomechanics through both experimental measurement and theoretical modeling analysis.

5.3 Anterior Malleolar Ligament

5.3.1 Mechanical Properties of the Anterior Malleolar Ligament

Figure 5.11A shows the transverse strain distribution of an AML specimen from the DIC analysis at four selected steps during the uniaxial loading test. Fig. 5.11B shows the comparison of the strain measured directly from the MTS (broken line) and that from the DIC (solid line). The strain distribution (Fig. 5.11A) was relatively uniform across the specimen at each step, with a slight increase from the left to right side of the specimen at last two steps. In Fig. 5.11B, the strain from MTS and DIC are in general agreement, although the strain from DIC is slightly lower than that from MTS. These differences maybe induced by geometric and structural non-uniformity of the AML tissue and sensitivity of the DIC method on calculating the local deformation of the tissue. In general, Fig. 5.11 indicates that the boundary effect of experiment is limited and the results are reliable.

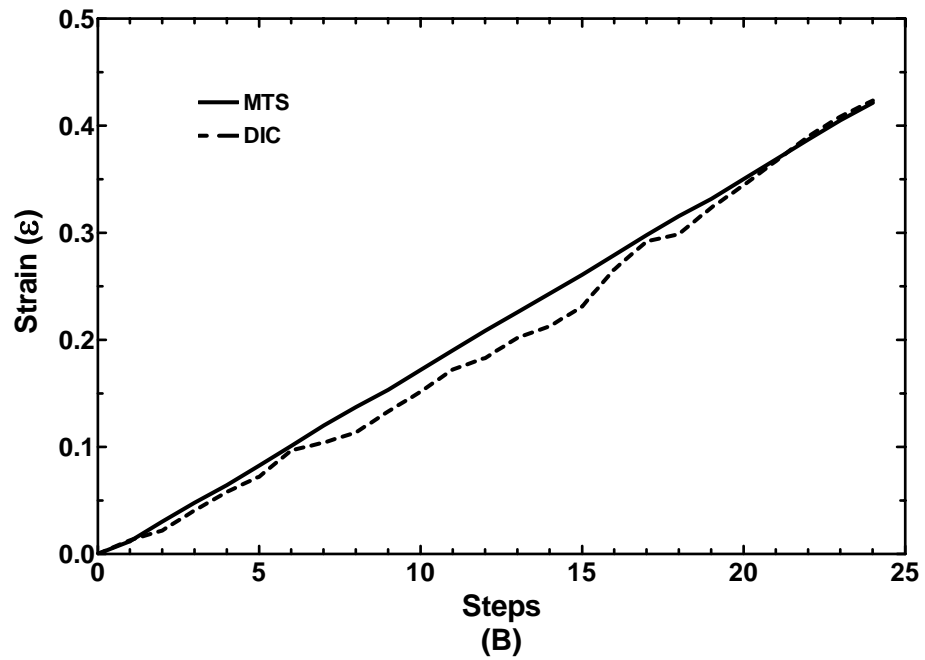
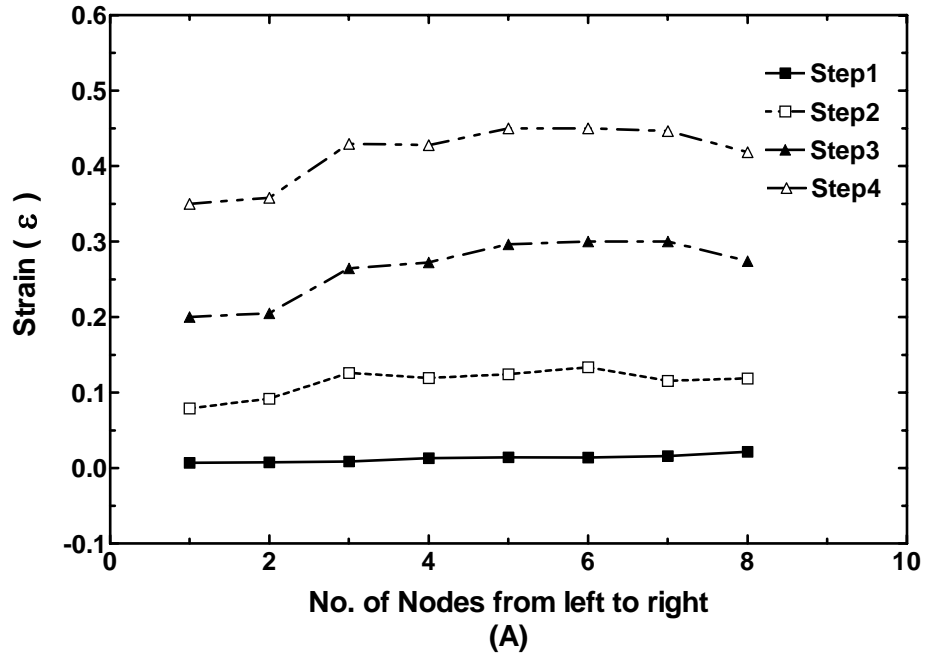
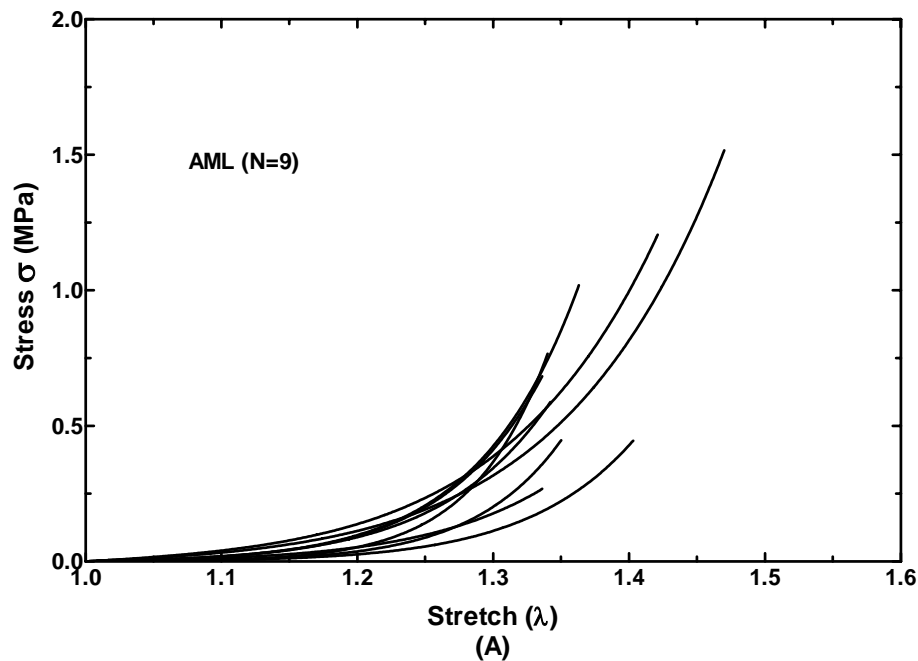


Figure 5.11 (A) Normal strain distribution across the transverse surface of the AML specimen calculated from DIC analysis at four time steps. The No. of nodes represents 8 locations (from left to right) across the specimen in the middle part of the grid. (B) Comparison of the strain obtained from MTS experiment (broken line) and DIC analysis (solid line).

Figure 5.12A shows stress-stretch curves of nine AML specimens derived from the stress measured in MTS and the stretch calculated from DIC for the loading process of uniaxial tensile tests. Fig. 5.12B displays the mean stress-stretch curve with standard deviation. A nonlinear stress-stretch relationship is clearly seen in Fig. 12. The standard deviation was increasing with the increasing stress, but the relative standard deviation remained the same at 0.50, which indicated that the variation between individual specimens was not changing with the stress level. It was also seen that the stress increased slowly at the beginning, and the stress-stretch curve was almost flat when the stretch ratio was less than 1.2. The curve became stiffer when the stretch ratio continued increasing.



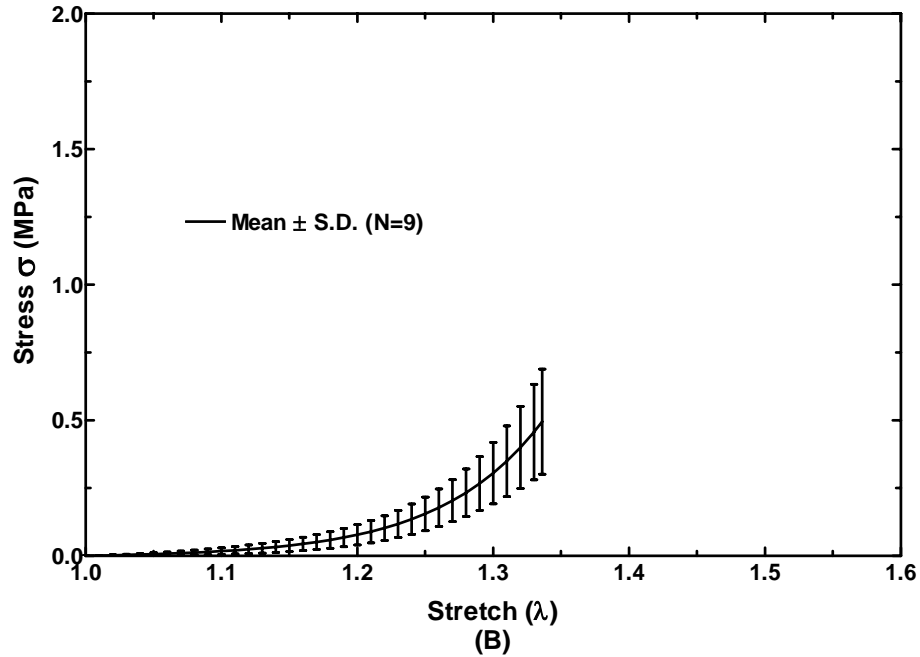


Figure 5.12 (A) Stress-stretch curves of nine AML specimens under uniaxial loading processes. The maximum stretch ratio λ was around 1.5 and the displacement rate was 0.01 mm/sec. (B) The mean curve of stress-stretch relationships obtained from nine AML specimens with standard deviation (S.D.) bars.

Figure 5.13A shows the stress relaxation behavior of the AML obtained from 9 specimens. The normalized stress relaxation function $G(t)$ decreased with time and finally reached a stable state at 120 sec, or the change rate of stress was less than 0.1% / sec. The stress was considered fully relaxed after 120 sec. The mean normalized stress relaxation function with standard deviation is shown in Fig. 5.13B. The mean initial stress was 1.13 MPa, and 33% of the initial stress, on average, was totally relaxed after fully relaxed.

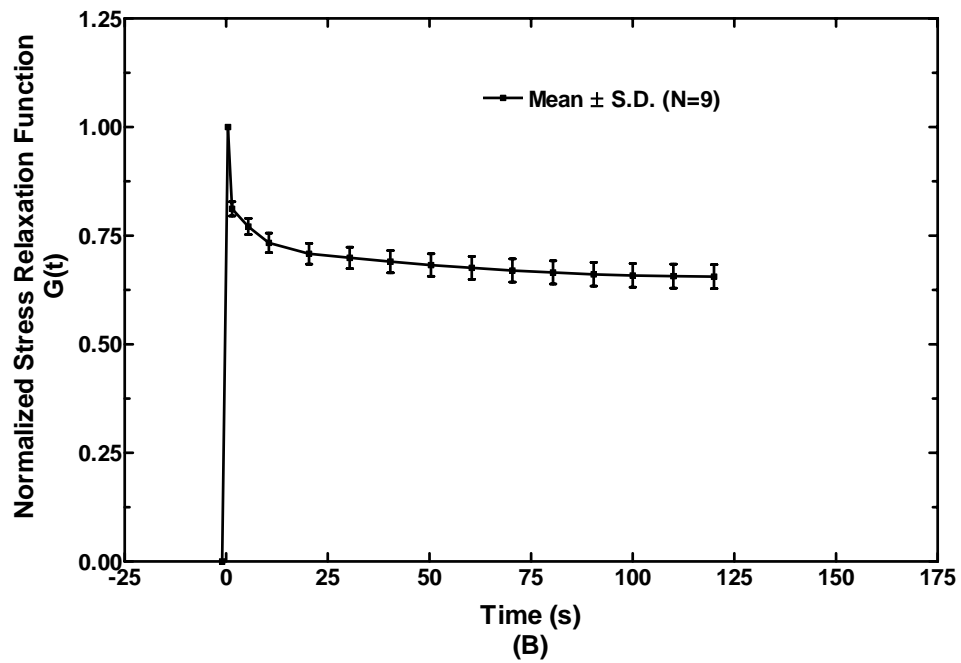
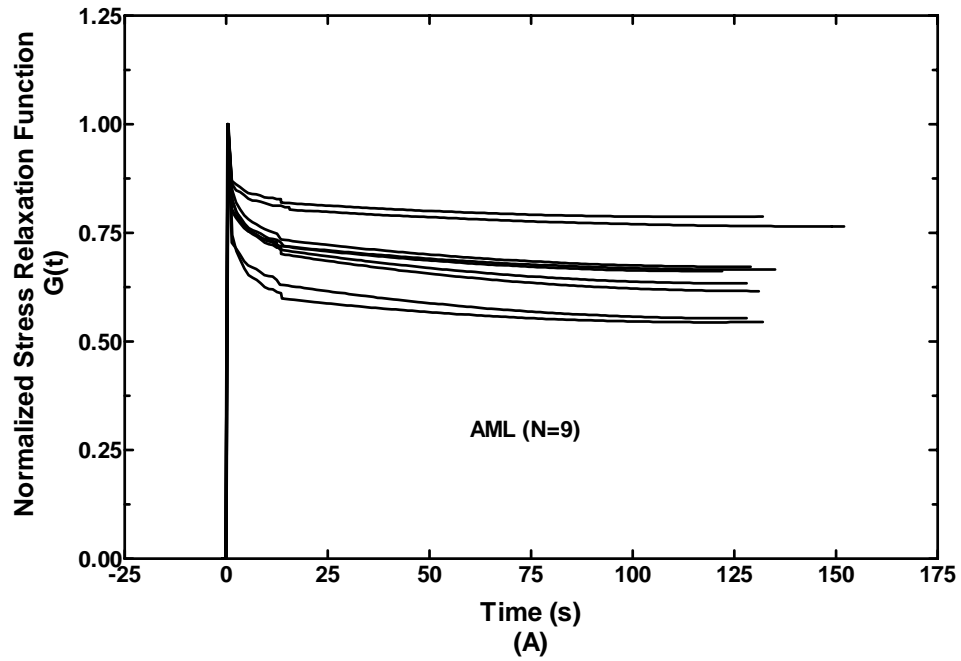


Figure 5.13 (A) Normalized stress relaxation function $G(t)$ obtained from nine AML specimens in stress relaxation tests. (B) The mean curve of $G(t)$ of nine AML specimens with standard deviation (S.D.) bars.

Table 5.4 lists the ultimate stress and stretch ratio of nine AML specimens obtained from failure tests. The breaking location of all specimens occurred around midsubstance in all the tests.

Table 5.4: Ultimate stress and stretch of anterior malleolar ligament (AML) specimens

	AML 1	AML 2	AML 3	AML 4	AML 5	AML 6	AML 7	AML 8	AML 9	Mean	S.D. (±)
Ultimate Stress (MPa)	1.00	0.43	1.34	1.83	2.06	1.54	0.44	0.71	0.68	1.11	0.60
Ultimate Stretch λ	1.50	1.46	1.33	1.71	1.50	1.56	1.51	1.42	1.37	1.48	0.11

S.D. Standard Deviation

5.3.2 Material Modeling Results

The mean experimental stress-stretch curve of nine AML specimens shown in Fig. 5.12B was used to determine material parameters, μ_1, α_1, β and k of Eq. (3.15). Table 5.5 lists the calculated values of μ_1, α_1 and β when k value was varied from 0 to 5, 10, and 20. When $k=0$, or the material is isotropic, we had $\mu_1=0.078$ MPa, $\alpha_1 = 13.69$, and β was not accounted for isotropic material. When k increased to 5, 10 and 20, the values of α_1 and β were almost equal (13.71 ~ 13.68), or the same as the α_1 value at $k = 0$. However, the μ_1 values were decreased as k value, the stiffness of material along the fiber direction, increased.

Table 5.5: Material parameters of the hyperelastic model for the AML

	μ_1	α_1	β
$k=0$	0.078	13.69	–
$k=5$	0.013	13.71	13.68
$k=10$	0.0071	13.68	13.69
$k=20$	0.0037	13.68	13.69

In Weiss's review on ligament mechanics [Weiss, 2002], the modulus of the ligament along the fiber direction was considered an order greater than the modulus in the transverse direction. The AML in this study was assumed with $k = 10$, and the constitutive equation of the AML was then derived as:

$$\sigma = 1.04 \times 10^{-3} (\lambda^{12.68} - \lambda^{-7.84}) + 0.01 (\lambda^{12.69} - \lambda^{-7.85}) \quad (5.5)$$

for stress level of 0 ~ 0.5 MPa, and stretch range of 1 ~ 1.4. Figure 5.14 displays the comparison of stress-stretch curves obtained from Eq. (5.5) and that measured from experiments. It shows that the material model (Eq. (5.5)) is generally able to describe the AML mechanical properties.

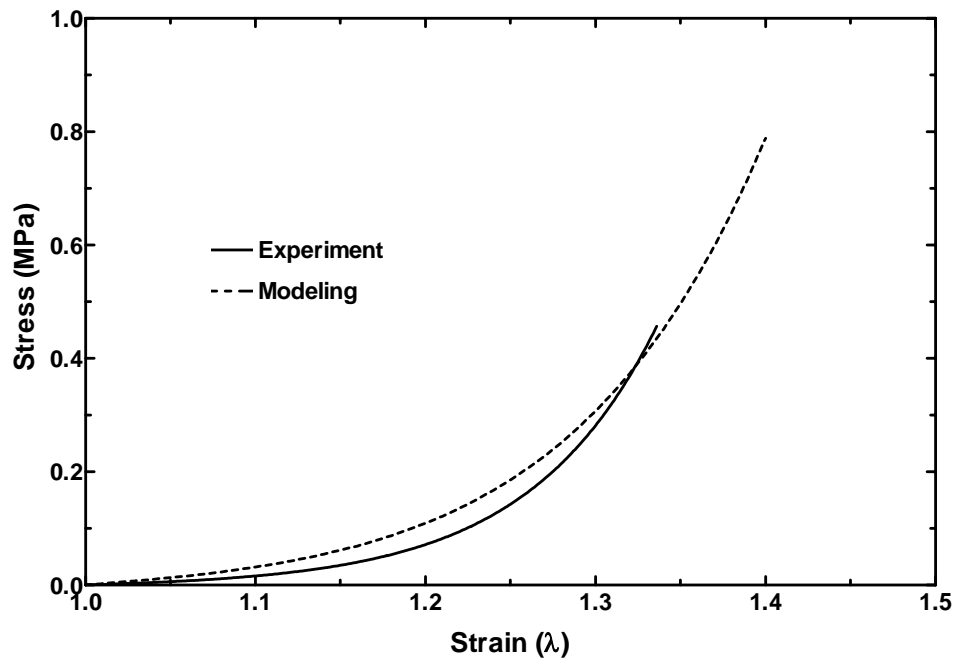


Figure 5.14 The stress-stretch curve of the AML obtained from modeling analysis and the mean stress-strain curve measured from nine AML specimens in uniaxial tensile tests.

Young's modulus of the AML was calculated from Eq. (3.16) and plotted against the stress in Fig. 5.15. It is clearly seen that the Young's modulus of the AML is linearly increasing with the stress. As a first approximation, Young's modulus of the AML is mathematically expressed as

$$\frac{d\sigma}{d\lambda} = 8.95\sigma + 0.22 \quad \text{for } 0 \leq \sigma \leq 0.5 \text{ MPa}, 1 \leq \lambda \leq 1.4 \quad (5.6)$$

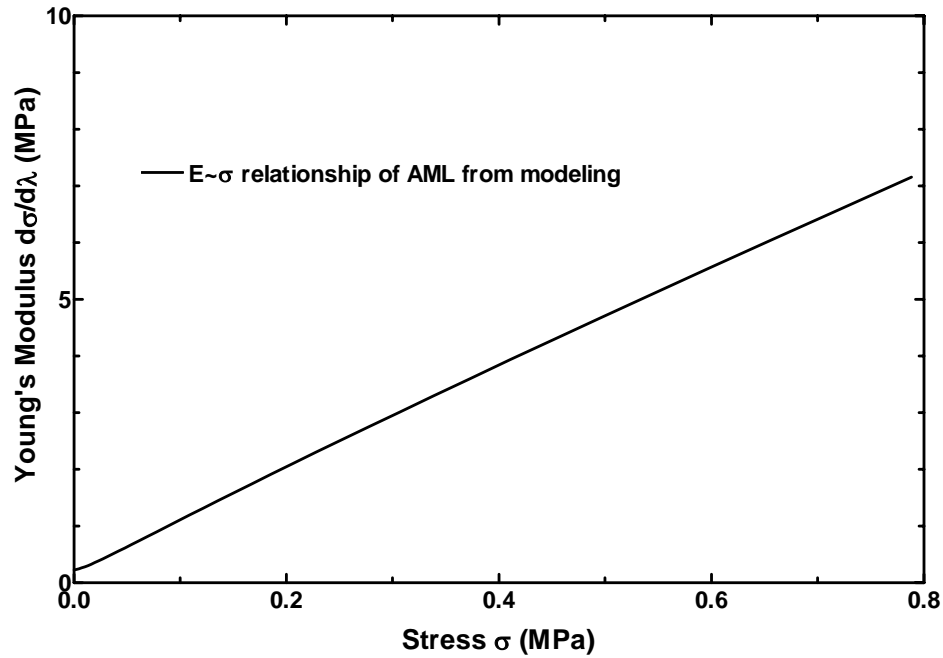


Figure 5.15 The Young's modulus-stress relationship of the AML obtained from the material model. The Young's modulus is linearly increasing with respect to the stress. The values varied from 0.12 to 6.5 MPa when the stress increases from 0 to 0.5 MPa.

5.3.3 Discussion on Anterior Malleolar Ligament Results

In this study, mechanical properties of the AML in human middle ear were first reported through experimental measurement and modeling analysis. The DIC method was used to assess the boundary effect in experiments (Fig. 5.11A) and calculate the

strain in middle portion of the specimen. The strain from DIC was compared with the strain measured in MTS (Fig. 5.11B). The consistent results from both methods were further analyzed to derive mechanical properties of the AML.

A transversely isotropic hyperelastic material model was employed to derive the constitutive equation of the AML. Four material parameters of the model, μ_1, α_1, β , and k , were determined based on regression of experimental data and material modeling results. The physical meaning of μ_1 and k has been stated in the Material Modeling section. The parameters α_1 and β are numbers without direct physical meaning. It is clearly seen from Table 5.5 that the value of k only affects μ_1 , which indicates that the increase of stiffness along the fiber direction (increase of k) results in the decrease of infinitesimal shear modulus (decrease of μ_1). Since α_1 and β are almost equal as k changes, Eqs. (3.15) and (3.16) can be simplified with three material parameters as

$$\sigma = \frac{2\mu_1(1+k)\lambda^{-0.5\alpha_1-1}(\lambda^{1.5\alpha_1} - 1)}{\alpha_1} \quad (5.7)$$

$$\frac{d\sigma}{d\lambda} = \frac{2\mu_1(1+k)}{\alpha_1} [(\alpha_1 - 1)\lambda^{\alpha_1-2} + (\frac{\alpha_1}{2} + 1)\lambda^{-(0.5\alpha_1+2)}] \quad (5.8)$$

The stress-strain relationships of the AML specimens shown in Fig. 5.12 are based on the stress measured in the middle portion of each specimen from the MTS and the strain measured at the same location from the DIC. For fibrous tissues like the ligament, the mechanical response of the tissue is mainly due to the strength of fibers inside ^[Weiss, 2001], especially when a uniaxial load is applied to the tissue along the fiber direction. In this

study, a local response of fibers in the middle portion of the AML was used to describe the mechanical properties of the ligament, which is often a good practical choice. However, due to the irregular geometry and inhomogeneous microstructure of biological tissues, the stress or strain distribution in the whole tissue is expected to be more complicated. A more accurate model including geometry and microstructure of the tissue, such as finite element (FE) model, is needed to investigate mechanical properties of the AML precisely.

The uniaxial tensile test is one of the simplest experiments to measure mechanical properties of soft tissue. The ligament is usually considered as a transverse isotropic material with collagen fibers embedded in substance matrix. The material behavior of ligament usually depends on fiber properties (main factor), matrix properties, fiber-matrix interaction, and fiber-fiber interaction. Thus, a single uniaxial test would be insufficient to characterize the three-dimensional material behavior of the tissue. Additional experiments on multiaxial quasi-static and viscoelastic material properties of the tissue are necessary for an accurate representation of ligament mechanics ^[Weiss, 2002].

The nonlinear stress-strain relationship of the AML shown in Fig. 5.14 resulted in the stress-dependent elastic modulus for the ligament (Fig. 5.15). The modulus increases as the stress increasing, which is a typical mechanical behavior of soft tissues. Therefore, the data reported in this study can be used to improve the FE model of human middle ear. A varying modulus of the AML at different stress levels may be used to simulate the middle ear response to the change of ear physiological condition such as the otitis media with effusion.

In conclusions, mechanical properties and dimensions of the AML in human ear are reported in this paper from experimental measurement and modeling analysis. This is the first investigation of material properties of the middle ear ligament. The data reported here may provide valuable information for understanding the AML and its function. However, the future work is needed such as using the FE modeling approach to include geometric configuration, micro-structural arrangement and interactions between fibers and ground substances on mechanical properties of the AML and developing new experimental methods on measurement of 2-dimensional or 3-dimensional mechanical properties of the AML.

CHAPTER 6

SUMMARY AND COMPARISON OF RESULTS

Mechanical properties of four middle ear tissues: the tympanic membrane (TM), stapedial tendon, tensor tympani tendon and anterior malleolar ligament (AML), have been obtained through experimental measurement and modeling analysis. During a normal hearing process, all components of the middle ear work together to maintain the normal function of the middle ear system. Therefore, it is meaningful to compare mechanical properties of these tissues in following aspects: (1) the constitutive equation or stress-strain relationship, (2) Young's modulus-stress relationship, (3) stress relaxation function, and (4) ultimate stress and strain level.

6.1 Constitutive Behaviors of Middle Ear Tissues

The constitutive equations or stress-strain relationships of the TM, stapedial tendon, tensor tympani tendon and AML are compared under the stress range from 0 to 1.0 MPa, or the stretch ratio from 1 to 1.4, as shown in Figure 6.1. It is clearly seen that within the same strain level, the stress induced in the TM raises faster than the stress increasing in the ligament and tendons, which indicates that the TM has a higher elastic modulus than the stapedial tendon, tensor tympani tendon and AML, therefore. The stress induced in the ligament and tendons are very small at the beginning of the tensile test compared to the stress in the TM. At a stretch ratio of 1.1, the stress in the TM reached 0.4 MPa, while the stresses in the stapedial tendon, tensor tympani tendon and AML were only 0.025,

0.016 and 0.0162 MPa, respectively. The stress response of the tensor tympani tendon is very close to that of the AML within the stretch ratio of 1.2. Among these tissues, the tensor tympani tendon has the lowest stress response over the stretch range from 1.0 to 1.3.

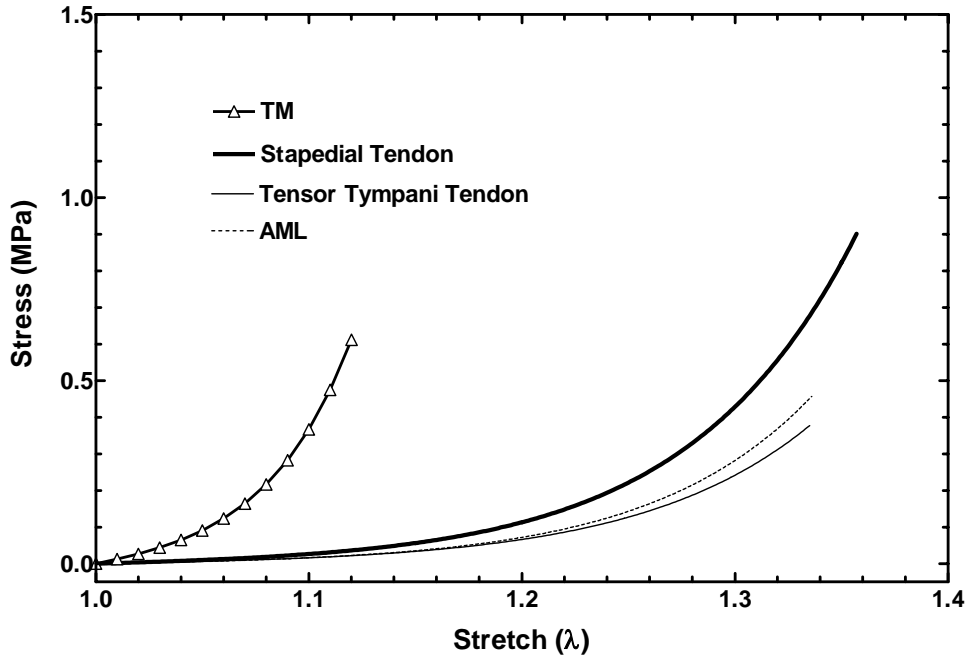


Figure 6.1 Stress-stretch relationships of tested middle ear tissues.

The constitutive equations of these middle ear tissues are summarized below:

$$\text{TM:} \quad \sigma = 0.03(\lambda^{25.76} - \lambda^{-14.38}) \quad (0 \leq \sigma \leq 1.0 \text{ MPa}, 1 \leq \lambda \leq 1.15) \quad (6.1)$$

$$\text{Stapedial Tendon:} \quad \sigma = 5.8 \times 10^{-3}(\lambda^{16.40} - \lambda^{-9.70}) \quad (0 \leq \sigma \leq 1.45 \text{ MPa}, 1.0 \leq \lambda < 1.4) \quad (6.2)$$

Tensor Tympani Tendon:

$$\sigma = 8.5 \times 10^{-4}(\lambda^{22.52} - \lambda^{-12.76}) \quad (0 \leq \sigma \leq 1.0 \text{ MPa}, 1 \leq \lambda < 1.4) \quad (6.3)$$

$$\begin{aligned} \text{AML:} \quad \sigma &= 1.04 \times 10^{-3}(\lambda^{12.68} - \lambda^{-7.84}) + 0.01(\lambda^{12.69} - \lambda^{-7.85}) \\ &\quad (0 \leq \sigma \leq 0.5 \text{ MPa}, 0 \leq \lambda \leq 1.4) \quad (6.4) \end{aligned}$$

Figure 6.1 shows nonlinear stress-strain relationships of four human middle ear tissues. The stress-strain behavior of the TM is significantly different from the behaviors of middle ear ligaments or tendons. It is clearly seen that the human TM is much stiffer than the middle ear ligaments or tendons, while the middle ear ligaments or tendons are more stretchable than the TM.

6.2 Young's Modulus-Stress Relationships of Middle Ear Tissues

The Young's modulus-stress relationships of the TM, stapedial tendon, tensor tympani tendon and AML are compared in Fig. 6.2 based on mean experimental data. The Young's modulus of the TM was derived over three stress ranges: 0~0.1 MPa, 0.1~0.3 MPa and 0.3~1 MPa, while the modulus of the ligament or tendons was derived in an overall stress range of 0~1.5 MPa.

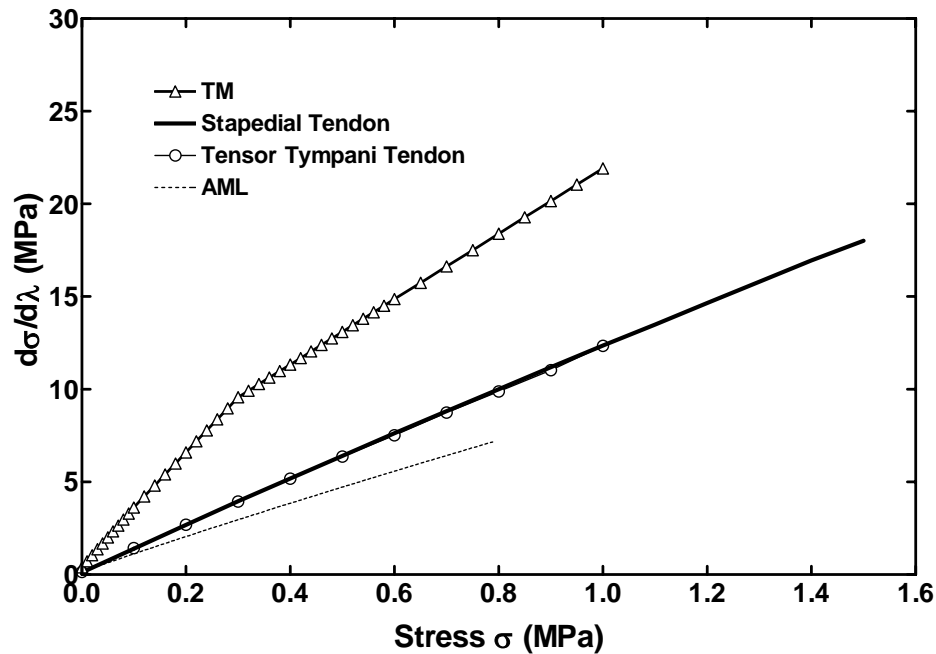


Figure 6.2 Young's modulus-stress relationships of tested middle ear tissues.

It is not surprised to see that the TM has the highest Young's modulus than the middle ear ligament and tendons as being predicted from their stress-strain relationships shown in Fig 6.1. However, two tendons (stapedial tendon and tensor tympani tendon) have almost the same Young's modulus, and the ligament (AML) has the lower Young's modulus than other tissues.

Again, quantified Young's modulus-stress relationships of four middle ear tissues are summarized here:

$$\begin{aligned} \text{TM:} \quad \frac{d\sigma}{d\lambda} &= 32.16\sigma + 0.398 \quad (0 \leq \sigma < 0.1 \text{ MPa}) \\ \frac{d\sigma}{d\lambda} &= 29.75\sigma + 0.645 \quad (0.1 \leq \sigma \leq 0.3 \text{ MPa}) \end{aligned} \quad (6.5)$$

$$\frac{d\sigma}{d\lambda} = 17.65\sigma + 4.274 \quad (0.3 < \sigma \leq 1.0 \text{ MPa})$$

$$\text{Stapedial Tendon: } \frac{d\sigma}{d\lambda} = 11.93\sigma + 0.35 \quad (0 \leq \sigma \leq 1.5 \text{ MPa}) \quad (6.6)$$

$$\text{Tensor Tympani Tendon: } \frac{d\sigma}{d\lambda} = 12.08\sigma + 0.26 \quad (0 \leq \sigma \leq 1.0 \text{ MPa}) \quad (6.7)$$

$$\text{AML: } \frac{d\sigma}{d\lambda} = 8.95\sigma + 0.22 \quad (0 \leq \sigma \leq 0.5 \text{ MPa}) \quad (6.8)$$

In conclusion, the Young's modulus of human middle ear tissues shows a linear relationship to the stress induced in the tissue. The TM has a higher Young's modulus than middle ear ligament or tendons at the same stress level, while the AML has the lowest Young's modulus at that stress.

6.3 Stress Relaxation Functions of Middle Ear Tissues

The normalized stress relaxation function of the TM, stapedial tendon, tensor tympani tendon and AML are compared in Fig. 6.3. The mean initial stress and the mean relaxed stress obtained after fully relaxation from each group of specimens are listed in Table 6.1.

Table 6.1: The mean initial stress and fully relaxed stress of middle ear tissues

	Mean Initial Stress (MPa)	Mean Relaxed Stress (MPa)
TM	1.02	0.64
Stapedial Tendon	2.62	1.44
Tensor Tympani Tendon	1.33	0.84
AML	1.13	0.76

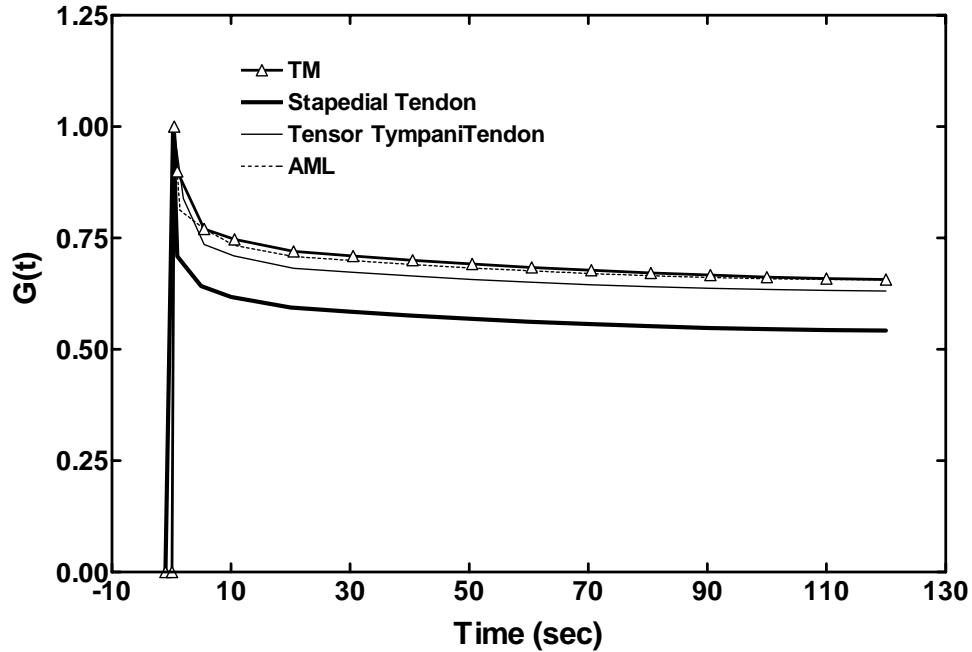


Figure 6.3 Normalized stress relaxation functions of tested middle ear tissues.

It is noted that all the tissues tested in this study are fully relaxed in about 120 seconds. The stapedial tendon has the highest initial and relaxed stress on average from Table 6.1, while the lowest normalized stress relaxation function in Fig. 6.3.

6.4 Ultimate Stress and Stretch Ratio of Middle Ear Tissues

The mean ultimate stress and stretch ratio of the TM, stapedial tendon, tensor tympani tendon and AML are summarized in Table 6.2, with standard deviation (S.D.). We can see that the ligament or tendons are more stretchable than the TM with higher strength along the longitudinal or fiber direction of the tissue. The AML has the lower ultimate stress than other tissues. On average, the stapedial tendon has the highest ultimate stress and stretch ratio among these middle ear tissues.

Table 6.2: The ultimate stress and stretch ratio of tested middle ear tissues

	Mean Ultimate Stress (\pm S.D.)	Mean Ultimate Stretch (\pm S.D.)
TM	1.66 MPa \pm 0.67	1.23 \pm 0.06
Stapedial Tendon	4.04 MPa \pm 1.95	1.65 \pm 0.13
Tensor Tympani Tendon	2.25 MPa \pm 1.47	1.66 \pm 0.10
AML	1.11 MPa \pm 0.6	1.48 \pm 0.11

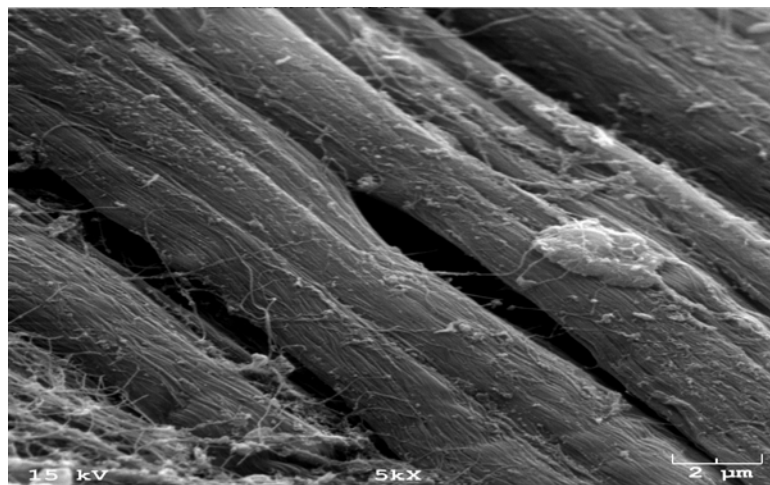
In summary, mechanical properties of four middle ear tissues were summarized and compared in sections 6.1 to 6.4. The human TM has significantly different properties comparing to middle ear ligament and tendons, while the behaviors of middle ear ligament and tendons are close to each other.

6.5 Comparison based on Structures and Functions

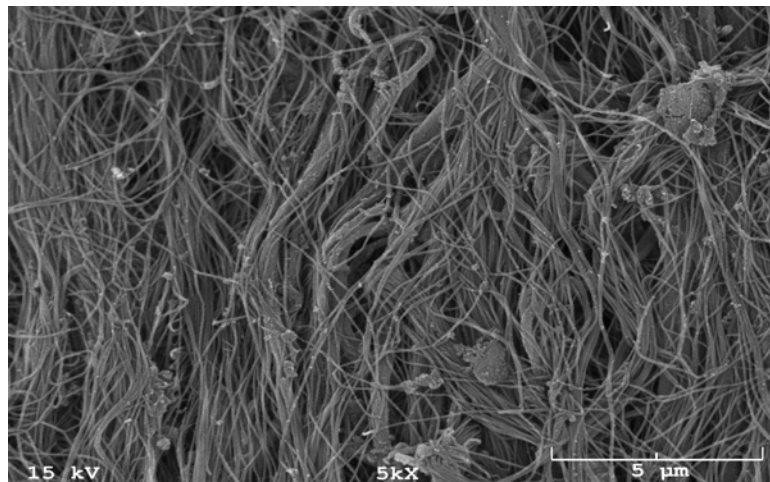
The differences of mechanical properties among these middle ear tissues are related to their distinctive structures. The TM and middle ear ligament or tendons have fibrous microstructure with collagen fibers organized into the matrix of ground substance. However, the TM has multi-layers with collagen fibers along radial and circumferential directions ^[Lim, 1970], while the tendon or ligament is generally considered as a collagenous tissue with the parallel-fibered structure ^[Kastelic *et al.*, 1978]. The variations of fibril density of a single fiber and the packing density of the fibers within the layer or cross-section area of these tissues have been reported ^[Fay *et al.*, 2005] and observed in our study under the scanning electron microscope (SEM). The SEM pictures of the tensor tympani tendon and AML are shown in Fig. 3.18A and Fig. 3.19 in Chapter 3, and the SEM pictures of the TM and the stapedial tendon are given in Fig. 6.4A and 6.4B here. The SEM pictures at the same magnification (5000×) illustrate that the TM has different packed fiber density from the stapedial tendon, as well as different microstructure inside the tissue. The fiber bundles of the TM are probably taut in the relaxed state, therefore the fibers of the TM respond to the tension immediately at the beginning of the tensile test (Fig. 6.1). While the fiber bundles of the stapedial tendon are somehow wavy in the relaxed condition, but become much straight under the tension. Therefore, the stress-strain curve of the stapedial tendon (Fig. 6.1) is relatively “flat” at the beginning of the tension when fibers are still coiled or buckled, but the curve stiffens rapidly when these fibers are fully straightened or taut and start to respond to the high tension.

The microstructures of the tensor tympani tendon and AML show similar wavy fibers as the stapedial tendon but different packed fiber density. Therefore, the stress-strain

relationships of the ligament and tendons are different as shown in Fig. 6.1. Moreover, the properties imparted by the structure enable tissues to perform their physiological functions well. The middle ear ligament or tendons function as a suspensory element in the middle ear while the TM receives sound pressure and initiates the motion of the ossicular chain. Therefore, the TM sustains more strength than the middle ear ligaments and tendons, and shows higher Young's modulus than other tissues.



(A)



(B)

Figure 6.4 (A) Microstructure of the TM under SEM (5000x). (B) Microstructure of the stapedial tendon under SEM (5000x).

CHAPTER 7

APPLICATION

Mechanical properties of the tympanic membrane (TM), stapedial tendon, tensor tympani tendon and anterior malleolar ligament (AML) have been obtained through mechanical experiments and theoretical analysis. The geometric information of these middle ear tissues was also measured by image processing techniques and presented with statistic significance. The results were used in a 3-dimensional finite element (FE) model of human ear developed by our group [Gan *et al.*, 2004] to investigate the change of middle ear function under the normal and pathological conditions, such as the detaching of middle ear ligaments or tendons caused by middle ear diseases, such as otitis media with effusion. The results presented in the following sections have been reported by Gan *et al.* in the 4th international symposium on middle ear mechanics in research and otology [Gan *et al.* 2007].

7.1 Finite Element Model of Human Ear

A 3-dimensional FE model of human ear (Fig. 7.1) reported by Gan *et al.*, 2004 was used in this study. The FE ear model was created based on a complete set of histological sections from a left human temporal bone. Geometric configurations and material properties of the components of the model were listed in Tables 1-3 in Gan's paper [Gan *et al.*, 2004]. Based on the measured results in Chapters 4 and 5 or Chapter 6, the Young's modulus of the TM, stapedial tendon, tensor tympani tendon and AML would be 15, 6.5, 6.5 and 4.5 MPa, respectively, at the physiological stress level of 0.5 MPa [Prendergast 1999].

These data were employed in the FE model, and the material parameters used for Gan's model and the model in this study are listed in Table 7.1.

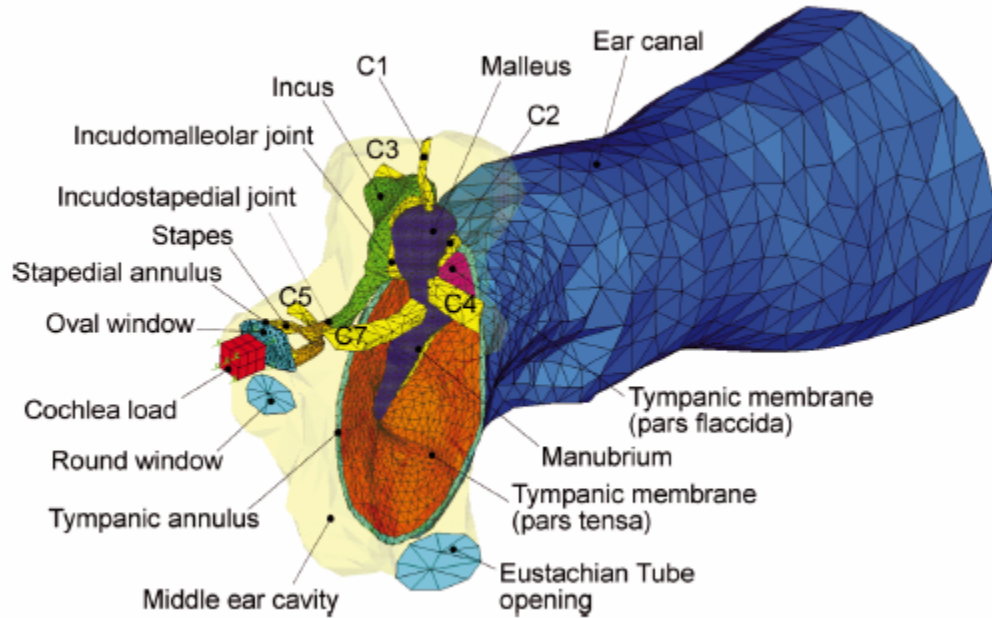


Figure 7.1 A 3-dimensional finite element model of human left ear with outer and middle ear parts.

Table 7.1: Young's modulus of middle ear tissues in Gan's model and this study

Young's Modulus	Gan's Model (MPa)	This Study (MPa)
TM	35, 20	15,10
Stapedial Tendon	52	6.5
Tensor Tympani Tendon	70	6.5
AML	21	4.5

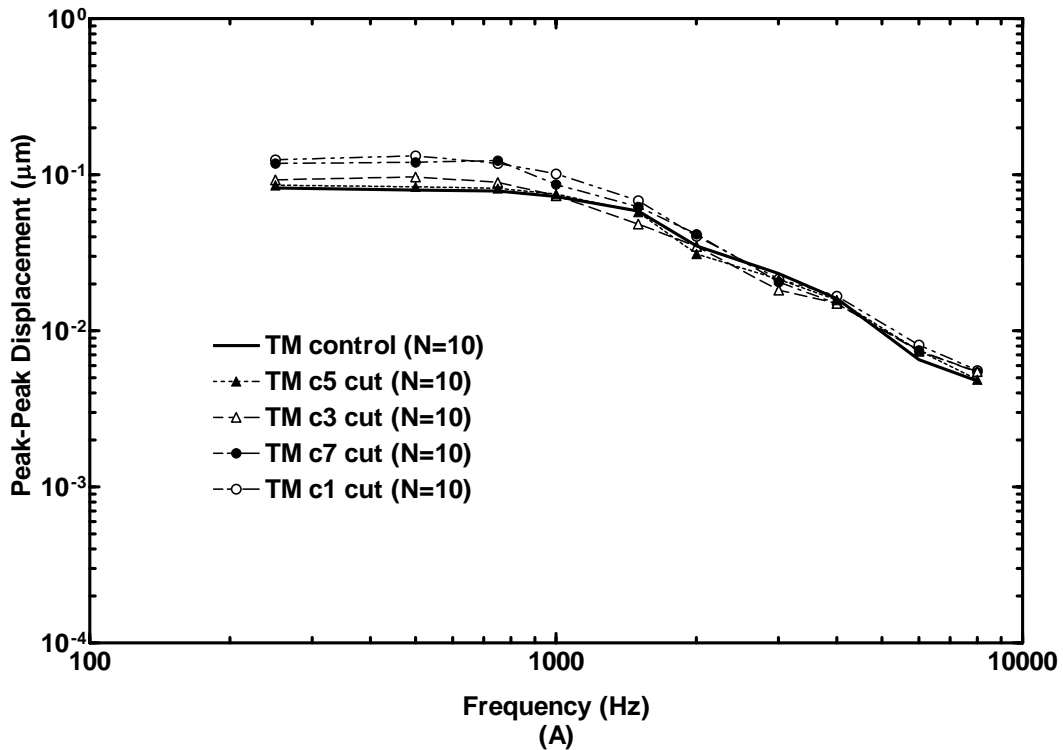
Note: The first number in the TM row represents the modulus along the radial direction, the second number represents the modulus along the circumferential direction.

7.2 Finite Element Analysis

The acoustic-structural coupled analysis was employed to investigate the acoustic effect on mechanical vibration transmission in the ear using the FE model with material properties from this study. A uniform pressure of 90 dB SPL (0.632 Pa, rms value) was applied in the canal side at a location of 2 mm away from the TM. The harmonic analysis was conducted on the model over the frequency range of 200–8000 Hz in ANSYS (ANSYS Inc, Canonsburg, PA). To simplify the FE calculation, the acoustic-mechanical coupled analysis was only involved between the external ear canal air and middle ear ossicular structure. This ear canal-TM coupling is called “one-chamber” acoustic-mechanical analysis ^[Gan 2004]. The magnitudes of displacements of the TM at the umbo and stapes footplate were calculated and compared with temporal bone experimental results ^[Gan 2007]. One of pathological conditions of the middle ear, i.e., the detachment of middle ear ligaments and tendons, was simulated in FE model by setting a very low Young’s modulus (0.1 MPa) for the detached ligament or tendon, and created in temporal bones by cutting the ligament or tendon through the surgical approach. Four middle ear ligaments and tendons were selected for this study: superior malleus ligament (C1), posterior incus ligament (C3), stapedial tendon (C5), and tensor tympani tendon (C7) in the order of cutting C5, C3, C7, and C1. Following the ligament cutting sequence in bone experiments, we created the same sequence of removing ligaments in the FE model and performed the FE analysis sequentially. The displacements at the umbo of the TM and footplate of the stapes were calculated and the results were compared with the bone experimental data.

7.3 Results

Figure 7.2 shows mean frequency response curves of displacement at the umbo of the TM measured from 10 bones following the ligament cutting sequence: control or intact ossicular chain → C5 → C3 → C7 → C1 cut. Figure 7.2A displays the magnitude and Figure 7.2B the phase angle. The results in Fig. 7.2 show that destruction of ligaments C5, C3, C7 and C1 affects the umbo movement at low frequencies ($f < 2$ kHz). The first cut C5 did not show much effect on the umbo vibration (< 0.5 dB) and the C7 cut showed stronger influence on TM displacement than other ligaments.



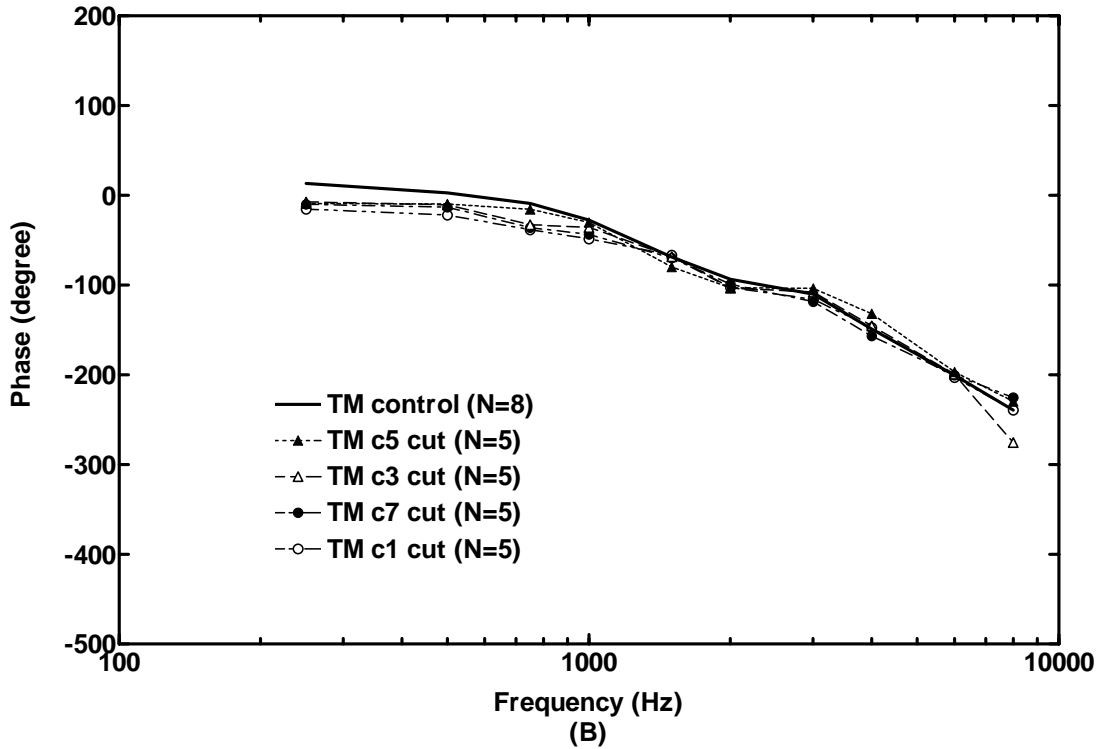


Figure 7.2 Mean peak-to-peak displacement curves measured at the umbo of the TM under the control and ligament cut sequence: C5→C3→C7→C1. (A) Magnitude; (B) phase angle.

The mean displacement curves of the stapes footplate from 10 bones following the ligament cutting sequence are shown in Fig. 7.3. Figure 7.3A represents the magnitude and Figure 7.3B the phase angle. Compared with the umbo displacement data, the destruction of ligaments limited its effect on the footplate movement at frequency below 1 kHz.

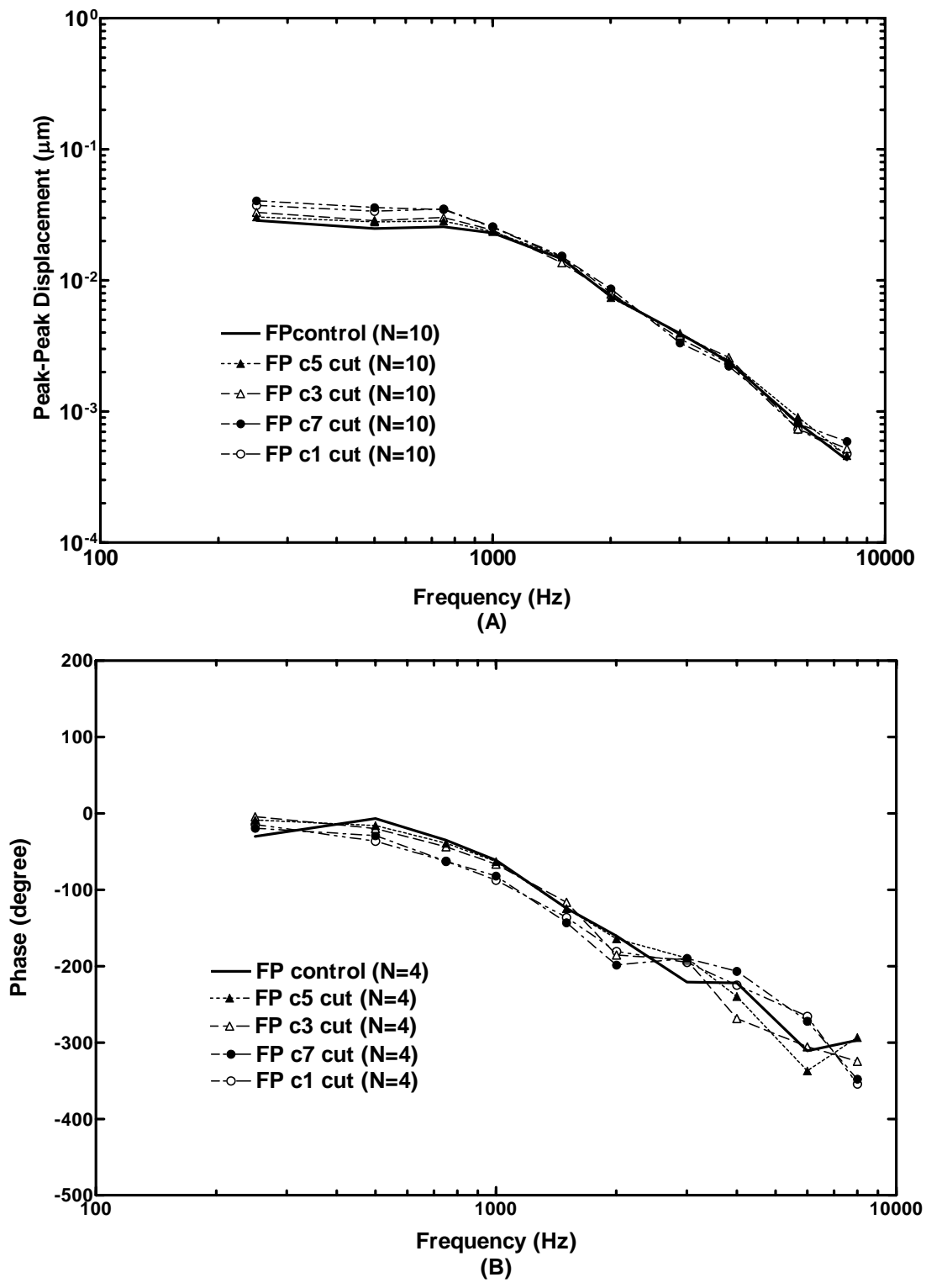
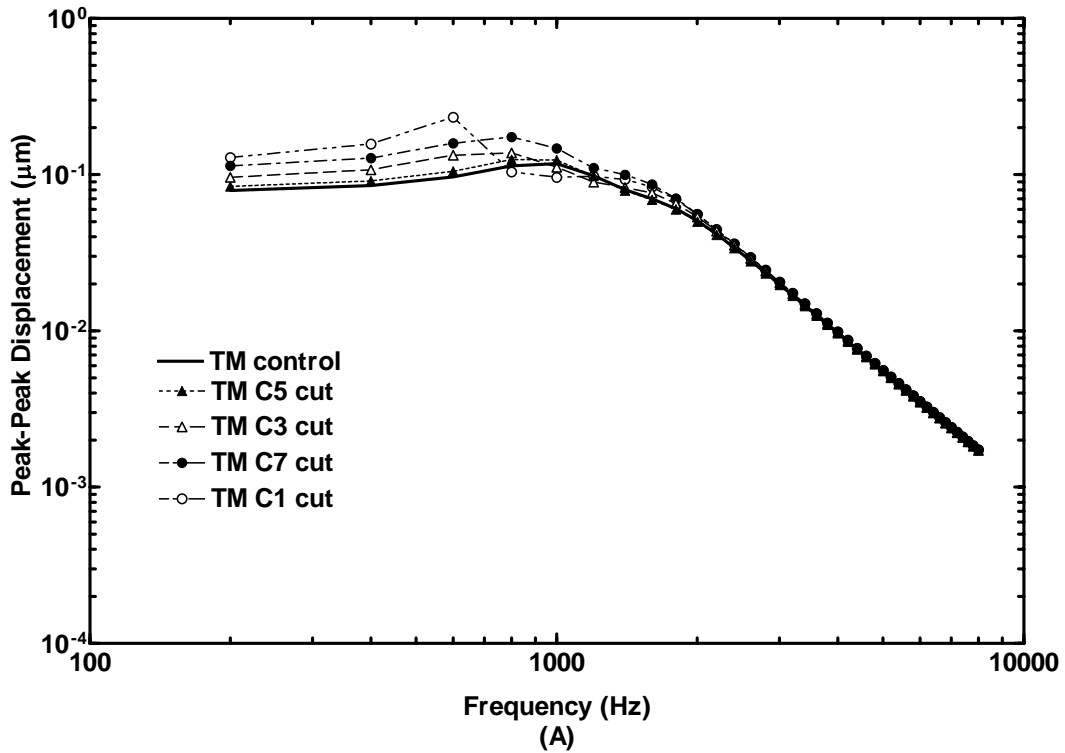


Figure 7.3 Mean peak-to-peak displacement curves measured at the stapes footplate under the control and ligament cut sequence: C5→C3→C7→C1. (A) Magnitude; (B) phase angle.

Figure 7.4 displays the FE model-predicted displacement at the umbo of the TM with the magnitude (Fig. 7.4A) and phase (Fig. 7.4B) in response to the ligament removal sequential. The model results show that ligaments C5 and C3 did not have much effect on the umbo movement, but C7 and C1 had considerable effect on the umbo movement at low frequencies ($f < 2$ kHz). Compared with the experimental data in Fig. 7.2, the model-predicted umbo displacement was increased more after C7 or C1 removal at $f \leq 1$ kHz. It is also noticed that the ligament removal did not affect the umbo movement at high frequencies ($f \geq 2$ kHz) shown in the experiments (Fig. 7.2) and FE model (Fig. 7.4). However, the umbo displacement from the model was decreased faster than that measured from the bones at frequencies 2 to 8 kHz.



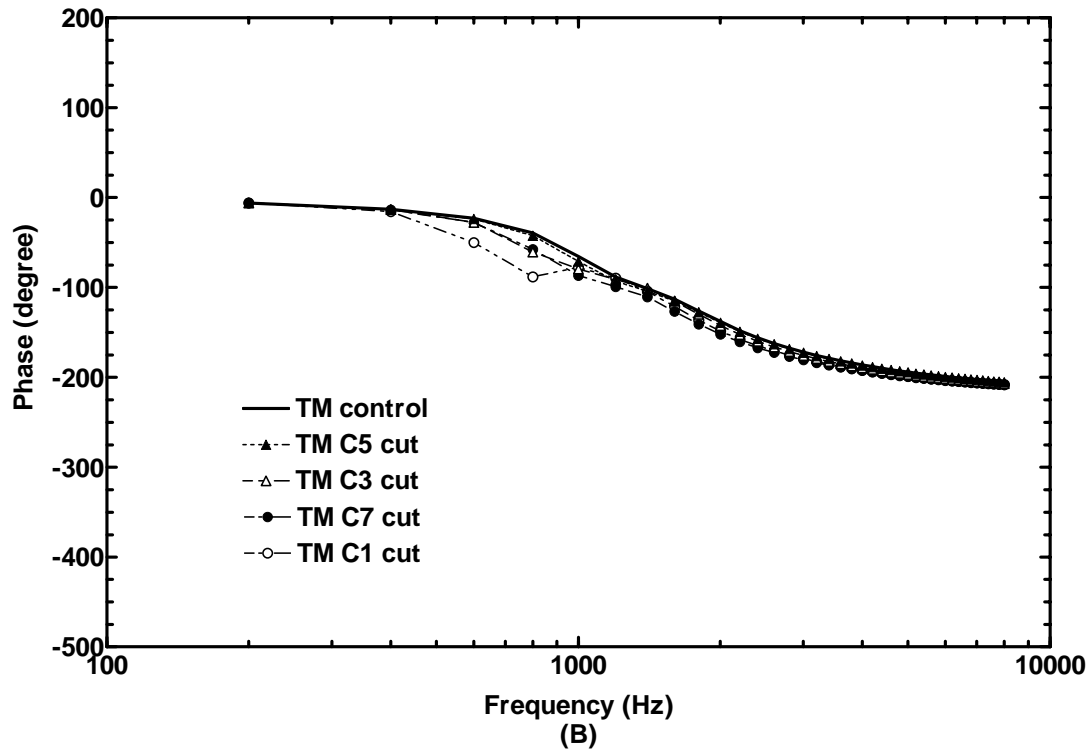


Figure 7.4 FE model-derived umbo displacement curves under the normal and ligament removal sequence: C5→C3→C7→C1. (A) Magnitude; (B) phase angle.

Fig. 7.5 shows the FE model-derived displacement curves of the stapes footplate under destruction of each ligament following the bone experimental sequence. The model results indicate that the removal of middle ear ligaments only affected the footplate displacement at $f < 1$ kHz and there was no obvious difference observed between ligaments. Similar to the umbo, the footplate displacement from the model was decreased faster than that measured in bones at frequencies 1 to 8 kHz.

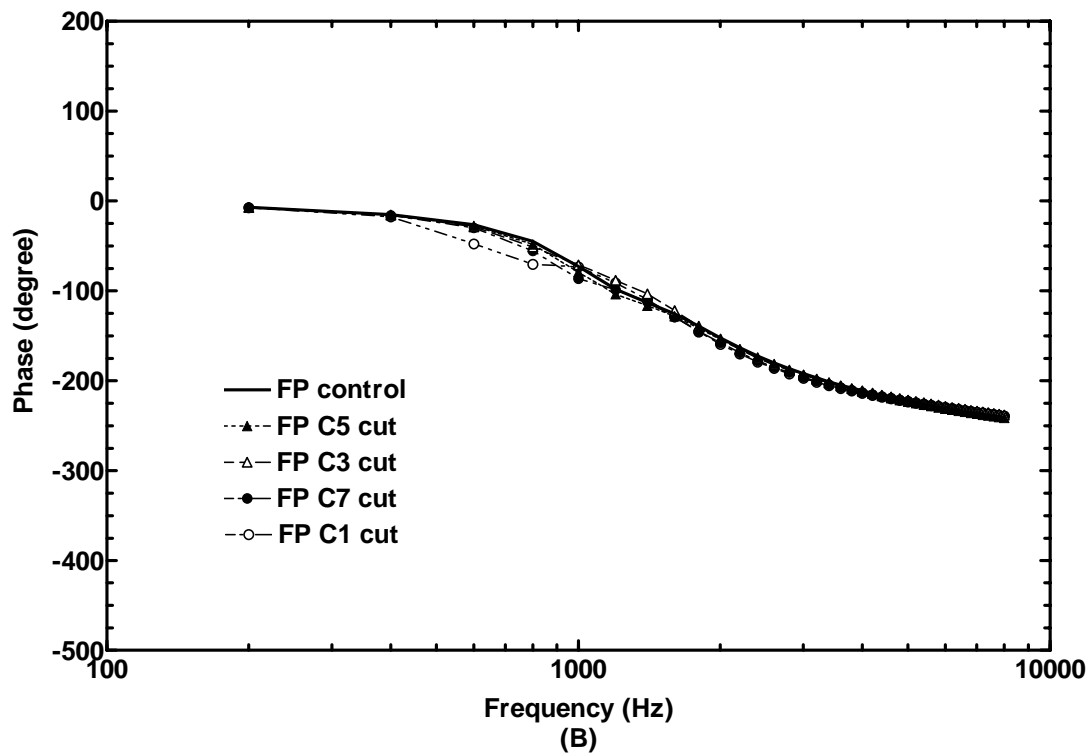
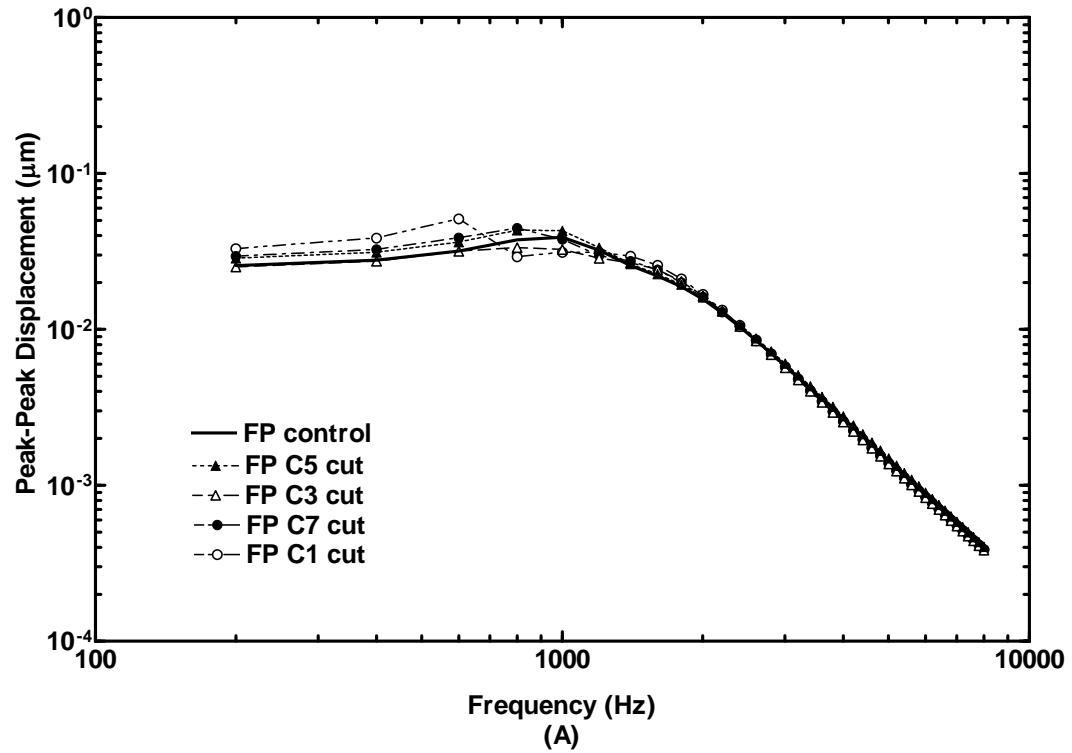


Figure 7.5 FE model-derived stapes footplate displacement curves under the normal and ligament removal sequence: C5→C3→C7→C1. (A) Magnitude; (B) phase angle.

7.4 Discussion

Both experimental and FE modeling results show that destruction of middle ear ligaments/tendons affects the TM and stapes footplate vibrations at low frequencies ($f \leq 1$ kHz). The tensor tympani tendon (C7) and superior malleus ligament (C1) may play more important role for acoustic-mechanical transmission compared with other ligaments. The effects of ligaments on transfer function of the middle ear are frequency sensitive and varying with individual ligament.

Mechanical tests of middle ear ligaments and tendons have shown that the ear tissues are viscoelastic materials and the Young's modulus changes with stress level. In this study, we employed the preliminary data obtained from uniaxial tensile tests on the TM, stapedial tendon, tensor tympani tendon and anterior malleolar ligament into our model, and the results showed that the new mechanical property of the tissue had improved the accuracy of the model for predicting the ligament function on umbo and stapes movements.

CHAPTER 8

CONCLUSIONS AND FUTURE WORK

8.1 Conclusions

The research works presented in this dissertation include:

1. a review on mechanical properties of four middle ear tissues (tympanic membrane, stapedial tendon, tensor tympani tendon and anterior malleolar ligament) published in literature through either experimental measurement or modeling analysis;
2. a review on fundamentals of biomechanics study including mechanical experiments and computational modeling analysis such as constitutive modeling and FE method;
3. mechanical properties of four middle ear tissues (tympanic membrane, stapedial tendon, tensor tympani tendon and anterior malleolar ligament) obtained from experimental measurement and theoretical analysis;
4. the microstructure of four middle ear tissues observed under the SEM and their geometric information with statistic significance;
5. a practicable method to determine mechanical properties of middle ear tissues through experimental measurement (with the aid of DIC method to evaluate boundary effects of experiments) and theoretical analysis (material modeling and FE method);

6. an application of determined mechanical properties of four middle ear tissues in a FE human ear model to predict the transfer function of middle ear in the normal and pathological condition (detachment of middle ear ligaments or tendons), which were compared with temporal bone experimental results.

The objectives formulated for this research in Chapter 1 are all fulfilled. First, the results of Chapter 4 described viscoelastic properties of the TM. Second, the results of Chapter 5 gave mechanical properties of three middle ear ligament and tendons. Third, applications of determined mechanical properties of middle ear tissues were performed in Chapter 7 with improved FE analysis results. Finally, based on results presented in this study, methods introduced in Chapter 3 are proved to be practical and reliable in determining mechanical properties of middle ear tissues with limited dimensions. Five approaches proposed at the end of Chapter 1 were thus feasible and this research work was successfully accomplished.

The major contribution of this research is to provide the new and useful data on mechanical properties of middle ear tissues for study of ear mechanics, which are unavailable in literature. The other contribution of this study is to develop a practical method to determine mechanical properties of middle ear tissues, and the method can be extended to the study of other biological soft tissues in the future. However, the challenge of this research is to dealing with middle ear tissues with small dimensions in the order of 1 or 2 mm. The reliability of experimentally measured data has to be verified carefully through image processing techniques and modeling analysis approaches. All the results presented in this study have been evaluated through those steps.

8.2 Future Work

Following our current works on mechanical properties of middle ear tissues, additional research issues that ought to be explored to extend our understanding on ear tissue mechanics are discussed in this section.

8.2.1 Age-Related Study

It is realized that mechanical properties of biological soft tissue are related to the age or disease state of the donor. For example, an old person or a person with otitis media with effusion might have thickened eardrum or thinner middle ear ligaments or tendons due to the structural change of the tissue by the age or disease. The mechanical behaviors of the tissue from this donor were different compared to the performance of tissues from a young or healthy person. Therefore, the mechanical tests on tissues from different age groups will be meaningful to explain age effect on mechanical properties of middle ear tissues.

8.2.2 Micro-Structural Modeling

In current study, a simple FE model of the tensor tympani tendon has been created to estimate the relationship between collagen fibers and ground substances of the tissue. In our future study, a more complicated FE model of the tissue will be developed, which will evaluate the effect of collagen fibers, effect of ground substances, and interactions between fibers and ground substances, in order to better understand the constitutive behavior of middle ear tissues.

8.2.3 Dynamic Experiment

As we have mentioned in Chapter 1, the middle ear functions as a transformer to transmit input sound waves into mechanical vibrations through the TM. In another word, the TM is the first structure which initiates the hearing process under the acoustic excitation across the auditory frequency range (200 ~ 8000 Hz). Therefore, it would be an interesting topic to measure the dynamic property of the TM corresponding to acoustic excitation at frequency domain. In the future dynamic experiment, the vibration of the TM driven by sound waves will be measured through the laser Doppler vibrometer or opto-electronic holography. The experimental data can be analyzed through the modeling approach to determine the dynamic modulus of the TM in frequency domain. The method could be extended to rest of middle ear tissues for modeling dynamic response of the whole middle ear system.

REFERENCES

- [1] Anson, B. J., Donaldson, J. A. *Surgical anatomy of temporal bone*. W B Saunders Company, 1981
- [2] Beer, H. J., Bornitz, M., Drescher, J., Schmidt, R. and Harddtke, H. J. *Finite element modeling of the human eardrum and application*. In: Hüttenbrink KB (ed) Middle ear mechanics in research and otosurgery. Department of Oto-Rhino-Laryngology, Dresden University of Technology, Dresden, Germany, pp. 40-47, 1996
- [3] Causse, J. B., Vincent, R., Michat, M. and Gherini, S., *Stapedius Tendon Reconstruction during Stapedotomy: Technique and Results*, Ear Nose Throat J., 76(4), pp. 256-258, 260-269, 1997
- [4] Cheng, T., Dai, C., Gan, R. Z. *Viscoelastic Properties of human tympanic membrane*. Annals of Biomedical Engineering, 35(2), pp. 305-314, 2007a
- [5] Cheng, T. and Gan, R. Z. *Mechanical Properties of Stapedial Tendon in Human Middle Ear*, Transactions of the ASME, Journal of Biomechanical Engineering, (in press), 2007b
- [6] Cheng, T. and Gan, R.Z. *Experimental Measurement and Modeling Analysis on Mechanical Properties of Tensor Tympani Tendon*, Medical Engineering & Physics, (in press), 2007c
- [7] Cheng, T. and Gan, R.Z. *Mechanical Properties of Anterior Malleolar Ligament from Experimental Measurement and Material Modeling Analysis*, Biomechanics and Modeling in Mechanobiology, (under review), 2007d

- [8] Decraemer, W. F., Maes, M. A. and Vanhuyse, V. J. *An elastic stress-strain relation for soft biological tissues based on a structural model*. J Biomech. 13(6), pp. 463-468, 1980
- [9] Donaldson, J. A., Duckert, L. G., Lambert, P.M., and Rubel, E.W. *Surgical anatomy of the temporal bone*, 4th ed., Raven Press, New York, 1992
- [10] Fay, J., Puria, S., Decraemer, W. F. and Steele, C. *Three approaches for estimating the elastic modulus of the tympanic membrane*. J Biomech. 38(9), pp. 1807-1815, 2005
- [11] Ferrazzini, M. *Virtual middle ear: a dynamic mathematical model based on the finite element method*. Ph.D. Dissertation, Swiss federal institute of technology, 2003
- [12] Ferris, P. and Prendergast, P. J. *Middle-ear dynamics before and after ossicular replacement*. J. of Biomech. 33, pp. 581-590, 2000
- [13] Flanagan, J. L. *Speech Analysis and Perception*, Springer-Verlag, Berlin, 2nd edition, 1965
- [14] Fung, Y. C. *Elasticity of soft tissues in simple elongation*, American Journal of Physiology, 213(6), pp. 1532-1544, 1967
- [15] Fung, Y.C. *Biomechanics: mechanical properties of living tissues*. Springer-Verlag New York, Inc., 1993
- [16] Funnell, W. R. and Laszlo, C. A. *A critical review of experimental observations on ear-drum structure and function*. ORL J. Otorhinolaryngol. Relat. Spec. 44(4):181–205, 1982

- [17] Gan, R. Z., Sun, Q., Dyer, R. K., Chang, K. H. and Dormer, K. J. *Three-dimensional modeling of middle ear biomechanics and its application*. *Otology & Neurotology*, 23, pp. 271-280, 2002
- [18] Gan, R. Z., Feng, B. and Sun, Q. *Three-dimensional finite element modeling of human ear for sound transmission*. *Annals of Biomedical Engineering*, 32(6), pp. 847-859, 2004
- [19] Gan, R.Z., Cheng, T., Nakmali, D., and Wood, M. W. *Effects of middle ear suspensory ligament on acoustic-mechanical transmission in human ear*. *The Proceedings of the 4th International Symposium on Middle Ear Mechanics in Research and Otology*, Zurich, Switzerland, pp. 216-222, 2007
- [20] Gardiner, J. C. and Weiss, J. A. *Simple shear testing of parallel-fibered planar soft tissues*. *ASME J. Biomech Eng.*, 123, pp. 170-175, 2001
- [21] Geisler, C. Daniel. *From Sound to Synapse*. Oxford, 1998
- [22] Guyton, A., and Hall, J. *Textbook of medical physiology*, 10th Edition, W. B. Saunders Company, Philadelphia, PA, 2000
- [23] Helmholtz H. F. L. (translated by Hinton J). *The mechanics of the ossicles and the membrane Tympani*. New Sydenham Society, London. Vol 62. pp. 97-155, 1874
- [24] Kastelic, J., Galeski, A., and Baer, E. *The multicomposite structure of tendon*. *J. Connective Tissue Research*. 6, pp. 11-23, 1978
- [25] Kelly D. J. and Prendergast P. J. *An investigation of middle-ear biomechanics using finite element modeling*. *Proc. Summer Bioengineering Conference, BED Vol.50*, ASME, 2001

- [26] Kelly, D. J., Prendergast, P. J. and Blayney, A. W. *The effect of prosthesis design on vibration of the reconstructed ossicular chain: a comparative finite element analysis of four prostheses*. *Otology & Neurotology*, 24, pp. 11-19, 2003
- [27] Kirikae I. *The structure and function of the middle ear*. Tokyo: University of Tokyo Press, 1960
- [28] Koike, T., Wada, H. and Kobayashi, T. *Modeling of the human middle ear using the finite-element method*. *J. Acoust. Soc. Am.*, 111(3), pp. 1306-1317, 2002
- [29] Lanir, Y. and Fung, Y. C. *Two-dimensional mechanical properties of rabbit skin. I. Experimental system*. *J. Biomech.*7, pp. 29-34, 1974
- [30] Lim, D. J. *Human tympanic membrane: An ultrastructural observation*. *Acta Otolaryngol.* 70(3), pp. 176-186, 1970
- [31] Love, J. T. Jr., and Stream, R. W., *The Biphasic Acoustic Reflex: a New Perspective*, *Laryngoscope*, 88, pp. 298-313, 1978
- [32] Lu, H. and Cary, P. D. *Deformation measurements by digital image correlation: Implementation of a second-order displacement gradient*. *Experimental Mechanics*. 40(4), pp. 1-8, 2000
- [33] Miller, K. and Chinzei, K. *Mechanical properties of brain tissue in tension*. *J Biomech.* 35(4), pp. 483-490, 2002
- [34] Møller A. R. *Function of the middle ear*, Chapter 15 of *Handbook of Sensory Physiology Vol.1: Auditory System, Anatomy Physiology (Ear)*, Edited by Keidel W.D. and Neff W.D., Springer-Verlag, New York, 1974
- [35] Møller A. R. *Hearing: Anatomy, Physiology and Disorders of the Auditory System*, 2nd edition, Elsevier, 2006

- [36] Ogden, R. W. *Nonlinear Elasticity, Anisotropy, Material Stability and Residual Stresses in Soft Tissue*. In: Holzapfel GA, Ogden RW (eds) *Biomechanics of Soft Tissue in Cardiovascular System*, CISM Courses and lecture Series 441. Springer-Verlag, Wien New York, 2003
- [37] Peters, W. H. and Ranson, W. F. *Digital imaging techniques in experimental stress analysis*. *Opt. Eng.* (21), pp. 427-432, 1982
- [38] Prendergast, P. J., Ferris, P., Rice, H. J. and Blayney, A. W. *Vibro-acoustic modeling of the outer and middle ear using the finite-element method*. *Audiol Neurootol*, 4, pp. 185-191, 1999
- [39] Rossing T. D., *The science of sound*, Addison-Wesley Publishing Co., 1990
- [40] Sarma, P. A., Pidaparti, R. M., Moulik, P. N. and Meiss, R. A. *Non-linear material models for tracheal smooth muscle tissue*. *Biomed Mater Eng.* 13(3), pp. 235-245, 2003
- [41] Singh R. P. *Anatomy of hearing and speech*, Oxford University Press, New York, 1980
- [42] Sutton, M. A., Wolters, W. J., Peters, W. H., Ranson, W. F., and McNeil, S. R. *Determination of displacements using an improved digital image correlation method*. *Image Vision Computing.* 1(3), pp. 133-139, 1983
- [43] Sun, Q., Gan, R. Z., Chang, K. H. and Dormer, K. J. *Computer-integrated finite element modeling of human middle ear*. *Biomechan Model Mechanobiol*, 1, pp. 109-122, 2002
- [44] Tsai, S. W., Hahn, H. T. *Introduction to Composite Materials*. Technomic Publishing Company, Inc., Lancaster, Pennsylvania, 1980

- [45] Vendroux, G. and Knauss, W. G. *Submicron deformation field measurements: Part2. Improved digital image correlation. Experimental Mechanics.* (38), pp. 86-91, 1998
- [46] von Békésy, G. *The structures of the middle ear and the hearing of one's own voice by bone conduction.* J Acoust Soc Am. Vol 21(3), pp. 217-232, 1949
- [47] Wada, H., Metoki, T., and Kobayashi, T. *Analysis of dynamic behavior of human middle ear using a finite-element method.* J Acoust Soc Am. 92(6), pp. 3157-3168, 1992
- [48] Wang, B., Lu, H. and Kim, G. *A damage model for the fatigue life of elastomeric materials. Mechanics of Materials.* (34), pp. 475-483, 2002
- [49] Weiss, J. A. and Gardiner, J. C. *Computational modeling of ligament mechanics. Critical Review. Biomed Eng.,* 29(3), pp. 303-371, 2001
- [50] Weiss, J. A., Gardiner, J. C., Bonifasi-Lista, C. *Ligament Material Behavior is Nonlinear, Viscoelastic and Rate-Independent under Shear Loading.* J. of Biomech, 35, pp. 943-950, 2002
- [51] Wever E. G., Lawrence M. *Physiological acoustics.* Princeton University Press. Princeton. Pp. 416-417, 1954
- [52] Wellman P., Howe R. H., Dalton E. and Kern K. A. *Breast tissue stiffness in compression is correlated to histological diagnosis.* Technical report. Harvard Biorobotics Laboratory. 1999. <http://biorobotics.harvard.edu/pubs/mechprops.pdf>
- [53] Williams, K. R., Blayney, A. W. and Lesser, T. H. J. *Mode shapes of a damaged and repaired tympanic membrane as analyzed by the finite element method.* Clin. Otolaryngol., 22, pp. 126-131, 1997

- [54] Wood M.G. *Laboratory textbook of anatomy and physiology*, Prentice Hall, New Jersey, 1998
- [55] Wu, J. Z., Dong, R. G., Smutz, W. P. and Schopper, A. W. *Non-linear and viscoelastic characteristics of skin under compression: experiment and analysis*. Biomed Mater Eng. 13(4), pp. 373-385, 2003